THE QUARTERLY JOURNAL OF
MECHANICS AND APPLIED MATHEMATICS

VOLUME IV PART 3

SEPTEMBER 1951

UNIV RS
OF MICHIGAN
OCT 1 1 1951
ENGINEERING
LIBRARY

OXFORD
AT THE CLARENDON PRESS
1951

Price 12*s.* 6*d. net*

PRINTED IN GREAT BRITAIN BY CHARLES BATEY AT THE UNIVERSITY PRESS, OXFORD

THE QUARTERLY JOURNAL OF MECHANICS AND APPLIED MATHEMATICS

Editorial Board

S. GOLDSTEIN — R. V. SOUTHWELL
G. I. TAYLOR — G. TEMPLE

together with

A. C. AITKEN — H. JEFFREYS
S. CHAPMAN — J. E. LENNARD-JONES
A. R. COLLAR — M. J. LIGHTHILL
T. G. COWLING — N. F. MOTT
C. G. DARWIN — W. G. PENNEY
W. J. DUNCAN — A. G. PUGSLEY
A. A. HALL — L. ROSENHEAD
D. R. HARTREE — ALEXANDER THOM
WILLIS JACKSON — A. H. WILSON
J. R. WOMERSLEY

Executive Editors

G. C. McVITTIE — V. C. A. FERRARO

THE QUARTERLY JOURNAL OF MECHANICS AND APPLIED MATHEMATICS is published at 12*s.* 6*d.* net for a single number with an annual subscription (for four numbers) of 40*s.* post free.

NOTICE TO CONTRIBUTORS

1. *Communication.* Papers should be communicated to one or other of the Executive Editors, by name, at King's College, Strand, London, W.C. 2.

2. *Presentation.* Manuscripts should preferably be typewritten, and each paper should be preceded by a summary not exceeding 300 words in length. References to literature should be given in standard order, *author, title of journal, volume number, date, page.* These should be placed at the end of the paper and arranged according to the order of reference in the paper.

3. *Diagrams.* The number of diagrams should be kept to the minimum consistent with clarity. The lines of the figures should be drawn in ink either on draughtsman's paper or on good quality white paper. Each individual line in the figure should bear reducing to one-half of the size of the original, and great care should be exercised to see that the lines are regular in thickness, especially where they meet. Lettering of the figure should be in pencil and should be sufficient to define clearly the lines and curves in it. The writing of formulae or of explanations on the diagram itself should be avoided. All explanations of symbols, etc., should be given in underline. Contributors should indicate on their manuscripts where figures should be inserted.

4. *Tables.* Tables should preferably be arranged so that they can be printed with the columns parallel to the longer edge of the page.

5. *Notation.* All single letters used to denote vectors in the manuscript should be marked by underlining with a wavy line. Scalar and vector products should be denoted by $\underset{\sim}{a} . \underset{\sim}{b}$ and $\underset{\sim}{a} \wedge \underset{\sim}{b}$ respectively. Real and imaginary parts of complex quantities should be denoted by re and im respectively.

6. *Offprints.* Authors of papers will be entitled to 25 free offprints. This number is available for sharing between authors of joint papers.

7. All correspondence other than that dealing with contributions should be addressed to the Publisher:

GEOFFREY CUMBERLEGE
OXFORD UNIVERSITY PRESS
AMEN HOUSE, LONDON, E.C. 4

ICS

cs is
ption

utive

ould
ature
page.
er of

with
aper
cing
t the
ould
The
All
ndi-

the

ould
l be
ities

r is

ssed

BUCKLING OF A TRIANGULAR PLATE BY SHEARING FORCES

By J. M. KLITCHIEFF (*Belgrade*)

[Received 13 February 1951]

SUMMARY

The dimensions of built-up plate girders are often taken so as to eliminate buckling of the web under service conditions. The corresponding spacing of transverse stiffeners is usually determined by considering a portion of the web between two stiffeners as a simply supported rectangular plate under the action of shearing forces.

In addition to transverse stiffeners, the web is often reinforced by diagonal stiffening ribs. To estimate their effect it is necessary, however, to know the value of the shearing force for which a simply supported triangular plate first begins to buckle (Fig.).

In what follows the spacing of transverse stiffeners is assumed equal to the depth of the web, so that the problem is that of the buckling of a right-angled isosceles triangle.

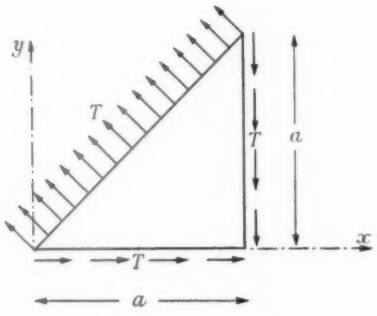

Notation

w deflexion of plate at point (x, y).
D its flexural rigidity.
T shearing force per unit length.
m, i even integers.
n, j odd integers.
C_{mn}, C_{ij} constants.

$$\lambda = \frac{\pi^4}{32}\frac{D}{a^2 T}.$$

[Quart. Journ. Mech. and Applied Math., Vol. IV, Pt. 3 (1951)]
5092.15

Details of solution

LET us consider a right-angled isosceles triangular plate, simply supported along its edges, and acted on by shearing forces T, uniformly distributed along the edges (Fig.) $x = a$ and $y = 0$, and by normal forces of the same magnitude T, uniformly distributed along the edge $y = x$. The differential equation of the deflected middle surface then becomes

$$D\left(\frac{\partial^2}{\partial x^2}+\frac{\partial^2}{\partial y^2}\right)\left(\frac{\partial^2 w}{\partial x^2}+\frac{\partial^2 w}{\partial y^2}\right)+2T\,\frac{\partial^2 w}{\partial x \partial y}=0.$$

The boundary conditions for a simply supported plate can be expressed in the form

$$\text{along the edge } x = a\text{: } w = 0,\quad \frac{\partial^2 w}{\partial x^2}=0;$$

$$\text{along the edge } y = 0\text{: } w = 0,\quad \frac{\partial^2 w}{\partial y^2}=0;$$

$$\text{along the edge } y = x\text{: } w = 0,\quad \frac{\partial^2 w}{\partial x^2}+\frac{\partial^2 w}{\partial y^2}=0.$$

These conditions will be satisfied if the solution of the differential equation is taken in the form

$$w=\sum_{m=2,4\ldots}^{\infty}\ \sum_{n=1,3\ldots}^{\infty} C_m\left(\sin\frac{m\pi x}{a}\sin\frac{n\pi y}{a}-\sin\frac{n\pi x}{a}\sin\frac{m\pi y}{a}\right).$$

Substituting in the differential equation

$$\sum_{m=2,4\ldots}^{\infty}\ \sum_{n=1,3\ldots}^{\infty} C_{mn}\left\{D\left(\frac{\pi}{a}\right)^2(m^2+n^2)^2\left(\sin\frac{m\pi x}{a}\sin\frac{n\pi y}{a}-\sin\frac{n\pi x}{a}\sin\frac{m\pi y}{a}\right)+\right.$$

$$\left.+2Tmn\left(\cos\frac{m\pi x}{a}\cos\frac{n\pi y}{a}-\cos\frac{n\pi x}{a}\cos\frac{m\pi y}{a}\right)\right\}=0.$$

Multiplying this equation by

$$\sin\frac{j\pi x}{a}\sin\frac{i\pi y}{a}\,dxdy\quad (i = 2, 4,\ldots,\ j = 1, 3\ldots),$$

integrating with respect to x and y, from 0 to a, and observing that

$$\int_0^a \cos\frac{m\pi x}{a}\sin\frac{j\pi x}{a}\,dx=\frac{2a}{\pi}\,\frac{m}{m^2-j^2},\qquad \int_0^a \cos\frac{n\pi x}{a}\sin\frac{j\pi x}{a}\,dx=0,$$

there results

$$\lambda(m^2+n^2)^2C_{mn}+mn\sum_{i=2,4\ldots}^{\infty}\ \sum_{j=1,3\ldots}^{\infty} C_{ij}\,\frac{ij}{(m^2-j^2)(n^2-i^2)}=0.$$

The condition that these equations should have a non-zero solution gives the infinite determinantal equation

$$\begin{vmatrix} 5^2\lambda+\frac{4}{9} & -\frac{4}{5} & -\frac{8}{25} & -\frac{8}{63} & -\frac{4}{49} & . & . \\ -\frac{4}{5} & 13^2\lambda+\frac{36}{25} & -\frac{72}{35} & -\frac{40}{49} & -\frac{20}{63} & . & . \\ -\frac{8}{25} & -\frac{72}{35} & 25^2\lambda+\frac{144}{49} & -\frac{80}{21} & -\frac{40}{27} & . & . \\ -\frac{8}{63} & -\frac{40}{49} & -\frac{80}{21} & 41^2\lambda+\frac{400}{81} & -\frac{200}{33} & . & . \\ -\frac{4}{49} & -\frac{20}{63} & -\frac{40}{27} & -\frac{200}{33} & 61^2\lambda+\frac{900}{121} & . & . \\ . & . & . & . & . & . & . \\ . & . & . & . & . & . & . \end{vmatrix} = 0.$$

If the first row and the first column of this determinant is divided by 5, the second row and the second column by 13, and so on, the equation becomes a secular equation of symmetrical type, having only real roots, the largest of which determines the critical value of the shearing force T_{cr}.

The calculation can be effected by a process of successive approximation. The determinantal equation formed by ignoring all elements except those common to the first three rows and columns gives $\lambda = 0{\cdot}0047$; including elements common to the first four, five, and seven rows and columns gives $\lambda = 0{\cdot}0061$, $\lambda = 0{\cdot}00666$, and $\lambda = 0{\cdot}00666$ respectively.†

Conclusion

The magnitude of the critical shearing force corresponding to $\lambda \approx 0{\cdot}0067$ is

$$T_{cr} = 46\pi^2 \frac{D}{a^2},$$

since the value of the critical shearing force applied to a square plate is (**1**)

$$T_{cr} = 9{\cdot}4\pi^2 \frac{D}{a^2},$$

it follows that the effect on the value of the critical shearing force of reinforcing the web by additional diagonal stiffeners is considerable.

† The roots were calculated for the writer by Mrs. I. Yassensky.

REFERENCE

1. S. Timoshenko, *Elastic Stability* (New York, 1933), p. 360.

ON THE TWO-DIMENSIONAL PROBLEM OF A SEMI-INFINITE ELASTIC BODY COMPRESSED BY AN ELASTIC PLANE

By H. ŌKUBO

(*Institute of High Speed Mechanics, Tōhoku University, Sendai, Japan*)

[Received 21 March 1950]

SUMMARY

An approximate solution of the two-dimensional problem of an elastic foundation compressed by a pillar is given, account being taken of the elasticity of the pillar. It is found that the contact pressure between the two elastic planes in contact has a tendency to concentrate at both edges of the prism.

1. The object of this paper is to find an approximate solution of the two-dimensional problem of an elastic foundation compressed by a pillar with a rectangular cross-section. The solution of the problem may be of interest in the problem of a shaft, press-fitted with a collar or a wheel,† since if the diameter of the shaft is very large compared with the dimensions of the collar or the wheel, we can consider the problem two-dimensionally as one of a semi-infinite body compressed by an elastic plane.

The problem of a semi-infinite body compressed by a rigid plane has been considered by several writers (**1**, **2**). But the case when it is compressed by an elastic plane has not yet been treated. We shall derive an approximate solution of the problem and examine the pressure distribution on the contact surface of two bodies.

2. Let us consider a semi-infinite body compressed by a rectangular prism, with the width 2 and the height $2h$, which is compressed by a vertical force P, distributed uniformly over the upper surface of the prism as shown in Fig. 1. The origin of the coordinates is chosen at the centre of the contact surface of the prism and the directions of the axes of x and y are taken parallel and perpendicular to the boundary of the semi-infinite body, respectively. To simplify the calculation we shall not consider the condition to be satisfied on the vertical surfaces of the prism, since it can be assumed that the traction σ_x on the vertical surfaces will not appreciably

† The solution for the problem of a shaft press-fitted with a collar will be given in a later paper.

affect the distribution of σ_y on the contact surface.† Then the boundary conditions for the prism are

$$\left.\begin{aligned} &\left.\begin{aligned} \sigma_y &= -\frac{P}{2} + \sum_{n=1}^{\infty} P_n \cos n\pi x \\ \tau_{xy} &= 0 \end{aligned}\right\} \text{ at } y = 0 \\ &\left.\begin{aligned} \sigma_y &= -\frac{P}{2} \\ \tau_{xy} &= 0 \end{aligned}\right\} \text{ at } y = -2h \end{aligned}\right\}, \tag{1}$$

where the P_n are unknown constants. In (1) we assume that τ_{xy} vanishes over the contact surface, but the assumption is far from the actual condition, since the friction between the two bodies in contact gives the

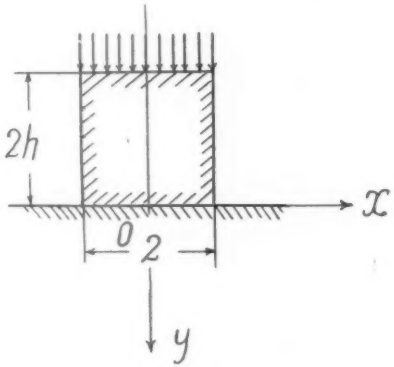

FIG. 1.

shearing stress. But in so far as the distribution of pressure on the contact surface is concerned, the influence of the friction between the bodies can be neglected, as the writer has pointed out previously (**3**).

We shall assume h to be large so that $\sinh n\pi h \doteqdot \cosh n\pi h$ and

$$\sinh n\pi h \cosh n\pi h \pm n\pi h \doteqdot \cosh^2 n\pi h;$$

then the stresses which satisfy the boundary condition (1) are approximately given by

$$\left.\begin{aligned} \sigma_x &= \sum_{n=1}^{\infty} P_n e^{n\pi y}(1 + n\pi y)\cos n\pi x \\ \sigma_y &= -\frac{P}{2} + \sum_{n=1}^{\infty} P_n e^{n\pi y}(1 - n\pi y)\cos n\pi x \\ \tau_{xy} &= \sum_{n=1}^{\infty} n\pi y e^{n\pi y} \sin n\pi x \end{aligned}\right\}. \tag{2}$$

† See the Appendix.

The displacements in question are obtained from the following relations:

$$\frac{\partial u}{\partial x}=\frac{1}{E_1}(\sigma_x-\nu_1\sigma_y),\qquad \frac{\partial v}{\partial y}=\frac{1}{E_1}(\sigma_y-\nu_1\sigma_x),\qquad \frac{\partial v}{\partial x}+\frac{\partial u}{\partial y}=\frac{2(1+\nu_1)}{E_1}\tau_{xy}, \tag{3}$$

where E_1 and ν_1 denote Young's modulus and Poisson's ratio of the prism, respectively.

The vertical displacement on the contact surface can then be easily shown to be

$$v=\frac{2}{\pi E_1}\sum_{n=1}^{\infty}\frac{P_n}{n}\cos n\pi x,\quad \text{at } y=0, \tag{4}$$

which is independent of the distribution of load on the upper surface of the prism.

At the contact surface ($1\geqslant x\geqslant -1$), we may expand σ_y and v as power series in x,

$$\sigma_y=\sum_{n=0}^{\infty}a_n x^{2n},\qquad v=\sum_{n=0}^{\infty}b_n x^{2n}, \tag{5}$$

and x^{2n} can be expanded in a Fourier series of the form

$$x^{2n}=\sum_{m=0}^{\infty}c_{nm}\cos m\pi x,$$

in the interval $1\geqslant x\geqslant -1$, where

$$c_{n0}=\frac{1}{2n+1},\qquad c_{0m}=0,\qquad c_{1m}=\frac{4(-1)^m}{m^2\pi^2},$$

$$c_{nm}=\frac{4n(-1)^m}{m^2\pi^2}-\frac{2n(2n-1)}{m^2\pi^2}c_{n-1,m}\qquad (m=1,2,3,\ldots).$$

Then (5) can be transformed into

$$\left.\begin{aligned}\sigma_y&=\sum_{m=0}^{\infty}\cos m\pi x\sum_{n=0}^{\infty}a_n c_{nm}\\ v&=\sum_{m=0}^{\infty}\cos m\pi x\sum_{n=0}^{\infty}b_n c_{nm}\end{aligned}\right\}. \tag{6}$$

Inserting these relations into (1) and (4), and equating the coefficients of P_n, we have the following relations between a_n and b_n:

$$\left.\begin{aligned}\sum_{n=0}^{\infty}a_n c_{n0}+\frac{P}{2}&=0\\ \sum_{n=0}^{\infty}b_n c_{n0}&=0\\ \sum_{n=0}^{\infty}\left(a_n-\frac{m\pi E_1}{2}b_n\right)c_{nm}&=0\qquad (m=1,2,3,\ldots)\end{aligned}\right\}. \tag{7}$$

The boundary conditions for the semi-infinite body are

$$\left.\begin{aligned} &\left.\begin{aligned} &\tau_{xy} = 0 \\ &\sigma_y = 0 \end{aligned}\right\} \quad (x > 1 \text{ and } x < -1) \\ &\left.\begin{aligned} &\sigma_y = \sum_{n=0}^{\infty} a_n x^{2n} \\ &v = C + \sum_{n=0}^{\infty} b_n x^{2n} \end{aligned}\right\} \quad (1 \geqslant x \geqslant -1) \end{aligned}\right\}, \quad \text{at } y = 0. \tag{8}$$

If we assume that a point on the y-axis at a distance l from the origin does not move vertically, the vertical displacement on the contact surface is expressed as (4)

$$v = -\frac{2}{\pi E_2}\int_0^{1-x} \sigma_y(r+x)\log\frac{l}{r}\,dr + \frac{1+\nu_2}{\pi E_2}\int_0^{1-x} \sigma_y(r+x)\,dr - \\ -\frac{2}{\pi E_2}\int_0^{1+x} \sigma_y(r-x)\log\frac{l}{r}\,dr + \frac{1+\nu_2}{\pi E_2}\int_0^{1+x} \sigma_y(r-x)\,dr, \tag{9}$$

where E_2 and ν_2 denote Young's modulus and Poisson's ratio of the semi-infinite body, respectively.

Equating the values of v in (8) and (9), we have

$$C + \sum_{n=0}^{\infty} b_n x^{2n} = \frac{2}{\pi E_2}\sum_{n=0}^{\infty} a_n \int_0^{1-x} (r+x)^{2n}\log r\,dr + \\ + \frac{2}{\pi E_2}\sum_{n=0}^{\infty} a_n \int_0^{1+x} (r-x)^{2n}\log r\,dr - \frac{4\log l - 2(1+\nu_2)}{\pi E_2}\sum_{n=0}^{\infty}\frac{a_n}{2n+1}. \tag{10}$$

Putting $x = 0$ in (10), we have

$$C + b_0 = -\frac{4}{\pi E_2}\sum_{n=0}^{\infty}\frac{a_n}{(2n+1)^2} - \frac{4\log l - 2(1+\nu_2)}{\pi E_2}\sum_{n=0}^{\infty}\frac{a_n}{2n+1}, \tag{11}$$

from which C is obtained.

Differentiating both sides of (10) twice with respect to x, and putting $x = 0$, we have

$$\left.\begin{aligned} b_1 &= -\frac{2}{\pi E_2}\sum_{n=0}^{\infty}\frac{a_n}{2n-1} \\ b_2 &= -\frac{2}{2\pi E_2}\sum_{n=0}^{\infty}\frac{a_n}{2n-3} \\ b_3 &= -\frac{2}{3\pi E_2}\sum_{n=0}^{\infty}\frac{a_n}{2n-5} \\ &\cdots\cdots\cdots \end{aligned}\right\}, \tag{12}$$

Inserting the above expressions for the b_n's into (7), we find the following simultaneous equations for the a_n's.

$$\sum_{n=1}^{\infty}\left(\frac{a_n}{km}+\frac{1}{n}\sum_{j=0}^{\infty}\frac{a_j}{2j-2n+1}\right)c_{nm}=0 \qquad (m=1,\,2,\,3,\ldots), \tag{13}$$

where $k=E_1/E_2$.

From (13) and the first of equations (7) we can determine the a_n's, and P_m is obtained from the relation

$$P_m=\sum_{n=0}^{\infty}a_n c_{nm} \qquad (m=1,\,2,\,3,\ldots).$$

Then the stresses in the semi-infinite body are obtained from the following equations (5)

$$\left.\begin{aligned}
\sigma_x &= -P\int_0^{\infty}\frac{(\alpha y-1)e^{-\alpha y}\sin\alpha\cos\alpha x}{\alpha}\,d\alpha- \\
&\qquad -2\sum_{n=1}^{\infty}P_n(-1)^n\int_0^{\infty}\frac{\alpha(\alpha y-1)e^{-\alpha y}\sin\alpha\cos\alpha x}{n^2\pi^2-\alpha^2}\,d\alpha \\
\sigma_y &= -P\int_0^{\infty}\frac{(\alpha y+1)e^{-\alpha y}\sin\alpha\cos\alpha x}{\alpha}\,d\alpha- \\
&\qquad -2\sum_{n=1}^{\infty}P_n(-1)^n\int_0^{\infty}\frac{\alpha(\alpha y+1)e^{-\alpha y}\sin\alpha\cos\alpha x}{n^2\pi^2-\alpha^2}\,d\alpha \\
\tau_{xy} &= P\int_0^{\infty}ye^{-\alpha y}\sin\alpha\sin\alpha x\,d\alpha+ \\
&\qquad +2\sum_{n=1}^{\infty}P_n(-1)^n\int_0^{\infty}\frac{\alpha^2 ye^{-\alpha y}\sin\alpha\sin\alpha x}{n^2\pi^2-\alpha^2}\,d\alpha
\end{aligned}\right\}. \tag{14}$$

In the particular case when E_1 is very small compared with E_2, we can put $k=0$, and from (7) and (13), we have

$$a_1=a_2=\ldots=0, \qquad a_0=-\frac{P}{2}.$$

When E_1 is very large compared with E_2 we also have

$$b_1=b_2=\ldots=0,$$

or

$$\sum_{n=0}^{\infty}\frac{a_n}{2n-1}=0, \qquad \sum_{n=0}^{\infty}\frac{a_n}{2n-3}=0,\ldots.$$

Putting

$$a_n=\frac{1\cdot3\cdot5\ldots(2n-1)}{n!\,2^n}a_0,$$

we can readily show that a_n satisfies the above equations and a_0 is determined from the following relation:

$$-\frac{P}{2} = \sum_{n=0}^{\infty} a_n c_{n0} = \frac{\pi}{2} a_0 \quad \text{or} \quad a_0 = -\frac{P}{\pi}.$$

Then the normal stress on the contact surface is

$$\sigma_y = \sum_{n=0}^{\infty} a_n x^{2n} = -\frac{P}{\pi} \sum_{n=0}^{\infty} \frac{1.3.5...(2n-1)}{n!\,2^n} x^{2n} = -\frac{P}{\pi\sqrt{(1-x^2)}},$$

which agrees with the result obtained by M. Sadowsky.

In the case when the two bodies are of the same material, k is unity, and when one of them is of steel with Young's modulus 21,500 kg./mm.^{2} and the other is of duralumin with Young's modulus 7,220 kg./mm.^{2}, then k is 2·978 or 0·3358. In these cases, values of a_n calculated from (7) and (13) are tabulated in Table 1 (unit P).

TABLE 1

k	0·3358	1	2·978
a_0	−0·462	−0·417	−0·377
a_1	−0·044	−0·152	0·129
a_2	0·432	0·634	−2·154
a_3	−1·260	−2·006	4·409
a_4	−1·613	0·817	−0·634
a_5	3·193	2·062	−8·003
a_6	7·781	−0·798	8·115
a_7	−14·577	−0·916	−1·405
a_8	5·650	−0·482	−1·662

and the values of b_n and C calculated from (7), (11), and (12) are tabulated in Table 2 (unit P/E_2, $\nu_2 = 0$, 3, $l = 1$, 5).

TABLE 2

k	0·3358	1	2·978
b_0	0·094	0·065	0·035
b_1	−0·253	−0·157	−0·133
b_2	−0·101	−0·161	0·418
b_3	0·314	0·442	−1·196
b_4	−0·118	−0·484	0·912
b_5	−0·724	−0·170	0·789
b_6	−0·173	0·336	−1·589
b_7	1·914	0·080	0·696
b_8	−1·381	−0·030	0·124
b_9	0·178	−0·052	−0·106
b_{10}	0·012	−0·019	−0·028
b_{11}	0·000	−0·011	−0·015
b_{12}	−0·002	−0·007	−0·009
C	0·347	0·332	0·313

The pressure distributions and the vertical displacements at the contact surface for several values of k are shown in Figs. 2 and 3. Fig. 2 shows

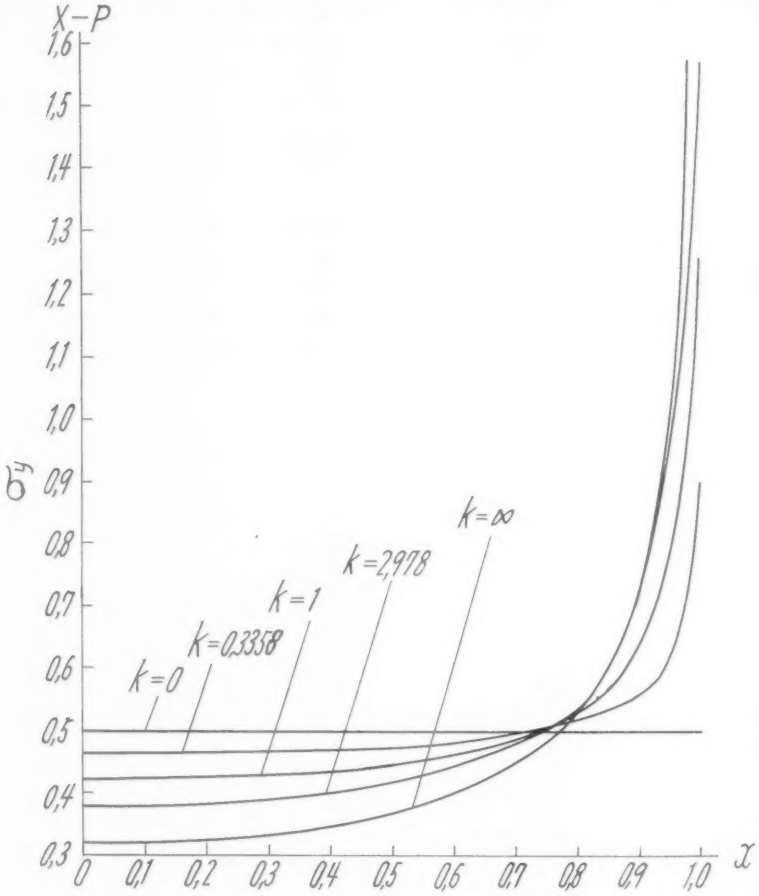

FIG. 2.

that the contact pressure between two elastic planes has a tendency to concentrate at both edges of the prism, and the tendency is more pronounced as the value of k increases. The values of the stress at the edges for several values of k are tabulated in the following table:

TABLE 3

k	0	0·3358	1	2·978	∞
$(\sigma_y)_{max}/P$	−0·50	−0·90	−1·26	−1·58	−∞

By means of the previous calculations, we readily find that the values of $(\sigma_y)_{\max}$, tabulated in Table 3, are valid under the assumption that the contact pressure σ_y can be represented approximately by the sum of the

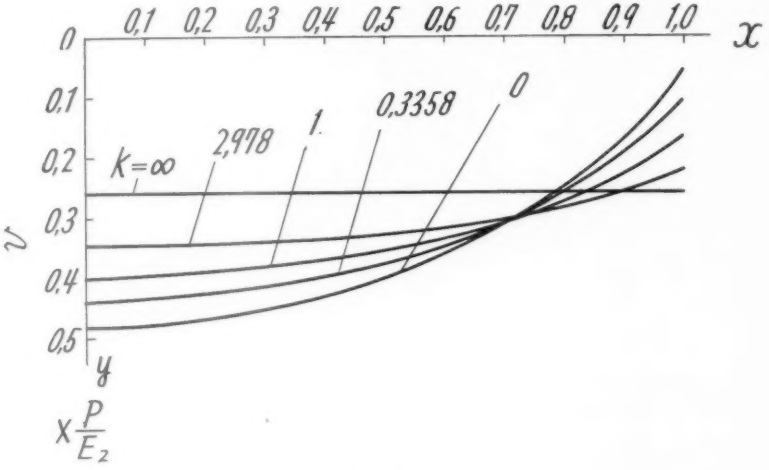

FIG. 3.

first few terms in the series of x^{2n}, in the closed interval $1 \geqslant x \geqslant -1$. Otherwise the contact pressure obtained in this way differs from the substantial one when x approaches the values ± 1. But even in this case, the solution is valid at every point in the semi-infinite body except at the points in the close neighbourhood of the edges of the prism.

APPENDIX

In our previous discussions the influence of the traction σ_x acting on the vertical surfaces of the prism upon the displacement v on the contact surface has been neglected. We shall find a more accurate solution, by using a numerical method, in which the effect of the traction acting on the vertical surfaces is taken into consideration. Now, consider a rectangular prism of the height 2, compressed by distributed loads acting on its upper and lower surfaces, as shown in Fig. 4. If we represent the distribution of the load by

$$-\frac{P}{2}+\sum_{n=1}^{\infty} P_n \cos n\pi x,$$

then the boundary conditions become

$$\left.\begin{aligned} &\left.\begin{aligned} &\sigma_y = -\frac{P}{2}+\sum_{n=1}^{\infty} P_n \cos n\pi x \\ &\tau_{xy} = 0 \end{aligned}\right\} \quad \text{at } y = \pm 1, \\ &\sigma_x = 0, \qquad \tau_{xy} = 0 \qquad\qquad \text{at } x = \pm 1 \end{aligned}\right\}. \tag{15}$$

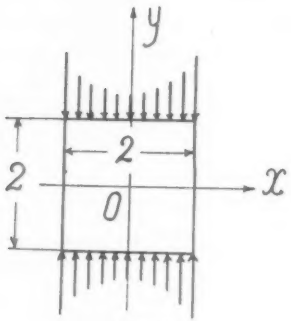
y
2
2
x
0

FIG. 4.

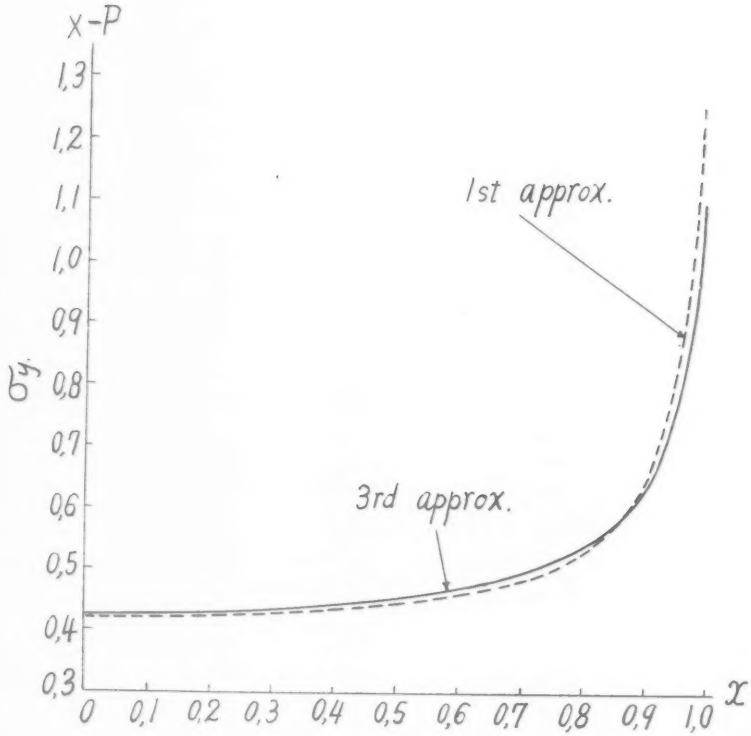
X-P
1,3
1,2
1,1
1,0
0,9
0,8
0,7
0,6
0,5
0,4
0,3
σy
1st approx.
3rd approx.
0
0,1
0,2
0,3
0,4
0,5
0,6
0,7
0,8
0,9
1,0
x

FIG. 5.

The stresses which satisfy the boundary condition (15) are (6)

$$\left.\begin{aligned}\sigma_x &= \sum_{n=1}^{\infty}\{P'_n\xi_n(y)\cos n\pi x + Q_n\eta_n(x)\cos n\pi y\}\\ \sigma_y &= -\frac{P}{2} + \sum_{n=1}^{\infty}\{P'_n\eta_n(y)\cos n\pi x + Q_n\xi_n(x)\cos n\pi y\}\\ &\quad\cdots\cdots\cdots\cdots\end{aligned}\right\}, \tag{16}$$

where

$$\xi_n(y) = \frac{\sinh n\pi\cosh n\pi y + n\pi y\sinh n\pi\sinh n\pi y - n\pi\cosh n\pi\cosh n\pi y}{\sinh n\pi\cosh n\pi + n\pi},$$

$$\eta_n(y) = \frac{\sinh n\pi\cosh n\pi y - n\pi y\sinh n\pi\sinh n\pi y + n\pi\cosh n\pi\cosh n\pi y}{\sinh n\pi\cosh n\pi + n\pi},$$

. . . . . .

and P'_n are the solutions of the simultaneous equations

$$P'_n + \sum_{m=1}^{\infty}P_m(-1)^{m+1}\sum_{j=1}^{\infty}(-1)^j I(j,n)I(m,j) = P_n \qquad (n = 1, 2, 3,\ldots), \tag{17}$$

in which

$$I(n,j) = \frac{4(-1)^j nj^2\sinh^2 n\pi}{\pi(n^2+j^2)^2(\sinh n\pi\cosh n\pi + n\pi)}.$$

Using (16) in place of (2) and the approximations $\sinh n\pi \doteqdot \cosh n\pi$ and $\sinh n\pi\cosh n\pi + n\pi \doteqdot \cosh^2 n\pi$, the more accurate formula for v on the contact surface is (the constant term being omitted)

$$v = \frac{2}{\pi E_1}\sum_{n=1}^{\infty}\frac{P'_n}{n}\cos n\pi x, \tag{18}$$

since the displacements v due to the stress σ_x and the second term in the expression of σ_y vanish on the contact surface.

Accordingly, in our accurate calculation, (13) should be replaced by

$$\sum_{n=1}^{\infty}\left(\frac{a_n\alpha_m}{km} + \frac{1}{n}\sum_{j=0}^{\infty}\frac{a_j}{2j-2n+1}\right)c_{nm} = 0, \tag{19}$$

where $\alpha_m = P'_m/P_m$.

As an example, we shall consider the case for $k = 1$, and take the values of a_n obtained in the previous example and the corresponding values of P_n as the first approximation. Inserting the numerical values of P_n into (17), and solving the simultaneous equations, we can find P'_n and subsequently the corresponding values of α_n for the first approximation, as are shown in Table 4. Inserting these values of α_n into (19), and solving the simultaneous equations, we have the values of a_n for the second approximation. Repeating this operation, we have finally the values of α_n which do not vary by the operation, and subsequently the corresponding values of a_n, which are the ones for the exact solution.

The pressure distribution on the contact surface, calculated in this way, is shown in Fig. 5† and the approximate one, previously obtained, is also shown by a dotted line in the figure. From the figure we see that the influence of the normal traction acting on the vertical surfaces of the prism, upon the pressure distribution on the contact surface, is not perceptible except at the edges of the prism. The accurate

† The pressure distribution in the second approximation almost agrees with that for the third approximation.

TABLE 4

1st approximation $a_0 = -0{\cdot}417$, $(\sigma_y)_{\max} = -1{\cdot}26P$

n	1	2	3	4	5	6	7	8
a_n	−0·152	0·634	−2·006	0·817	2·062	−0·798	−0·916	−0·482
α_n	1·25	1·41	1·49	1·55	1·57	1·58	1·60	1·64

2nd approximation $a_0 = -0{\cdot}423$, $(\sigma_y)_{\max} = -1{\cdot}11P$

n	1	2	3	4	5	6	7	8
a_n	−0·128	−0·052	0·856	−2·871	2·360	−0·360	1·866	−2·353
α_n	1·24	1·43	1·52	1·60	1·64	1·65	1·69	1·69

3rd approximation $a_0 = -0{\cdot}421$, $(\sigma_y)_{\max} = -1{\cdot}10P$

n	1	2	3	4	5	6	7	8
a_n	−0·115	−0·451	2·567	−4·975	2·051	0·080	4·330	−4·168
α_n	1·24	1·43	1·52	1·60	1·67	1·69	1·70	1·70

value of $(\sigma_y)_{\max}$ is $-1{\cdot}10P$, while the approximate value previously obtained is $-1{\cdot}26P$, which is about 15 per cent. larger compared with that obtained here.

From these results we can conclude that the approximate solution previously obtained, where the effect of σ_x acting on the vertical surfaces of the prism is neglected, can be used with sufficient accuracy for the calculations of technical problems.

In conclusion the writer wishes to express his thanks to Miss E. Itagaki, his assistant, for her earnest help in numerical calculations.

REFERENCES

1. M. SADOWSKY, *Z. angew. Math. Mech.* **8** (1928), 107.
2. H. ŌKUBO, ibid. **20** (1940), 271.
3. —— ibid., p. 276.
4. S. TIMOSHENKO, *Theory of Elasticity* (McGraw-Hill, **1934**), p. 92.
5. H. ŌKUBO, *Science Reports of the Tōhoku Imperial University*, Ser. 1, **28** (1940), 291.
6. —— *J. App. Phys.* **11** (1940), 720.

THE MOTION OF AN ELASTICO-VISCOUS LIQUID CONTAINED BETWEEN COAXIAL CYLINDERS. I

By J. G. OLDROYD

(*Courtaulds Limited, Research Laboratory, Maidenhead, Berks.*)

[Received 20 December 1950]

SUMMARY

The theory of periodic and steady states of motion of a liquid in a narrow annular gap between long vertical coaxial cylinders is considered, when the viscous and elastic properties of the material at small rates of shear are measured by three constants, a viscosity coefficient and two relaxation times. When the outer cylinder undergoes forced harmonic angular oscillations about its axis, and the inner cylinder is constrained by a torsion wire, the amplitude of uniform oscillation attained by the inner cylinder is calculated. The ratio of the angular amplitudes of the two cylinders has been plotted as a function of the frequency, for different values of the constants of the material and of an available apparatus. From observations of the frequency, amplitude-ratio curves for some actual liquids which are approximately of the type considered, values can be deduced for their elastic and viscous constants. In steady flow between rotating cylinders, elastico-viscous liquids behave like purely viscous liquids whose viscosity is a function of the rate of shear. Additional information about the rheological equations of state of actual liquids can be deduced from steady rotational experiments.

1. Introduction

It is well known that elastic properties of liquids in shear can be detected and measured by observing suitable types of oscillatory motion (see, for example, **1**). For the purpose of investigating the rheological properties of dilute polymer solutions (**2**), an elastoviscometer has been built in this laboratory which provides a means of maintaining a liquid in a state of uniform oscillation in a narrow annular gap between vertical coaxial cylinders (**3**). The outer cylinder can be either rotated steadily at any speed between 0·3 and 3,000 r.p.m., or maintained in a state of harmonic angular oscillation about its axis at any frequency between 0·25 and 25 c/s; either the constant deflexion or the amplitude of uniform oscillation attained by the inner cylinder, when constrained by a torsion wire of known restoring constant, can be observed. It is the purpose of the present paper to outline the mathematical theory underlying the quantitative interpretation of observations made on different liquids. Only two-dimensional motion need be considered, since it is known that end-effects in steady

rotational experiments can be eliminated by repeating the experiments with the apparatus filled to different heights; in oscillatory experiments, in which the annular gap is always completely filled, the observations on Newtonian liquids of known viscosity have confirmed that end-effects are negligible.

It is hoped to establish the rheological properties of certain polymer solutions in two or more stages, the first stage being the investigation of the behaviour in a simple shearing motion at small rates of strain. It has been found that this behaviour can be approximately described by a linear equation

$$\tau+\lambda_1\dot{\tau} = \eta_0(\gamma+\lambda_2\dot{\gamma}) \tag{1}$$

relating the velocity gradient γ, the associated shear stress τ, and their rates of change $\dot{\gamma}$ and $\dot{\tau}$. The properties at sufficiently small rates of strain are measured by three constants, a coefficient of viscosity η_0, and two relaxation times λ_1 and λ_2, with the direct physical significance that if the motion is suddenly stopped the shear stress decays as $\exp(-t/\lambda_1)$, and if the stress is removed the rate of strain decays as $\exp(-t/\lambda_2)$. The viscosity η_0 is that obtained from experiments in the elastoviscometer involving slow steady rotation of the outer cylinder. The values of λ_1 and λ_2 can be deduced from observations of the amplitude of uniform oscillation of the inner cylinder, plotted as a function of frequency in the range 0·25–25 c/s, when the outer cylinder undergoes forced harmonic oscillations of known small amplitude. The estimation of λ_1 and λ_2 is made by comparing an observed frequency-amplitude curve for a given material with a set of theoretical curves based on the equation (1) with different values of λ_1 and λ_2. The justification for associating the equation (1) with an actual material depends on the results of experiments with different inner cylinders and torsion wires being consistent with the same values of η_0, λ_1, and λ_2.

An equation of the type (1) was first proposed as a possible stress, rate-of-strain relation by Jeffreys (**4**). It was shown to be associated with a suspension of elastic particles in a Newtonian liquid by Fröhlich and Sack (**5**), and some of the consequences of such an equation have been discussed by Burgers (**6**). With (1) must be associated the auxiliary condition that $\lambda_1\tau-\eta_0\lambda_2\gamma$ is continuous at a discontinuous change in stress (cf. **5**). It follows that, at a sudden application of a shear stress to the material at rest, the initial rate of shear is λ_1/λ_2 times the corresponding rate in a steady state under the same conditions. This factor can only represent an *increased* response to suddenly applied stress due to elasticity, so that

$$\lambda_1 > \lambda_2 \tag{2}$$

in all cases of physical interest.

A single equation (1), associated with simple shearing of a material at sufficiently small rates of strain, together with the usual assumption of negligible bulk compressibility, does not suffice to specify the rheological properties of the material completely. In order to describe the behaviour in general motion, a set of equations of state with the right invariance properties is required (7), and there is not a unique way of recasting (1) in an invariant form. On the other hand, in order to present a mathematical treatment of the type of motion involved in the determination of λ_1 and λ_2, which is not strictly a simple shearing motion, it is desirable to specify precisely the idealized material to be studied and therefore to select an invariant generalization of (1) on which to base the theory.

When it has been established that an equation (1), with certain values of the constants, can be associated with a particular liquid, one must then consider what further experiments are required in order to distinguish between the various possible sets of equations of state which reduce to (1) under simplifying conditions. In the present paper it will be shown how different generalizations of (1) can give rise to different types of non-Newtonian viscous behaviour in steady-state experiments.† Hence the investigation of rheological properties might in principle be carried to a second stage by making quantitative observations on the liquid in the elastoviscometer when the outer cylinder is rotated steadily.

2. Idealized types of elastico-viscous liquid

We consider (almost) incompressible elastico-viscous liquids in which the stresses p_{ik} at any point may be considered as the superposition of two independent stress systems, one represented by a tensor p'_{ik} related to the distortion, and the other an isotropic tensor $-p''g_{ik}$ related to the dilatation:

$$p_{ik} = p'_{ik} - p''g_{ik}. \tag{3}$$

It is of interest here to examine those in which the relation between p'_{ik} and the rate-of-strain tensor $e^{(1)}_{ik}$ reduces to

$$\left(1+\lambda_1 \frac{\partial}{\partial t}\right) p'_{ik} = 2\eta_0 \left(1+\lambda_2 \frac{\partial}{\partial t}\right) e^{(1)}_{ik} \tag{4}$$

in a sufficiently slow simple shearing motion, and in which the relationship between the scalar p'' and the dilatation reduces effectively to

$$e^{(1)i}_{i} = 0 \quad (\text{all } p''), \tag{5}$$

which represents ideal incompressibility. The notation is that of the earlier

† The possibility of *qualitative* differences in behaviour has already been demonstrated (7) by establishing that some generalizations would show the 'Weissenberg effect' while others would not. We are concerned here with differences which can be *measured* by recording the couple on the inner cylinder at different speeds of the outer.

paper (7), in which liquids of this type were used for the purposes of illustration: g_{ik} denotes the metric tensor of a general curvilinear coordinate system x^i fixed in space, covariant tensor suffixes are written below, contravariant suffixes above, and the usual summation convention is assumed.

In order to convert equations (3)–(5) into a possible set of equations of state of general validity, it is only necessary to recast (4) in an invariant form which reduces approximately to (4)—and therefore implies (1)—in a sufficiently slow simple shearing motion. This can be done in an infinite number of ways (cf. 7). When the incompressibility condition (5) is taken into account explicitly, the distinct invariant generalizations which are linear in the stresses, and quadratic in the stresses and the space derivatives of velocity taken together, are

$$\left(1+\lambda_1 \frac{\mathfrak{D}}{\mathfrak{D}t}\right) p'_{ik} = 2\eta_0 \left(1+\lambda_2 \frac{\mathfrak{D}}{\mathfrak{D}t}\right) e^{(1)}_{ik}, \tag{6}$$†

and equations obtained from this by adding an arbitrary linear combination of $e^{(1)}_{im} e^{(1)m}_{k}$, $e^{(1)}_{im} p'^{m}_{k}$, and $e^{(1)}_{km} p'^{m}_{i}$ to one side. Of these only equations in which each side is a symmetric tensor are relevant, since the required number of independent equations relating stress and rate-of-strain components is six. Hence the simplest‡ generalized forms of (4) are

$$\left(1+\lambda_1 \frac{\mathfrak{D}}{\mathfrak{D}t}\right) p'_{ik} - 2\kappa_1 (e^{(1)}_{im} p'^{m}_{k} + e^{(1)}_{km} p'^{m}_{i}) = 2\eta_0 \left(1+\lambda_2 \frac{\mathfrak{D}}{\mathfrak{D}t}\right) e^{(1)}_{ik} - 8\eta_0 \kappa_2 e^{(1)}_{im} e^{(1)m}_{k}, \tag{7}$$

where κ_1, κ_2 are arbitrary scalar constants. More complicated equations, involving contracted triple and higher products of the stress and rate-of-strain tensors (and, in general, arbitrary functions of scalar products), give other distinct generalizations. Such equations might well have to be invoked in order to explain the behaviour of actual materials, but the set of equations of state (3), (5), (7) suffices to illustrate how different types of behaviour can arise in steady-state experiments from different generalizations of (1).

The particular values $\kappa_1 = \lambda_1$, $\kappa_2 = \lambda_2$ define the idealized material B of the previous paper (7), which was shown to exhibit the 'Weissenberg effect' in steady rotation; they permit (7) to be written, after raising suffixes, as

$$\left(1+\lambda_1 \frac{\mathfrak{D}}{\mathfrak{D}t}\right) p'^{ik} = 2\eta_0 \left(1+\lambda_2 \frac{\mathfrak{D}}{\mathfrak{D}t}\right) e^{(1)ik}. \tag{8}$$

The particular values $\kappa_1 = 0$, $\kappa_2 = 0$ define the material A which would

† $\mathfrak{D}/\mathfrak{D}t$ denotes convected differentiation of a tensor quantity in relation to the material in motion, as defined in (7).

‡ There is no invariant generalization which is linear in the space derivatives of velocity.

not show this effect. These two materials are distinguished from the other possible types because, in either A or B, a simple shearing motion is possible in which (1) is satisfied *exactly*, without restriction to small rates of shear. More precisely, a velocity distribution given by $v_i = [0, v(x^1, t), 0]$, referred to orthogonal Cartesian coordinates x^i, can be maintained by non-vanishing stresses $p'_{12}(x^1, t)$, $p'_{11}(x^1, t)$ alone in A—or $p'_{12}(x^1, t)$, $p'_{22}(x^1, t)$ in B—where

$$p'_{12} + \lambda_1 \frac{\partial p'_{12}}{\partial t} = \eta_0 \left(\frac{\partial v}{\partial x^1} + \lambda_2 \frac{\partial^2 v}{\partial t \partial x^1} \right)$$

without approximation. It is seen that either of these types includes, as a limiting special case when λ_1 and λ_2 tend to equality, the incompressible Newtonian liquid in which

$$p'_{ik} = 2\eta_0 e^{(1)}_{ik} \quad \text{(and, equally, } p'^{ik} = 2\eta_0 e^{(1)ik}\text{)}.$$

3. Flow between coaxial cylinders

A liquid defined by the equations of state (3), (5), (7) is now supposed to be contained between long vertical coaxial cylinders. All tensor quantities associated with the liquid are most conveniently represented by their physical components in cylindrical polar coordinate directions r, ϕ, z; z is measured vertically upwards and $r = r_1$, $r = r_2$ ($> r_1$) represent the rigid boundaries. Two-dimensional axially symmetric flow is assumed, with velocity components $0, r\omega(r, t), 0$. The relations between ω and the physical components $\widehat{r\phi}'$, $\widehat{rr}'$, $\widehat{\phi\phi}'$, $\widehat{zz}'$ of p'_{ik}, all functions of r and t only, are obtained in the same way as for steady flow of particular types of liquid (cf. **7**, pp. 539–40), except that partial time derivatives cannot here be omitted. These relations are, from (7),

$$\widehat{r\phi}' + \lambda_1 \frac{\partial \widehat{r\phi}'}{\partial t} + r \frac{\partial \omega}{\partial r} [(\lambda_1 - \kappa_1) \widehat{\phi\phi}' - \kappa_1 \widehat{rr}'] = \eta_0 r \left(\frac{\partial \omega}{\partial r} + \lambda_2 \frac{\partial^2 \omega}{\partial t \partial r} \right), \tag{9}$$

$$\widehat{rr}' + \lambda_1 \frac{\partial \widehat{rr}'}{\partial t} + 2(\lambda_1 - \kappa_1) r \frac{\partial \omega}{\partial r} \widehat{r\phi}' = 2\eta_0 (\lambda_2 - \kappa_2) \left(r \frac{\partial \omega}{\partial r} \right)^2, \tag{10}$$

$$\widehat{\phi\phi}' + \lambda_1 \frac{\partial \widehat{\phi\phi}'}{\partial t} - 2\kappa_1 r \frac{\partial \omega}{\partial r} \widehat{r\phi}' = -2\eta_0 \kappa_2 \left(r \frac{\partial \omega}{\partial r} \right)^2, \tag{11}$$

$$\widehat{zz}' + \lambda_1 \partial \widehat{zz}' / \partial t = 0. \tag{12}$$

The equations of motion, expressed in terms of the same quantities, take the form

$$\frac{\partial \widehat{rr}'}{\partial r} + \frac{\widehat{rr}' - \widehat{\phi\phi}'}{r} = \frac{\partial p''}{\partial r} - \rho r \omega^2, \quad \frac{\partial \widehat{r\phi}'}{\partial r} + \frac{2\widehat{r\phi}'}{r} = \rho r \frac{\partial \omega}{\partial t}, \quad \frac{\partial \widehat{zz}'}{\partial z} = \frac{\partial p''}{\partial z} + \rho g, \tag{13}$$

where ρ is the density of the liquid and g the acceleration due to gravity.

The observations which can be made in the elastoviscometer can give, at the most, ω and $\widehat{r\phi}'$ at the boundaries, so that the equations of immediate interest are those not involving $\widehat{rr}'$, $\widehat{\phi\phi}'$, $\widehat{zz}'$, or p''. In the steady state, the relevant equations are the second of equations (13) and the following equation, obtained by eliminating $\widehat{rr}'$ and $\widehat{\phi\phi}'$ from (9)–(11) after putting $\partial/\partial t \equiv 0$:

$$\widehat{r\phi}' = \eta_0 \frac{1+2(\lambda_1\kappa_2+\kappa_1\lambda_2-2\kappa_1\kappa_2)(r\,\partial\omega/\partial r)^2}{1+4\kappa_1(\lambda_1-\kappa_1)(r\,\partial\omega/\partial r)^2} r\frac{\partial\omega}{\partial r}. \tag{14}$$

Hence the observed behaviour, so far as is revealed by measurements of the torque on the inner cylinder at various speeds of the outer, will be precisely that of a non-Newtonian viscous liquid whose viscosity η is a simple function of the velocity gradient γ defined by

$$\eta = \eta_0[1+2(\lambda_1\kappa_2+\kappa_1\lambda_2-2\kappa_1\kappa_2)\gamma^2]/[1+4\kappa_1(\lambda_1-\kappa_1)\gamma^2]. \tag{15}$$

The observed viscosity is the constant η_0 only in special cases, for example in a material of type A or B. For general values of κ_1 and κ_2, η_0 is the limiting viscosity at low rates of shear. When the annular gap between the cylinders is sufficiently small (or, when η is a constant, without this restriction) the usual formulae for a Couette viscometer,

$$\gamma = \frac{2r_1r_2\Omega}{r_2^2-r_1^2}, \qquad \eta = \frac{(r_2^2-r_1^2)G}{4\pi r_1^2 r_2^2 h\Omega}, \tag{16}$$

define the γ, η relationship parametrically. Here, Ω denotes the angular velocity of the outer cylinder, G the couple on the inner, and h is the height of liquid between the cylinders plus an end-correction; this correction is readily eliminated by measuring the couples at different heights of filling. In this way different values of κ_1 and κ_2 could be distinguished experimentally if λ_1, λ_2, and η_0 were known.

In the case of periodic motion of frequency n, it is observed that there is not an exact solution of equations (9)–(13) in which ω, $\widehat{r\phi}'$, $\widehat{rr}'$, $\widehat{\phi\phi}'$ all vary sinusoidally, because the equations are not linear in these quantities. For small rates of strain, however, there will be a solution in which

$$\widehat{r\phi}' = O(\eta_0 r\,\partial\omega/\partial r), \quad rr' = O[\eta_0\lambda_1(r\,\partial\omega/\partial r)^2], \quad \widehat{\phi\phi}' = O[\eta_0\lambda_1(r\,\partial\omega/\partial r)^2],$$

and

$$\widehat{r\phi}' + \lambda_1\frac{\partial\widehat{r\phi}'}{\partial t} = \eta_0 r\left(\frac{\partial\omega}{\partial r}+\lambda_2\frac{\partial^2\omega}{\partial t\partial r}\right) \tag{17}$$

with an error of the order of $\eta_0\lambda_1^2(r\,\partial\omega/\partial r)^3$. Equation (17) is exact in the case of a material A or B, since in A $\widehat{\phi\phi}'$ is seen to vanish, and in B $\widehat{rr}'$ vanishes. The following theory is an exact treatment for either of these prototypes, and will hold approximately when κ_1 and κ_2 have other values.

Equations (13) and (17) permit a solution of the form

$$\widehat{r\phi'} = \mathrm{re} f(r)e^{2\pi int}, \qquad \omega = \mathrm{re}\, F(r)e^{2\pi int}, \tag{18}$$

where $f(r)$ and $F(r)$ incorporate appropriate phase factors. The equations relating $\widehat{r\phi'}$ with ω reduce to

$$d(r^2 f)/dr = 2\pi in\rho r^3 F \tag{19}$$

and

$$(1+2\pi in\lambda_1)f = \eta_0(1+2\pi in\lambda_2)r\, dF/dr. \tag{20}$$

Eliminating F, we have

$$\left(r^2\frac{d^2}{dr^2}+r\frac{d}{dr}+\alpha^2 r^2-4\right)f = 0, \tag{21}$$

where $\alpha(n)$ is defined by

$$\alpha^2 = -\frac{2\pi in\rho(1+2\pi in\lambda_1)}{\eta_0(1+2\pi in\lambda_2)} \qquad (-\tfrac{1}{2}\pi < \arg\alpha < \tfrac{1}{2}\pi). \tag{22}$$

The solution of (19) and (20) can therefore be expressed, in terms of Bessel functions of complex argument, as

$$f = aJ_2(\alpha r)+bY_2(\alpha r); \qquad F = \alpha[aJ_1(\alpha r)+bY_1(\alpha r)]/(2\pi in\rho r), \tag{23}$$

where a and b are complex constants to be determined by the boundary conditions.

If θ_1, θ_2 are the amplitudes of angular oscillation of the inner and outer cylinders, I is the moment of inertia of the inner cylinder about its axis, L the length of the annular gap, and K the restoring constant of the torsion wire, we have

$$F(r_1) = 2\pi in\theta_1, \qquad F(r_2) = 2\pi in\theta_2 e^{ic}, \tag{24}$$

where c is a real constant. Also, from the equation of motion of the inner cylinder,

$$2\pi r_1^2 L f(r_1) = (K-4\pi^2 n^2 I)\theta_1. \tag{25}$$

These equations determine a, b, c, and θ_1/θ_2 in terms of the frequency. The most readily measurable quantity in oscillatory experiments with the elastoviscometer is the amplitude ratio

$$\vartheta(n) \equiv \frac{\theta_1}{\theta_2} = \frac{\left|\dfrac{2\pi\rho r_1^2 r_2 L}{\alpha}[J_2(\alpha r_1)Y_1(\alpha r_1)-Y_2(\alpha r_1)J_1(\alpha r_1)]\right|}{\left|\dfrac{2\pi\rho r_1^3 L}{\alpha}[J_2(\alpha r_1)Y_1(\alpha r_2)-Y_2(\alpha r_1)J_1(\alpha r_2)]+ \right.} \tag{26}$$

$$\left. +\left(\frac{K}{4\pi^2 n^2}-I\right)[J_1(\alpha r_1)Y_1(\alpha r_2)-Y_1(\alpha r_1)J_1(\alpha r_2)]\right|$$

It is observed that a radial variation of vertical normal stress zz $(= zz'-p'')$ is required to maintain strictly two-dimensional motion. It is easily verified that, in addition to the variation arising from the centripetal

acceleration $\rho r\omega^2$, the variation of zz across the annulus is of the order of $\eta_0\lambda_1(r_2-r_1)r(\partial\omega/\partial r)^2$. The departure from two-dimensional motion which must arise when a free surface is present at the top of the annular gap can therefore be made negligible by sufficiently reducing the annular gap and the amplitude of oscillation. In practice, a check is made experimentally that the amplitude is sufficiently small for the above theory to hold, by noting that the amplitude ratio is (very nearly) independent of the absolute value of the amplitude of oscillation of the outer cylinder.

4. Numerical calculations

The numerical constants associated with the three different inner cylinders at present available for oscillatory experiments are as follows.

Cylinder	r_1 (*cm.*)	r_2 (*cm.*)	L (*cm.*)	I (*gm. cm.*^{2})
I	2·1212	2·1712	25·40	2677·5
II	2·0701	2·1712	25·40	2468
III	1·9692	2·1712	25·40	2098

Calculations have been made with two values of K, corresponding to the torsion wires which have been used in most of the experimental work of Toms and Strawbridge (**2**), namely $0{\cdot}171\times10^6$ dyne cm./radian (Wire 5A) and $2{\cdot}79\times10^6$ dyne cm./radian (Wire 8).

The exact formula (26) is unsuitable for direct computation because there appear to be no tables of the Bessel functions J_2 and Y_2 for general complex arguments. An approximate formula, valid for sufficiently large n, is obtained by substituting for the Bessel functions their asymptotic expansions in powers of $(\alpha r)^{-1}$. After some reduction, the following approximate formula is obtained

$$\left(\frac{r_2}{r_1}\right)^{\frac{3}{2}}\frac{1}{\vartheta}=\left|\left(1-\frac{3(r_2-r_1)S}{8r_0^2}\right)\cos(r_2-r_1)\alpha+\right.$$
$$\left.+\left[\frac{15r_2-3r_1}{8r_0^2\alpha}+\frac{15}{16r_0^3\alpha^3}+\left(\alpha+\frac{3}{8r_0^2\alpha}-\frac{45}{128r_0^4\alpha^3}\right)S\right]\sin(r_2-r_1)\alpha\right|, \quad (27)$$

where $r_0=\sqrt{(r_1r_2)}$ and

$$S=\frac{1}{2\pi\rho r_1^3L}\left(\frac{K}{4\pi^2n^2}-I\right). \quad (28)$$

When the above numerical constants are used, it is estimated that the formula (27) gives ϑ with an error of less than about 1 per cent. for values of n sufficiently large to make $|\alpha|>2$ cm.$^{-1}$

It follows from (26) that the slope of the (n, ϑ) curve at the origin is given by

$$\lim_{n \to 0} \frac{\vartheta(n)}{n} = \frac{8\pi^2 r_1^2 r_2^2 L \eta_0}{(r_2^2 - r_1^2)K}, \tag{29}$$

a result which is independent of λ_1 and λ_2. The observation of this slope

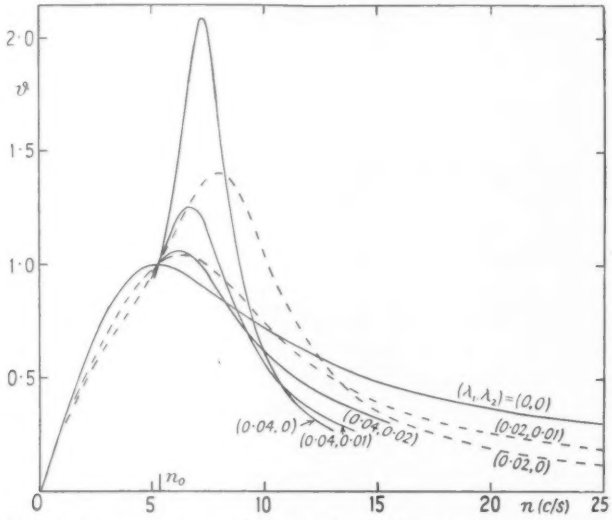

FIG. 1. The variation of $\vartheta(n)$ with λ_1 and λ_2 when $\rho = 1$, $\eta_0 = 8$ (Inner Cylinder II, Torsion Wire 8).

in an experimental (n, ϑ) curve gives an independent, though less accurate, method of obtaining η_0. (It has been found that the values of η_0 so obtained for polymer solutions are consistent with those obtained from steady-state experiments.)

The function $\vartheta(n)$ depends on six parameters which can take different values when the liquid or elastoviscometer components are changed: ρ, η_0, λ_1, λ_2, r_1, and K. An example of the variation of the theoretical (n, ϑ) curve with r_1 and K for a given liquid has already been quoted by Oldroyd, Strawbridge, and Toms (3, Fig. 7), and this need not be considered further. The results of numerical calculation show that the form of the curve is very little dependent on ρ, when the other parameters are fixed, in the range $0{\cdot}75 < \rho < 1{\cdot}5$ (g./ml.). The manner in which the curve varies with λ_1 and λ_2 is illustrated in Fig. 1, and the effect of changing η_0, other things being equal, is illustrated in Figs. 2 and 3. (Numerical values marked on the diagrams are in C.G.S. units.). The curves for Newtonian

liquids ($\lambda_1 = 0$, $\lambda_2 = 0$) show a peak in ϑ, not exceeding unity, at a value of n almost exactly equal to the frequency n_0 of free oscillation of the inner cylinder and torsion wire (defined by $S = 0$). Those based on values of

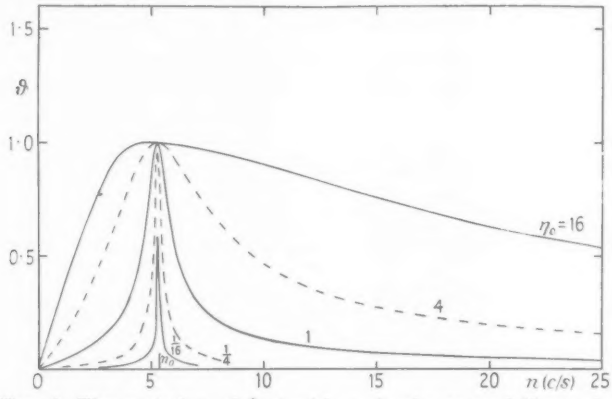

FIG. 2. The variation of $\vartheta(n)$ with η_0 in the case of Newtonian liquids ($\lambda_1 = 0$, $\lambda_2 = 0$, Inner Cylinder II, Torsion Wire 8).

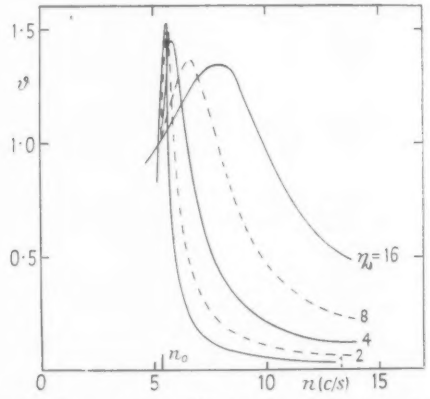

FIG. 3. The variation of $\vartheta(n)$ with η_0 when $\lambda_1 = 0{\cdot}05$, $\lambda_2 = 0{\cdot}01$ (Inner Cylinder II, Torsion Wire 8).

$\lambda_1 > 0$ show a higher peak at a frequency greater than n_0. The height of the peak increases with λ_1 and decreases with increasing λ_2.

The change in shape of the (n, ϑ) curve with λ_1 and λ_2, at constant density and viscosity (cf. Fig. 1) is sufficiently marked to permit approximate values of λ_1 and λ_2 to be assigned without ambiguity to an experimental curve, by comparing it with the theoretical curves based on the known ρ

and η_0 and a series of values of λ_1 and λ_2. For example, the values $\lambda_1 = 0{\cdot}065$ sec., $\lambda_2 = 0{\cdot}015$ sec. were assigned in this way to the solution of *poly*(methyl methacrylate) in pyridine ($\rho = 0{\cdot}98$ g./ml., $\eta_0 = 7{\cdot}9$ poises) the curves for which were given by Oldroyd, Strawbridge, and Toms (**3**, Fig. 6); the observed curves for the different cylinders and torsion wires were in general agreement with the predicted curves based on these values. A device which has been found useful in assigning values of the relaxation times rapidly is a graphical method such as the following. Two frequencies n_1 and n_2 ($> n_0$) are chosen, at which the variation of ϑ with λ_1 and λ_2 is considerable, and contours $\lambda_1 =$ constant, $\lambda_2 =$ constant are constructed, on a plot of $\vartheta(n_1)$ against $\vartheta(n_2)$, from the theoretical curves. Approximate values of λ_1 and λ_2 can then be assigned immediately by marking the point $\vartheta(n_1)$, $\vartheta(n_2)$ on this plot which corresponds to an actual material. The choice of n_1 and n_2 depends on the viscosity and density of the solution being examined.

In order to avoid extensive calculations for the analysis of every new experimental curve it has been decided to study polymer solutions of such compositions as to give $\eta_0 = 2^m$ poises only ($m = 0, \pm 1, \pm 2, \ldots$). The systematic computation of (n, ϑ) curves has been carried out for these viscosities and for $\rho = 1$ g./ml. (A small correction is necessary before these are suitable for direct comparison with experimental results for liquids of appreciably different density.) It has been found sufficient to consider values of λ_1, λ_2 increasing from zero in steps of 0·01 sec. up to about 0·08 sec., in order to assign values to the experimental curves so far considered. Most calculations have been done to correspond to the experimental set-up of Inner Cylinder II and Torsion Wire 8, and the first comparisons of observed curves have been made with the resulting theoretical curves.

The experimental results from steady rotational experiments show that the liquids exhibit marked non-Newtonian behaviour (cf. **3**, Fig. 5). The variation of η with γ, calculated from equations (16), indicates that more complicated equations of state than (7) are required to explain the rheological properties of the liquids so far observed at finite rates of shear.

Acknowledgement

The author is indebted to Mr. P. J. Evans and Miss M. E. Henry for computational assistance at different times, to Mrs. W. L. Wood for undertaking to continue the systematic calculation of the function $\vartheta(n)$ for different values of the physical constants, and to Dr. B. A. Toms and Dr. D. J. Strawbridge for access to their experimental results.

REFERENCES

1. J. M. Burgers, *Proc. Kon. Ned. Akad. v. Wetensch.* **51** (1948), 1211.
2. B. A. Toms and D. J. Strawbridge. (In preparation.)
3. J. G. Oldroyd, D. J. Strawbridge, and B. A. Toms, *Proc. Phys. Soc.* B, **64** (1951), 44.
4. H. Jeffreys, *The Earth*, 2nd ed. (Cambridge, 1929), 265.
5. H. Fröhlich and R. Sack, *Proc. Roy. Soc.* A, **185** (1946), 415.
6. J. M. Burgers, *First Report on Viscosity and Plasticity* (Royal Netherlands Academy of Sciences, 1935), chap. i.
7. J. G. Oldroyd, *Proc. Roy. Soc.* A, **200** (1950), 523.

THE SURFACE ELEVATION IN CELLULAR CONVECTION

By HAROLD JEFFREYS (*St. John's College, Cambridge*)

[Received 6 June 1950]

SUMMARY

Bénard observed that in cellular convection in a fluid heated below, the surface was depressed over the rising currents. His theoretical explanation is fallacious, and an analysis leads to the opposite result. A discrepancy remains between theory and observation. An alternative method of numerical solution was used as a check and may be capable of extension to other problems.

1. THE formation of cellular convection currents in a fluid heated below was studied experimentally by H. Bénard (**1**) and there have been many theoretical discussions. My attention was recently called by Miss M. E. M. Bland to a passage (**1**, p. 92) where Bénard states that the currents rise in the centres of the cells and that the surface of each cell is concave upward; thus to each centre of ascent corresponds a depression of the free surface. This appeared surprising in the light of several problems that have been solved with a view to the explanation of thermally produced winds. In these the disturbance of temperature is taken to be a function of the horizontal coordinates, varying slowly with the time, and the result in each case is a slow motion with the pressure in a heated column increased at the top and diminished on the bottom; while the flow at the top is outward from such a column. Thus the flow at the top is away from the elevated parts.

It appeared that the different conditions of the problems might provide an explanation, but a thermodynamical argument suggests that they cannot. In the steady state the dissipation of energy must be compensated by a supply, which can come only from the contraction of elements of the fluid where the pressure is high and expansion where it is low; that is, for an element describing a circuit, $\int p\,dv$ must be negative. Since the fluid is assumed incompressible, and since the temperature is taken constant over the free surface and the bottom, this implies that a particle must be under excess pressure when it is moving towards a place of lower temperature, that is, upwards; and hence the elevations must be over the rising currents.

Bénard gives a qualitative argument to show that his result could be inferred on physical grounds, by considering the currents near the bottom. These are being driven against viscosity and imply a decrease of pressure along the bottom from a region of descent to one of ascent. But the

conclusion does not follow for several reasons. (1) In the corresponding problems of wind formation the pressure gradients along level surfaces have opposite signs at the top and bottom, and this might be true here too. (2) The relevant stress components for bottom currents would be p_{11}, p_{22}, in a usual notation; while the surface elevation determines p_{33}, and the differences, even at the same place, are not negligible in a motion largely controlled by viscosity. (3) The shear stresses p_{13}, p_{23} are not zero, and play a part in driving the bottom current. Unfortunately (2) also vitiates the thermodynamical argument, because the normal stress at the free surface of a viscous fluid would differ from $-p$.

It might be argued directly that the rising current can be stopped at the free surface only by an opposing vertical stress, which can be provided only by an elevation of the surface. A full discussion is desirable.

2. *Notation*

$x_1, x_2, x_3 = x, y, z$ coordinates; z vertically upward.

$u_1, u_2, u_3 = u, v, w$ velocity components.

p_{ik} = stress components.

ρ = density.

κ = thermometric conductivity.

ν = kinematic viscosity.

V = temperature.

$\beta = \partial V/\partial z$ in undisturbed state.

α = coefficient of volume expansion.

h = depth of fluid.

Accents refer to departures from the undisturbed state.

Departures are taken to be of the forms $(\cos lx, \cos my)(\sin lx, \sin my)$.

It was only in the work of Pellew and Southwell (**2**) that the solution was first found for the motion with a free surface, and no discussion has attended explicitly to the variations of pressure and of surface elevation. I use the method of my original paper (**3**) to state the equations; the formal solution is found by Goldstein's method (**4**, section 14.062). This allows for Pellew and Southwell's adaptation to a free surface. It is necessary to notice, however, that in all treatments of the problem the equations of motion have been taken in the form

$$\frac{d}{dt}(u, v, w) = -\left(\frac{\partial}{\partial x}, \frac{\partial}{\partial y}, \frac{\partial}{\partial z}\right)p + \rho\nu\nabla^2(u, v, w) - (0, 0, g\rho), \tag{1}$$

which implies a special and rather unusual definition of pressure in relation to the stress components; (1) in fact is true only if

$$p_{ik} = -(p + \rho\nu\theta)\delta_{ik} + \rho\nu\left(\frac{\partial u_i}{\partial x_k} + \frac{\partial u_k}{\partial x_i}\right); \qquad \theta = \frac{\partial u_m}{\partial x_m}. \tag{2}$$

Since the fluid is taken to be incompressible, this is permissible because the pressure does not appear in the equation of state and is required only to be a scalar. But in studying the surface elevation, the only datum will be the variations of normal stress over $z = h$, and we need the relation between p and p_{33}. Considering only disturbances from the static state we have, with $\partial/\partial t = 0$,

$$\beta w = \kappa \nabla^2 V', \qquad \theta = \alpha\kappa \nabla^2 V', \tag{3}$$

$$-\frac{\partial p'}{\partial z} + \frac{\kappa\rho\nu}{\beta}\nabla^4 V' + g\alpha\rho V' = 0, \tag{4}$$

$$\nabla^2 p' - \alpha\kappa\rho\nu\nabla^4 V' - g\alpha\rho\frac{\partial V'}{\partial z} = 0, \tag{5}$$

whence

$$\nabla_1^2 p' + \frac{\kappa\rho\nu}{\beta}\frac{\partial}{\partial z}\nabla^4 V' - \alpha\kappa\rho\nu\nabla^4 V' = 0. \tag{6}$$

With

$$(l^2+m^2)h^2 = a^2, \tag{7}$$

we have

$$p' = -\frac{h^2}{a^2}\nabla_1^2 p', \tag{8}$$

and from (2), (3), (6)

$$p_{33} = -\frac{h^2}{a^2}\left(\frac{\kappa\rho\nu}{\beta}\frac{\partial}{\partial z}\nabla^4 V' - \alpha\kappa\rho\nu\nabla^4 V'\right)$$

$$-\rho\nu\alpha\kappa\nabla^2 V' + \frac{2\rho\nu\kappa}{\beta}\frac{\partial}{\partial z}\nabla^2 V' \tag{9}$$

$$= -\frac{\kappa\nu\rho}{\beta}\frac{\partial}{\partial z}\left(\frac{h^2}{a^2}\nabla^4 V' - 2\nabla^2 V'\right), \tag{10}$$

since the second and third terms of (9) can be neglected in comparison with the first and fourth when $\alpha\beta h$ is small. Put now

$$a = \pi b, \qquad z = h\xi/\pi, \qquad \mu = -\frac{g\alpha\beta h^4}{\pi^4\kappa\nu}. \tag{11}$$

Then

$$p_{33} = M\frac{d}{d\xi}\left(\frac{d^2}{d\xi^2} - b^2\right)\left(\frac{d^2}{d\xi^2} - 3b^2\right)V', \tag{12}$$

where

$$M = -\kappa\nu\rho\pi^3/\beta f^2 h^3 = g\alpha h/b^2\pi\mu; \tag{13}$$

μ, and therefore M, are positive since β is negative.

Take

$$V' = f(x,y)Z(z) = f(x,y)\sum A_n \sin n\xi. \tag{14}$$

Then*

$$p_{33} = M[-\tfrac{1}{2}B + \sum\{(n^2+b^2)(n^2+3b^2)nA_n - B\}\cos n\xi]. \tag{15}$$

* In (10) of (4) p. 414, π should be 2.

Since the case of a free surface corresponds to sums over even n, we use (18) of (**4**) and find

$$p_{33} = -MB\left(\frac{1}{2} - \sum \frac{b^2(n^4-b^4)+\mu b^2}{(n^2+b^2)^3-\mu b^2}\cos n\xi\right). \tag{16}$$

Put $n = 2m$, $b = 2s$; since we are concerned chiefly with $\xi = \frac{1}{2}\pi$ we need also the sums

$$\sum_1^\infty \frac{(-1)^m}{m^2+s^2} = -\frac{1}{2s^2} + \frac{\pi}{2s}\operatorname{cosech}\pi s, \tag{17}$$

$$\sum_1^\infty \frac{(-1)^m}{(m^2+s^2)^2} = -\frac{1}{2s^4} + \frac{\pi}{4s^3}\operatorname{cosech} s\pi + \frac{\pi^2}{4s^2}\operatorname{cosech} s\pi \coth s\pi. \tag{18}$$

Then

$$p_{33} = -MB\Big(\tfrac{1}{2}\pi^2 s^2 \operatorname{cosech} s\pi \coth s\pi - \\ - \sum (-1)^m \frac{m^2(m^2+3s^2)_{\frac{1}{16}}\mu s^2}{(m^2+s^2)^2\{(m^2+s^2)^3-\frac{1}{16}\mu s^2\}}\Big). \tag{19}$$

With the numerical values (**4**, p. 415)

$$b = 1{\cdot}70, \qquad \mu = 180{\cdot}8, \tag{20}$$

this gives

$$p_{33}/MB = -0{\cdot}501+(2{\cdot}854+0{\cdot}0929-0{\cdot}0099+\ldots) = +2{\cdot}436 \tag{21}$$

in which a correction has been made for the probable value of the remainder. Also

$$A_2 = -0{\cdot}01024B \tag{22}$$

and $\sin 2\xi$ is the only harmonic that does not change sign between 0 and $\frac{1}{2}\pi$. Hence a column of heated fluid corresponds to negative B, therefore to negative p_{33} at $z = h$, and therefore to an elevation of the free surface. Further, $\nabla^2 V'$ has the opposite sign to V', and β is negative; hence w is positive in the heated columns, and there is an elevation of the free surface over the rising currents, as expected. Thus there is an unexplained discrepancy between theory and observation. The surface elevation ζ satisfies

$$\frac{\zeta}{A_2} = -\frac{p_{33}}{g\rho} = 0{\cdot}15\alpha h \tag{23}$$

nearly. It must be remembered that h in this formula is twice the depth. Since α is the coefficient of volume expansion, the surface elevation is comparable with the direct effect of linear expansion.

In view of the result and of the possibility of a mistake in sign in the calculation, I sought for another method that would serve as a check. The formal solution of Pellew and Southwell would also, I think, involve

a risk of errors in sign, and the safest method appeared to be a numerical one. I first tried the method of finite differences of my original paper. This had never been applied with the correct boundary conditions. A test of the applicability of this method was desirable for other reasons. Both the Fourier series and the exponential solution are suited only for a differential equation with constant coefficients, and more complex cases may need to be considered; but a numerical method should still be applicable. We now take $\zeta = z/h = \pi\xi, \lambda = \pi^4\mu$. The method was applied to the case of two conducting rigid boundaries and to the lowest (symmetrical) mode. With intervals $\frac{1}{2}$, λ was found to be 604; with $\frac{1}{3}$, 955; with $\frac{1}{4}$, 1180. Extrapolation to zero interval by Richardson's method gave $\lambda = 1548$. As the correct value is 1708, the convergence is far too slow to be satisfactory. A possible explanation is that to form a centred third difference at the boundary it was necessary to take two extrapolated values of V''; but in fact only first and second centred differences were used in forming the boundary values of the first and second derivatives. With two extrapolated values available it would be possible to allow for third and fourth differences. When this was done, however, it was found that the signs of the extrapolated values were reversed. Thus it appeared that the method is precarious when used for a differential equation of high order containing a large numerical coefficient.

A method briefly mentioned in my first paper, but not completed, was then tried. This was to make up a polynomial that satisfies the boundary conditions exactly, and then to choose λ so as to satisfy the differential equation where the solution is a maximum. Since there are three conditions* $Z = 0$, $Z'' = 0$, $Z''' - a^2 Z' = 0$ at each boundary, and since the solution must be symmetrical or antisymmetrical about the mid-point, it seemed likely that the solution is very fully determined by these conditions alone. For the symmetrical case the simplest polynomial that satisfies them is

$$Z = \zeta(1-\zeta) + \zeta^2(1-\zeta)^2 + (2+\tfrac{1}{6}a^2)\zeta^3(1-\zeta)^3. \tag{24}$$

Then λ is chosen so that the differential equation

$$\left(\frac{d^2}{d\zeta^2} - a^2\right)^3 Z = -\lambda a^2 Z \tag{25}$$

is satisfied at $\zeta = \frac{1}{2}$. For various values of a the results were

$a^2 =$	8	9	10
$\lambda =$	1870	1833	1888

and by interpolation the minimum is for

$$a^2 = 8{\cdot}90, \qquad a = 2{\cdot}98, \qquad \lambda = 1833.$$

* Here accents denote derivatives.

As the correct values are $a = 3{\cdot}14$, $\lambda = 1708$, these results are very satisfactory for a first approximation. It could be improved by including an extra term in Z and fitting the differential equation at another point.

For the antisymmetrical case a suitable polynomial is

$$Z = (1-2\zeta)\zeta(1-\zeta)\{1+3\zeta(1-\zeta)+10\zeta^2(1-\zeta)^2+\tfrac{1}{6}a^2\zeta^2(1-\zeta)^2\}, \quad (26)$$

and by fitting the differential equation at $\zeta = \frac{1}{3}$ we get

$a^2 =$	15	20	22	23	25
$\lambda =$	17,539	16,839	16,772	16,796	16,891

By interpolation the minimum comes at $a^2 = 21{\cdot}7$, $a = 4{\cdot}66$, $\lambda = 16{,}771$. The correct values are $a = 5{\cdot}34$, $\lambda = 17{,}610$. Again the method leads easily to a fairly good approximation; λ must be divided by 16 to give the value for depth h with a free surface.

Returning now to (12) we have to evaluate at $\zeta = \frac{1}{2}$

$$Z^{(v)}-4a^2Z'''+3a^4Z' = -2520-450a^2-4{\cdot}31a^4-a^6/64 = -14745$$

with $a^2 = 21{\cdot}7$. At $\zeta = \frac{1}{8}$, which is near the maximum of Z, we have $Z = 0{\cdot}25$. The sign is therefore confirmed. We also have, nearly,

$$\frac{p_{33}}{g\rho V'_{(\max)}} = -0{\cdot}16\alpha h$$

in good agreement with the Fourier series solution.

Apart from its use as a check in the present problem, this method may be capable of extension, particularly if generalizations of the stationary principle proved by Southwell and Pellew should be possible. It seems that such generalizations should exist because the required value of λ is the lower bound of values such that distributions exist that make the supply of energy to the eddies enough to balance the loss by dissipation.

It appears desirable that Bénard's experimental work should be repeated. Chandra (**5**) has made a study of the conditions in air with rigid boundaries above and below, and finds that the motion is downward in the centres of the cells, whereas with a free surface above Bénard found it upward. He also found a second type of convection, which is not covered by the present theory. Similar work in CO_2 has been done by Dassanayake; for information about this I am indebted to Professor O. G. Sutton.

REFERENCES

1. H. Bénard, *Ann. Chim. Phys.* (7) **23** (1901), 62–144.
2. A. Pellew and R. V. Southwell, *Proc. Roy. Soc.* A, **176** (1940), 312–43.
3. H. Jeffreys, *Phil. Mag.* (7) **2** (1926), 833–44.
4. H. and B. S. Jeffreys, *Methods of Mathematical Physics* (Cambridge, 1946).
5. K. Chandra, *Proc. Roy. Soc.* A, **164** (1938), 231–42.

THE FORCES ACTING ON AN AEROFOIL OF APPROXIMATE JOUKOWSKI TYPE IN A STREAM BOUNDED BY A PLANE WALL*

By S. TOMOTIKA, Z. HASIMOTO, *and* K. URANO

(*University of Kyoto, Kyoto, Japan*)

[Received 3 October 1950]

SUMMARY

The investigation of the manner in which the effect of the ground on the lift and moment of an aerofoil is modified by its thickness and camber is of great interest not only from the theoretical point of view but also from the practical standpoint.

In this paper we discuss in detail the modifications introduced by the thickness of an aerofoil on the ground-effect upon its lift, by evaluating the forces acting on some aerofoils (especially approximately symmetrical aerofoils) of approximate Joukowski type placed in a stream bounded by an infinite plane wall.

It is found that when an aerofoil is placed in the vicinity of the ground at the small angles of attack used in practice, the lift on the aerofoil is in general increased by the presence of the ground, but the rate of increase of the lift becomes smaller as the thickness of the aerofoil increases.

1. Introduction

DETAILED theoretical investigations concerning the effect of the ground upon the lift and moment of a plane aerofoil have been carried out by one of us (S. T.) and co-workers (**1, 2, 3**). However, since such a plane aerofoil has no camber or thickness, it would not be appropriate to apply those theoretical results directly to the case of aerofoils used in practice, which have, in general, camber and thickness. Some modifications would be necessary when either, or both, the camber and thickness of an aerofoil becomes appreciable, though it may naturally be expected that the effect of the ground on the lift and moment of very thin aerofoils with negligible camber does not differ greatly from that of a plane aerofoil. Thus an interesting and important question arises: In what manner is the ground-effect on the lift and moment of an aerofoil modified by its camber and thickness?

A beginning has been made on this problem by Bonder (**4**) and Müller (**5**), but no definite results seem to have been obtained, as far as we are aware. We have therefore discussed the problem in detail, by evaluating the forces acting on a circular arc aerofoil as well as on an aerofoil of approximate Joukowski type with small camber, each of which is placed in a stream

* The work described in the present paper was carried out in 1941. Publication of the paper has been unavoidably delayed.

bounded by an infinite plane rigid wall. A circular arc aerofoil has been taken for the purpose of investigating the effect of the camber of the aerofoil upon the ground-effect, while an approximately symmetrical aerofoil of approximate Joukowski type has been considered for the purposes of finding what modifications, if any, are introduced in the ground-effect by the thickness of the aerofoil. In the present paper we describe our results

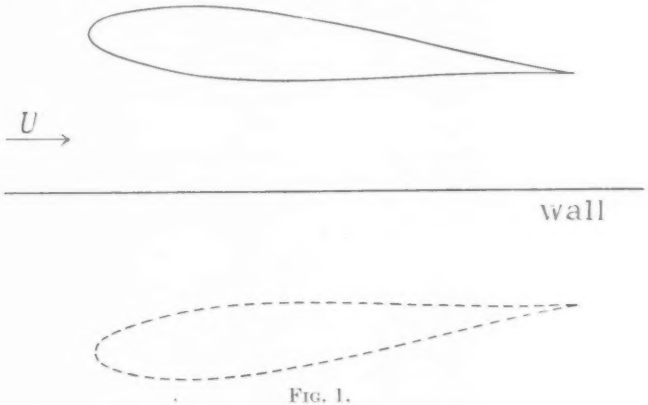

FIG. 1.

for the latter case. Results for the former case, i.e. for the case of a circular arc aerofoil, will be published elsewhere (**6**).

Although there are several different ways of dealing with the problem, we have used the convenient method of images, as used in Bonder's and Müller's papers. Thus by introducing on the lower side of the wall the mirror image of the aerofoil with respect to the wall (see Fig. 1) and then allowing the fluid to have access to the whole region, we replace the original problem by the two-dimensional continuous flow of an incompressible perfect fluid past a system of real and image aerofoils placed in an unbounded stream. The required flow pattern past such a system of real and image aerofoils can then be deduced by suitable conformal transformations from the flow past a system of two equal circular cylinders.

2. The flow past two equal circular cylinders

Following the lines of the argument laid down by Lagally (**7**), we shall first deal with the steady two-dimensional continuous potential flow of an incompressible inviscid fluid past two equal circular cylinders, under the assumption that the line joining their centres is perpendicular to the direction of the undisturbed flow at infinity and that there are no singularities in the field of flow.

We take the plane of fluid motion as the (ξ, η)-plane. If Q_1, Q_2 are

the points $(0, c)$ and $(0, -c)$ respectively and P any point in the plane, and if the radii from Q_1, Q_2 to P are of lengths r_1, r_2 and are inclined at angles ϑ_1, ϑ_2 to the ξ-axis, then the complex coordinates $\zeta = \xi + i\eta$ of the point P are expressed in either of the following two forms:

$$\zeta = ic + r_1 e^{i\vartheta_1}, \qquad \zeta = -ic + r_2 e^{i\vartheta_2}, \tag{1}$$

and we have

$$\log \frac{\zeta + ic}{\zeta - ic} = \log \frac{r_2}{r_1} + i(\vartheta_2 - \vartheta_1). \tag{2}$$

The curves $r_2/r_1 =$ constant are a set of co-axal circles having Q_1, Q_2 for limiting points. The circles corresponding to values of r_2/r_1 greater than unity lie above the ξ-axis and those corresponding to values less than unity below, while on the ξ-axis itself, which is the common radical axis, $r_2/r_1 = 1$. The curves $\vartheta_2 - \vartheta_1 =$ constant are circles, or rather arcs of circles passing through Q_1, Q_2 and cutting the first set of circles orthogonally. On the right-hand side of the η-axis $\vartheta_2 - \vartheta_1$ is positive and on the left-hand side negative, while on the η-axis $\vartheta_2 - \vartheta_1 = 0$, except on the segment $Q_1 Q_2$, where $\vartheta_2 - \vartheta_1 = \pm\pi$. At infinity $r_2/r_1 = 1$, $\vartheta_2 - \vartheta_1 = 0$, and at Q_1, Q_2 we have $r_2/r_1 = \infty$ and $r_2/r_1 = 0$ respectively; also, $\log r_2/r_1$, $\vartheta_2 - \vartheta_1$ are the bipolar coordinates.

We now take a circle C_1 defined by $r_2/r_1 =$ constant $\equiv \lambda$ (> 1) above the ξ-axis and another circle C_2 defined by $r_2/r_1 =$ constant $\equiv \mu$ (< 1) below, and we assume that these two circles are of the same radius a. Then there exists an obvious relation $\lambda\mu = 1$ between the two constants λ, μ and these two circles are symmetrically situated with respect to the ξ-axis (Fig. 2). Further, we denote the centres of the circles by O_1, O_2 respectively.

If we denote the centre distance $O_1 O_2$ by $2b$ and if we put

$$\log \lambda = -\log \mu \equiv \sigma \quad (> 0)$$

for convenience, we find

$$\sinh \sigma = \frac{c}{a}, \qquad \cosh \sigma = \frac{b}{a}. \tag{3}$$

Thus when the common radius a of the two equal circles and the distance apart of their centres, $2b$, are given, equations (3) enable us to calculate the values of c and σ.

Next we conformally transform the ζ-plane on to an s-plane by the relation

$$s = i \log \frac{\zeta + ic}{\zeta - ic}. \tag{4}$$

Then the region outside the two circles C_1, C_2 is transformed into a rectangle of sides 2π, 2σ (Fig. 3), the circles C_1, C_2 corresponding to the sides CD, AB respectively.

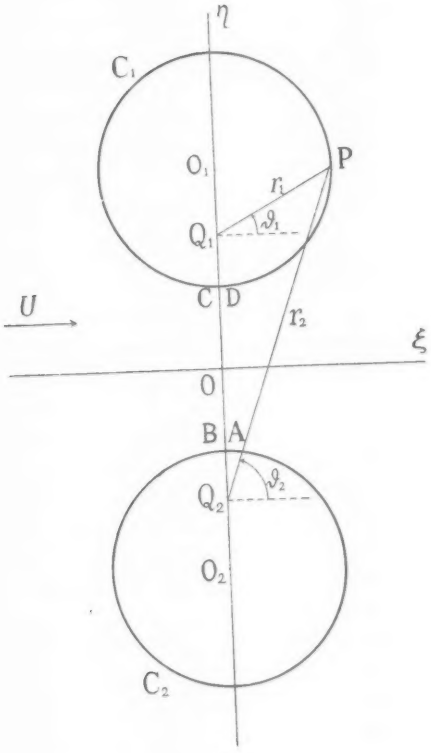

FIG. 2.

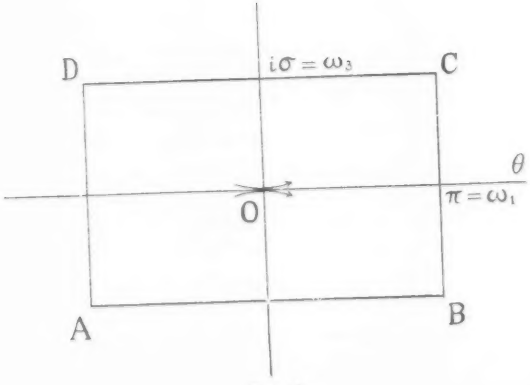

FIG. 3.

If, as shown in Fig. 2, we assume that at a great distance from the cylinders the fluid flows with a constant velocity U from left to right parallel to the ξ-axis, the complex velocity potential w for the flow under discussion takes the approximate form

$$w = U\zeta,$$

when ζ is very large.

From the relation
$$\zeta = -c \cot \tfrac{1}{2}s, \tag{5}$$

which follows immediately from (4), it is found that $\zeta = \infty$ corresponds to $s = 0$. Therefore, if we take account of the fact that $\cot \frac{1}{2}s$ behaves as $2/s$ when s is small, we readily find that in the neighbourhood of the origin ($s = 0$) of the s-plane the complex velocity potential w assumes the approximate form

$$w = -\frac{2cU}{s}, \tag{6}$$

which is the complex velocity potential due to a single doublet of strength $2cU$ at the origin $s = 0$. Since $cU > 0$, the axis of the doublet is in the positive direction of the real axis and the direction of flow in the vicinity of $s = 0$ is as shown in Fig. 3.

From (6) we have
$$\frac{dw}{ds} = \frac{2cU}{s^2}, \tag{7}$$

which shows that the required general expression for the conjugate complex velocity dw/ds must have a pole of the second order at the origin $s = 0$. Moreover, it has no other poles within the rectangle, since we have assumed that there are no singularities in the whole field of flow in the ζ-plane.

Our next problem is to obtain the general expression for the conjugate complex velocity dw/ds for the flow in the rectangle $ABCD$ in the s-plane, and this can be done by the use of Weierstrass's $\wp$-function.

We first note that the two sides AB, CD of the rectangle $ABCD$, which correspond respectively to the circles C_2, C_1 in the ζ-plane, are both streamlines of the flow; also since the homologous points on the remaining two sides AD, BC correspond to the same single point on the segment AD ($= BC$) in the ζ-plane, the values of the conjugate complex velocity at the homologous points are equal to each other. Further, we recall that there is, as mentioned above, a single doublet of strength $2cU$ at $s = 0$ with its axis in the positive direction of the real axis.

These conditions can be satisfied if we take the rectangle $ABCD$ as the fundamental period-parallelogram and we arrange a set of equal doublets of strength $2cU$ with similar axes, one at the point $s = 0$ and one at all the homologous points. It then follows that the conjugate complex velocity

for the flow due to such a system of infinitely many doublets has poles of the second order at $s = 0$ and at all the homologous points.

Thus, introducing Weierstrass's $\wp$-function with periods $2\omega_1 \equiv 2\pi$, $2\omega_3 \equiv 2i\sigma$, we may write the conjugate complex velocity dw/ds in the form

$$\frac{dw}{ds} = 2cU\,\wp(s)+k, \tag{8}$$

where k is a constant determined by the circulation round one of the circles (C_1, say) in the ζ-plane.

Moreover, the value of this constant can be determined if we assign the position of one of the stagnation points (e.g. that on the downstream side) on the circumference of the circle C_1.

Let the stagnation point on the downstream side on the circumference of the circle C_1 be denoted by $\zeta_1 = ib+ae^{-i\beta}$. Then, writing $\zeta_1 = \xi_1+i\eta_1$, we have immediately

$$\xi_1 = a\cos\beta, \qquad \eta_1 = b-a\sin\beta. \tag{9}$$

Further, let s_1 be the point in the s-plane which corresponds to the stagnation point ζ_1. Then, taking (3) into account, we have from (4)

$$s_1 = i\log\frac{ib+ic+ae^{-i\beta}}{ib-ic+ae^{-i\beta}} = i\sigma-\tan^{-1}\left(\frac{\sinh\sigma\cos\beta}{1-\cosh\sigma\sin\beta}\right), \tag{10}$$

or

$$s_1 = i\sigma+\theta_1 = \omega_3+\theta_1, \tag{11}$$

where we have put for simplicity

$$\theta_1 = -\tan^{-1}\left(\frac{\sinh\sigma\cos\beta}{1-\cosh\sigma\sin\beta}\right). \tag{12}$$

The condition that $\zeta = \zeta_1$ should be the stagnation point requires that

$$\left(\frac{dw}{d\zeta}\right)_{\zeta=\zeta_1} = \left(\frac{dw}{ds}\right)_{s=s_1}\left(\frac{ds}{d\zeta}\right)_{s=s_1} = 0, \tag{13}$$

which is also equivalent to the relation

$$\left(\frac{dw}{ds}\right)_{s=s_1} = 0, \tag{14}$$

since, in the present case, $(ds/d\zeta)_{s=s_1} \neq 0$, as can easily be proved.

Substituting (8) in (14), we have

$$2cU\,\wp(s_1)+k = 0,$$

which gives

$$k = -2cU\,\wp(s_1), \tag{15}$$

and if this value of k is substituted in (8), the conjugate complex velocity for the flow in the s-plane becomes

$$\frac{dw}{ds} = 2cU\{\wp(s)-\wp(s_1)\}. \tag{16}$$

Further, if we combine this with (4), we can immediately obtain, by using the relation $dw/d\zeta = (dw/ds)(ds/d\zeta)$, the conjugate complex velocity $dw/d\zeta$ in the ζ-plane.

3. Conformal transformation of two circles into two aerofoils

Making use of an appropriate transformation formula, the region outside the two equal circles C_1, C_2 in the ζ-plane can be conformally transformed on to the region exterior to two equal aerofoils in a z-plane, which are symmetrically situated with respect to the x-axis (cf. Fig. 1). A transformation formula suitable for the present problem has been suggested by Müller (**5**), who by employing similar transformations has discussed some special cases of little practical interest in which aerofoils are placed at zero angle of attack.

The suggested transformation formula is given by

$$z = \zeta + \frac{p^2 e^{i\gamma}}{\zeta + \zeta_0} + \frac{p^2 e^{-i\gamma}}{\zeta + \bar{\zeta}_0}, \tag{17}$$

where $\zeta_0 = \xi_0 + i\eta_0$, $\bar{\zeta}_0 = \xi_0 - i\eta_0$, and ξ_0, η_0, p, γ are all real constants which determine the shape and orientation of the aerofoils in the z-plane.

As will be shown later, suitable choice of these constants enables us to obtain a pair of equal aerofoils of approximate Joukowski type, symmetrical or unsymmetrical, which are situated symmetrically with respect to the x-axis, as shown in Fig. 1. Then if we assume that the fluid at infinity flows parallel to the x-axis, this axis becomes coincident with a particular streamline and can therefore be replaced by a plane rigid wall without causing any change in the field of flow.

We first consider the transformation formula (17). Separating real and imaginary parts we have

$$\left.\begin{aligned} x = \xi &+ \frac{p^2\cos\gamma}{(\xi+\xi_0)^2+(\eta-\eta_0)^2}\{\xi+\xi_0-(\eta-\eta_0)\tan\gamma\} + \\ &+ \frac{p^2\cos\gamma}{(\xi+\xi_0)^2+(\eta+\eta_0)^2}\{\xi+\xi_0+(\eta+\eta_0)\tan\gamma\} \\ y = \eta &- \frac{p^2\cos\gamma}{(\xi+\xi_0)^2+(\eta-\eta_0)^2}\{\eta-\eta_0+(\xi+\xi_0)\tan\gamma\} - \\ &- \frac{p^2\cos\gamma}{(\xi+\xi_0)^2+(\eta+\eta_0)^2}\{\eta+\eta_0-(\xi+\xi_0)\tan\gamma\} \end{aligned}\right\}. \tag{18}$$

In order to obtain an aerofoil section with a sharp trailing edge, it is necessary that one of the zeros of the transformation (17) should lie on the

circumference of the circle C_1, while the remaining zeros are enclosed within its circumference.

We now assume that the aforementioned stagnation point $\zeta = \zeta_1$ on the circumference of the circle C_1 is taken to be coincident with one of the zeros of the transformation (17) so that $dz/d\zeta = 0$ at $\zeta = \zeta_1$. Then the point ζ_1 is transformed to the sharp trailing edge of the aerofoil. Since, however,

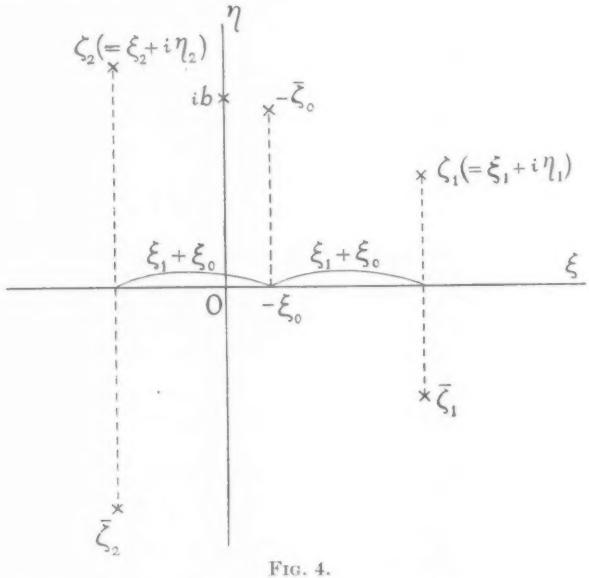

FIG. 4.

the value of the circulation round the circle C_1 (and consequently the circulation round the aerofoil obtained) has been so chosen that $dw/d\zeta = 0$ at $\zeta = \zeta_1$, the velocity at the trailing edge becomes finite and the fluid flows smoothly there.

Using (17), the equation $(dz/d\zeta)_{\zeta=\zeta_1} = 0$ becomes

$$1 - \frac{p^2 e^{i\gamma}}{(\zeta_1+\zeta_0)^2} - \frac{p^2 e^{-i\gamma}}{(\zeta_1+\bar{\zeta}_0)^2} = 0, \tag{19}$$

or

$$(\zeta_1+\zeta_0)^2(\zeta_1+\bar{\zeta}_0)^2 - p^2 e^{i\gamma}(\zeta_1+\bar{\zeta}_0)^2 - p^2 e^{-i\gamma}(\zeta_1+\zeta_0)^2 = 0. \tag{20}$$

It is easily found that the coefficient of ζ_1^3 on the left-hand side of (20) is equal to $4\xi_0$. Also, it is readily seen that the quartic equation in ζ obtained by replacing ζ_1 by ζ in (20) has two pairs of conjugate complex roots. Hence it will be found that the four roots may be written as ζ_1, $\bar{\zeta}_1$, ζ_2, $\bar{\zeta}_2$ and that they are situated as shown in Fig. 4.

Separating real and imaginary parts on the left-hand side of (19), we get, after some reduction, the following relations

$$\tan\gamma\left[\frac{(\xi_1+\xi_0)^2-(\eta_1-\eta_0)^2}{\{(\xi_1+\xi_0)^2+(\eta_1-\eta_0)^2\}^2}-\frac{(\xi_1+\xi_0)^2-(\eta_1+\eta_0)^2}{\{(\xi_1+\xi_0)^2+(\eta_1+\eta_0)^2\}^2}\right]$$

$$=-2(\xi_1+\xi_0)\left[\frac{\eta_1-\eta_0}{\{(\xi_1+\xi_0)^2+(\eta_1-\eta_0)^2\}^2}+\frac{\eta_1+\eta_0}{\{(\xi_1+\xi_0)^2+(\eta_1+\eta_0)^2\}^2}\right], \quad (21)$$

$$\frac{1}{p^2}=\frac{\cos\gamma}{\{(\xi_1+\xi_0)^2+(\eta_1-\eta_0)^2\}^2}[(\xi_1+\xi_0)^2-(\eta_1-\eta_0)^2-2(\xi_1+\xi_0)(\eta_1-\eta_0)\tan\gamma]+$$

$$+\frac{\cos\gamma}{\{(\xi_1+\xi_0)^2+(\eta_1+\eta_0)^2\}^2}[(\xi_1+\xi_0)^2-(\eta_1+\eta_0)^2+2(\xi_1+\xi_0)(\eta_1+\eta_0)\tan\gamma]. \quad (22)$$

Thus if we assign the values of $\xi_1+\xi_0$, η_0, η_1, these two equations enable us to determine the values of the two constants γ, p, and by using these values of γ and p we can also find the values of the remaining two roots ζ_2, $\bar{\zeta}_2$.

In order that the transformation may be conformal everywhere in the region outside the aerofoil above the real axis, the circle C_1 must be so chosen that the zero-point ζ_2 lies within its circumference, and this condition should be taken into account when we assign the values of the constants $\xi_1+\xi_0$, η_0, η_1. On the other hand, since, as we have seen, the other zero-point ζ_1 has been taken to be on the circumference of the circle C_1, it will be transformed into the sharp trailing edge of the aerofoil above the x-axis. In this case it is readily found from symmetry that the zero-point $\bar{\zeta}_2$ lies within the circumference of the circle C_2 and that the zero-point $\bar{\zeta}_1$ lies on the circumference of C_2 and is therefore transformed to the sharp trailing edge of the aerofoil below the x-axis. The transformation is now conformal everywhere in the whole region exterior to the two aerofoils.

We next consider the shape and orientation of the aerofoil which is obtained from the circle C_1 by the transformation (17). Let the chord length of the aerofoil be denoted by l and let the distance of the midpoint of the chord from the x-axis be denoted by H. Further, we denote by α the geometrical angle of attack, defined as the acute angle between the chord of the aerofoil and the x-axis.

Now let $z_T=x_T+iy_T$ and $z_L=x_L+iy_L$ be the complex coordinates of the points in the z-plane which correspond respectively to the points ζ_1 and ζ_2 in the ζ-plane. Then z_T is evidently the complex coordinate of the trailing edge of the aerofoil. If we choose the values of the various constants so that the point z_L becomes very nearly the leading edge of the aerofoil, the

distance between the two points z_L and z_T may be taken approximately as the chord length. Thus

$$l = |z_L - z_T| = \sqrt{\{(x_L - x_T)^2 + (y_L - y_T)^2\}}. \tag{23}$$

The distance H of the midpoint of the chord from the x-axis is given by

$$H = \tfrac{1}{2}(y_L + y_T),$$

and therefore the ratio l/H becomes

$$\frac{l}{H} = \frac{2\sqrt{\{(x_L - x_T)^2 + (y_L - y_T)^2\}}}{y_L + y_T}. \tag{24}$$

Lastly, the angle of attack α is given by

$$\alpha = \tan^{-1}\left(\frac{y_L - y_T}{x_T - x_L}\right). \tag{25}$$

From equations (18) or from Fig. 4 it is seen that the values of l, H, and α are completely determined if we assign the values of $\xi_1 + \xi_0$, η_0, η_1. However, it will be seen from (9) that even when the values of $\xi_1 + \xi_0$, η_0, η_1 are given, the values of the constants a and b, which determine the size and position of the circle C_1, remain indeterminate. Thus it is necessary to assign appropriate values to a and b.

Instead of assigning appropriate values to a and b, we have adopted the more convenient method of assigning appropriate values to ξ_0 and β which, together with the prescribed values of $\xi_1 + \xi_0$ and η_1, determine easily (by (9)), the values of a and b. The advantage of this lies in the fact that the thickness of the aerofoil is intimately connected with the value of ξ_0, while the value of β has a close relation to the camber of the aerofoil. The details of numerical calculations as well as the results obtained will be given later.

It may be added here that the geometrical angle of attack α is approximately equal to $\frac{1}{2}\gamma$, as was to be expected from the fact that the transformation (17) is but a slight modification of the well-known Joukowski transformation.

4. The general expression for the lift acting on the aerofoil

By combining the results obtained in the preceding sections we can obtain the steady uniform flow in the positive direction past two equal aerofoils of approximate Joukowski type which are placed symmetrically with respect to the x-axis, and since in this case the x-axis can be replaced by an infinite plane rigid wall, we can thus obtain the flow past an aerofoil of approximate Joukowski type placed close to a plane rigid wall.

We now proceed to the calculation of the lift acting on the aerofoil placed in the vicinity of the wall. We denote the x- and y-components of the force acting on the aerofoil by P_x and P_y respectively.

If, in the first place, we take into account the fact that the flow is steady, irrotational, and continuous, we can easily prove by the use of the principle of momentum that the aerofoil does not experience any resistance, i.e. P_x is equal to zero, just as in the case of an aerofoil in an unlimited stream.

Next, by applying the same principle of momentum, it can be readily proved that the lift acting on the aerofoil is equal in magnitude but opposite in sign to the total fluid thrust acting on the bounding plane wall. Thus, denoting the latter by P'_y, we have

$$P_y = -P'_y. \tag{26}$$

We shall now calculate P'_y. To avoid confusion with the constant p, let us denote the fluid pressure at any point in the fluid by p_r. Then, by Bernoulli's theorem, we have

$$p_r = \tfrac{1}{2}\rho(U^2 - |\mathbf{v}|^2),$$

where $|\mathbf{v}|$ denotes the magnitude of the fluid velocity at any point and ρ the density of the fluid concerned. Therefore, the total pressure P'_y acting on the bounding wall is given by

$$P'_y = -\int_{-\infty}^{\infty} p_r\,dx = -\tfrac{1}{2}\rho\int_{-\infty}^{\infty}(U^2 - |\mathbf{v}|^2)\,dx, \tag{27}$$

where the integral is taken from $-\infty$ to ∞ along the x-axis; and combining this with (26), we have

$$P_y = \tfrac{1}{2}\rho\int_{-\infty}^{\infty}(U^2 - |\mathbf{v}|^2)\,dx. \tag{28}$$

Denoting the lift acting on the aerofoil by L in place of P_y and remembering that along the x-axis, $dz = dx$ and $|\mathbf{v}| = u = \partial\phi/\partial x = \partial w/\partial x = dw/dz$, we have, from (28),

$$L = \tfrac{1}{2}\rho\int_{-\infty}^{\infty}\left\{U^2 - \left(\frac{dw}{dz}\right)^2\right\}dz. \tag{29}$$

5. Evaluation of the lift

For convenience in the evaluation of the above integral we transform it to the s-plane. Thus, remembering that the x-axis in the z-plane corresponds to the real axis of the ζ-plane as well as to the real axis of the s-plane, we have

$$L = \tfrac{1}{2}\rho\int_{-\pi}^{\pi}\left\{U^2 - \left(\frac{dw}{ds}\frac{ds}{d\zeta}\frac{d\zeta}{dz}\right)^2\right\}\left(\frac{dz}{d\zeta}\right)_{\zeta=\xi}\left(\frac{d\zeta}{ds}\right)_{s=\theta}d\theta, \tag{30}$$

where θ denotes the real axis of the s-plane.

We shall next calculate the value of the integrand. From (3), (5), and (16) we have

$$\left.\begin{aligned} \xi &= -a\sinh\sigma\cot\tfrac{1}{2}\theta, \\ \left(\frac{ds}{d\zeta}\right)_{s=\theta} &= \frac{1-\cos\theta}{a\sinh\sigma}, \\ \left(\frac{dw}{ds}\right)_{s=\theta} &= 2aU\sinh\sigma\{\wp(\theta)-\wp(s_1)\} \end{aligned}\right\}. \tag{31}$$

Also, we have from (17)

$$\left(\frac{dz}{d\zeta}\right)_{\zeta=\xi} = 1-\frac{2p^2\cos\gamma}{\{(\xi+\xi_0)^2+\eta_0^2\}^2}\{(\xi+\xi_0)^2-\eta_0^2+2(\xi+\xi_0)\eta_0\tan\gamma\}. \tag{32}$$

Thus, writing also

$$\left(\frac{dz}{d\zeta}\right)_{\zeta=\xi} \equiv S, \tag{33}$$

we have

$$\left(\frac{dw}{ds}\frac{ds}{d\zeta}\frac{d\zeta}{dz}\right)_{\substack{s=\theta\\ \zeta=\xi}} = 2U\{\wp(\theta)-\wp(s_1)\}(1-\cos\theta)S^{-1} \tag{34}$$

We now express the function $\wp(\theta)-\wp(s_1)$ in a form suitable for numerical calculations. Writing $u = s/2\omega_1$ we have in general

$$\wp(s)-e_1 = \left[\frac{\sigma_1(s)}{\sigma(s)}\right]^2 = \left[\frac{1}{2\omega_1}\frac{\vartheta_1'(0)\vartheta_2(u)}{\vartheta_2(0)\vartheta_1(u)}\right]^2. \tag{35}$$

If a complex variable v satisfies the relation

$$-\mathrm{re}\left(\frac{\tau}{i}\right) < \mathrm{re}\left(\frac{v}{i}\right) < \mathrm{re}\left(\frac{\tau}{i}\right), \tag{36}$$

we have (**8**)

$$\begin{aligned} &\frac{1}{4\pi}\frac{\vartheta_1'(0)\vartheta_1(v+w)}{\vartheta_1(v)\vartheta_1(w)} \\ &\quad = \tfrac{1}{4}\cot\pi v+\tfrac{1}{4}\cot\pi w+\sum_{n=1}^{\infty}\frac{q^{2n}\sin 2\pi(nv+w)-q^{4n}\sin 2n\pi v}{1-2q^{2n}\cos 2\pi w+q^{4n}}, \end{aligned} \tag{37}$$

from which, by putting $v = \frac{1}{2}$ and $w = u$, we obtain immediately

$$\frac{1}{4\pi}\frac{\vartheta_1'(0)\vartheta_2(u)}{\vartheta_2(0)\vartheta_1(u)} = \tfrac{1}{4}\cot\pi u+\sum_{n=1}^{\infty}(-1)^n\frac{q^{2n}\sin 2\pi u}{1-2q^{2n}\cos 2\pi u+q^{4n}}. \tag{38}$$

In our case, $\omega_1 = \pi$ and $\omega_3 = i\sigma$, and therefore, when s is equal to θ, we have $u = \theta/2\pi$. Thus, combining (35) with (38), we have

$$\wp(\theta)-e_1 = \left[\tfrac{1}{2}\cot\tfrac{1}{2}\theta+2\sum_{n=1}^{\infty}(-1)^n\frac{q^{2n}\sin\theta}{1-2q^{2n}\cos\theta+q^{4n}}\right]^2. \tag{39}$$

The parameter q is given by $q = e^{\tau\pi i}$. But, since $\tau = \omega_3/\omega_1 = i\sigma/\pi$, we have, using (3)

$$q = e^{-\sigma} = \frac{b}{a}-\sqrt{\left\{\left(\frac{b}{a}\right)^2-1\right\}}. \tag{40}$$

Next, when $s = s_1 = \omega_3 + \theta_1$, we have $u = s/2\omega_1 = \theta_1/2\omega_1 + \frac{1}{2}\tau$. Hence, if we put $u_1 = \theta_1/2\omega_1$, we have $u = u_1 + \frac{1}{2}\tau$ and

$$\wp(s_1) - e_1 = \left[\frac{1}{2\omega_1}\frac{\vartheta_1'(0)\vartheta_2(u_1+\frac{1}{2}\tau)}{\vartheta_2(0)\vartheta_1(u_1+\frac{1}{2}\tau)}\right]^2 = -\left[\frac{1}{2\omega_1}\frac{\vartheta_1'(0)\vartheta_4(u_1-\frac{1}{2})}{\vartheta_2(0)\vartheta_3(u_1-\frac{1}{2})}\right]^2. \quad (41)$$

In general, when a complex variable v satisfies the relation

$$-\mathrm{re}\left(\frac{\tau}{i}\right) < \mathrm{re}\left(\frac{v}{i}\right) < \mathrm{re}\left(\frac{\tau}{i}\right),$$

we have (9)

$$\frac{1}{4\pi}\frac{\vartheta_1'(0)\vartheta_3(v+w)}{\vartheta_1(v)\vartheta_3(w)} = \frac{1}{4\sin\pi v} - \\ - \sum_{n=1}^{\infty} \frac{q^{2n-1}\sin\pi[(2n-1)v+2w] + q^{4n-2}\sin(2n-1)\pi v}{1+2q^{2n-1}\cos 2\pi w + q^{4n-2}},$$

whence we have, by putting $v = \frac{1}{2}$ and replacing w by v,

$$\frac{1}{4\pi}\frac{\vartheta_1'(0)\vartheta_4(v)}{\vartheta_2(0)\vartheta_3(v)} = \frac{1}{4} - \sum_{n=1}^{\infty}(-1)^{n+1}\frac{q^{2n-1}\cos 2\pi v + q^{4n-2}}{1+2q^{2n-1}\cos 2\pi v + q^{4n-2}}. \quad (42)$$

By putting $v = u_1 - \frac{1}{2}$ in this formula and remembering that $\omega_1 = \pi$ and consequently $u_1 = \theta_1/2\pi$, we get

$$\frac{1}{2\omega_1}\frac{\vartheta_1'(0)\vartheta_4(u_1-\frac{1}{2})}{\vartheta_2(0)\vartheta_3(u_1-\frac{1}{2})} = \tfrac{1}{2} + 2\sum_{n=1}^{\infty}(-1)^{n+1}\frac{q^{2n-1}\cos\theta_1 - q^{4n-2}}{1-2q^{2n-1}\cos\theta_1+q^{4n-2}}, \quad (43)$$

and hence, by (41),

$$\wp(s_1) - e_1 = -\left[\tfrac{1}{2} + 2\sum_{n=1}^{\infty}(-1)^{n+1}\frac{q^{2n-1}\cos\theta_1 - q^{4n-2}}{1-2q^{2n-1}\cos\theta_1+q^{4n-2}}\right]^2. \quad (44)$$

Subtracting this from (39) we have

$$\wp(\theta) - \wp(s_1) = P + Q, \quad (45)$$

with

$$\left.\begin{aligned} P &= \left[\tfrac{1}{2}\cot\tfrac{1}{2}\theta + 2\sum_{n=1}^{\infty}(-1)^n\frac{q^{2n}\sin\theta}{1-2q^{2n}\cos\theta+q^{4n}}\right]^2 \\ Q &= \left[\tfrac{1}{2} + 2\sum_{n=1}^{\infty}(-1)^{n+1}\frac{q^{2n-1}\cos\theta_1 - q^{4n-2}}{1-2q^{2n-1}\cos\theta_1+q^{4n-2}}\right]^2 \end{aligned}\right\}, \quad (46)$$

and this formula is conveniently used for numerical calculation of the values of $\wp(\theta) - \wp(s_1)$.

Taking (31), (33), and (45) into account, the expression (30) for the lift becomes, after some reduction,

$$L = \tfrac{1}{2}\rho U^2 a \sinh\sigma \int_{-\pi}^{\pi}\left\{\frac{S}{1-\cos\theta} - 4(1-\cos\theta)(P+Q)^2\frac{1}{S}\right\}d\theta. \quad (47)$$

If, by using the chord length l of the aerofoil, we define the lift coefficient C_L as $C_L = L/(\frac{1}{2}\rho U^2 l)$, we have

$$C_L = \frac{a\sinh\sigma}{l}\int_{-\pi}^{\pi}\left\{\frac{S}{1-\cos\theta} - 4(1-\cos\theta)(P+Q)^2\frac{1}{S}\right\}d\theta. \tag{48}$$

Since the integrals in (47) and (48) are intractable, we have evaluated them numerically, and used the limiting values of the integrand when $\theta \to 0$, which are given by

$$\lim_{\theta\to 0}\left\{\frac{S}{1-\cos\theta} - 4(1-\cos\theta)(P+Q)^2\frac{1}{S}\right\}$$
$$= 1 - 2\left(\frac{p}{a\sinh\sigma}\right)^2\cos\gamma + 16\sum_{n=1}^{\infty}\frac{(-1)^{n+1}q^{2n}}{(1-q^{2n})^2} - 4Q. \tag{49}$$

6. Numerical calculations

As mentioned already, an aerofoil of approximate Joukowski type placed close to the ground can be obtained, in general, by transforming a circle in the vicinity of a plane wall by the aid of the transformation equation (17). But, in order to investigate the manner in which the ground-effect upon the lift of an aerofoil is modified by its thickness, it is convenient to take, if possible, a symmetrical aerofoil with no camber. Thus we have obtained a few approximately symmetrical aerofoils with very small camber by choosing appropriate numerical values for various constants contained in the transformation equation (17). For the purpose of computing the effect of the camber of an aerofoil, however, we have also investigated some aerofoils with slightly larger camber.

There are several ways of assigning appropriate numerical values for the constants in the transformation equation (17). But the most convenient way seems to be to assign at the outset appropriate numerical values for the three quantities $\xi_1+\xi_0$, η_1 and η_0. Then the values of p and γ can be determined by (21) and (22), and if we then obtain the second root ζ_2 of the equation $dz/d\zeta = 0$, by making use of those values of p and γ, we can determine, by (23), (25), and (24), the values of the chord length l, the angle of attack α, and the ratio l/H of the chord length l to the distance H from the midpoint of the chord to the ground respectively.

After some trials we found that an approximately symmetrical aerofoil of approximate Joukowski type placed near the ground, at an angle of attack as used in practice, can be obtained by assuming $\xi_1+\xi_0 = 1$, $\eta_1 = 1{\cdot}43$, and $\eta_0 = 1{\cdot}57$. The values of p, γ, l, α and l/H in this case are shown in Table 1 below.

The thickness of the aerofoil is determined mainly by the value of ξ_0, while the camber is determined by the value of β. Since our principal

object lies in the discussion of the manner in which the ground-effect on the lift of an aerofoil is modified by its thickness, we have taken the values of ξ_0 and β as shown in the table. Aerofoils A and B are both approximately symmetrical aerofoils of approximate Joukowski type with very small camber, while aerofoil C is an aerofoil of approximate Joukowski type with slightly larger camber. The values of $\xi_1+\xi_0$, η_1 and η_0, and consequently those of p, γ, l, α, and l/H as given in the table are all common to these three aerofoils. The values of the thickness ratio and camber for these three

TABLE 1

$\xi_1+\xi_0 = 1$, $p = 1{\cdot}04738$, $l/H = 3{\cdot}486$,
$\eta_1 = 1{\cdot}43$, $\gamma = 11^\circ 33' 50''$, $\alpha = 5^\circ 11' 45''$,
$\eta_0 = 1{\cdot}57$, $l = 4{\cdot}39343$

	Aerofoil A	*Aerofoil B*	*Aerofoil C*
ξ_0	−0·05	−0·1	−0·1
ξ_1	1·05	1·1	1·1
β	10°	10°	11° 30′
a	1·06620	1·11697	1·12254
b	1·61514	1·62396	1·65380
Thickness ratio	0·085	0·137	0·144
Camber	0·004	0·004	0·017
Lift coefficient C_L	0·2421π (= 0·761)	0·2415π (= 0·759)	0·3002π (= 0·943)

aerofoils are shown in the table.* The values of the constants a and b as calculated from (9) are also given in the table.

The aerofoils A, B, and C are shown in Fig. 5. As shown in Table 1, the thickness ratios of the aerofoils A and B are 0·085 and 0·137 respectively, while the aerofoil C has the thickness ratio of 0·144. The cambers of both aerofoils A and B are nearly equal to 0·004, while that of the aerofoil C is 0·017 approximately. Since the two aerofoils A and B have cambers nearly equal to each other, comparison of these two aerofoils enables us to anticipate the manner in which the ground-effect upon the lift of an aerofoil is modified by its thickness. Also, comparison of two aerofoils B and C with nearly equal thickness ratios enables us to anticipate the effect of the camber of the aerofoil upon the ground-effect of the lift.

Evaluating the integral in the formulae (47) and (48) numerically, the values of the lift L and the lift coefficient C_L of each of the three aerofoils have been obtained. To do this use has been made of the values of θ_1 and q

* As usual, the thickness ratio of an aerofoil is here defined as the ratio of the maximum thickness to the chord length of the aerofoil. Also, the camber of an aerofoil is here defined as the maximum distance of the camber line from the chord divided by the chord length.

which have been calculated with the aid of (12) and (40) respectively, by employing the values of a and b as shown in Table 1.

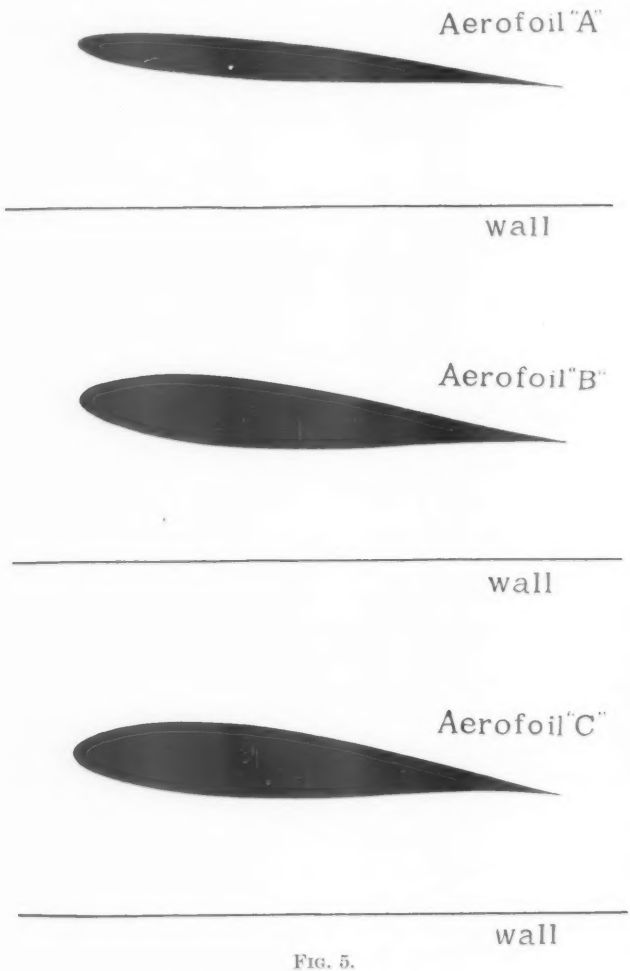

FIG. 5.

The values of the lift coefficient C_L thus calculated are given in Table 1. It is found that the value of C_L for the aerofoil C is much greater than that for the aerofoil B, despite the fact that these two aerofoils have nearly equal thickness ratios. This is perhaps due to difference between the cambers of these two aerofoils.

7. The lift on the aerofoils when placed in an unlimited stream

In order to investigate the manner in which the lift of an aerofoil is changed by the presence of the ground, we have calculated the lift L_0 experienced by the preceding three aerofoils when placed in an unlimited stream. There are in general several methods of calculating the lift of any given aerofoil placed in an infinite mass of fluid, but we have employed the method used by Kármán, Trafftz, Müller, and others.*

The values of the lift coefficient C_{L_0} thus calculated are shown in Table 2, where the values of C_L have been reproduced in the first row. The values of the ratio C_L/C_{L_0} are also given in the last row. For the sake of comparison, the values of the corresponding quantities for the plane aerofoil are given in the last column.†

TABLE 2

	Aerofoil A	*Aerofoil B*	*Aerofoil C*	*Plane aerofoil*
C_L	$0{\cdot}2421\pi$	$0{\cdot}2415\pi$	$0{\cdot}3002\pi$	$0{\cdot}2237\pi$
C_{L_0}	$0{\cdot}2092\pi$	$0{\cdot}2195\pi$	$0{\cdot}2795\pi$	$0{\cdot}1811\pi$
C_L/C_{L_0}	1·157	1·100	1·074	1·235

The results are shown in Fig. 6, where L/L_0 $(= C_L/C_{L_0})$ and l/H are the ordinate and abscissa respectively. In this figure the solid line curve shows the values of L/L_0 for the plane aerofoil placed at an angle of attack $\alpha = 5^\circ\ 11'\ 45''$, which have been calculated by using the general formula given some years ago by one of the present writers (**1**).

From Table 2 and Fig. 6 it will be seen that when an aerofoil of approximate Joukowski type with small thickness ratio is placed in the vicinity of the ground at a small angle of attack as used in practice, the lift is increased by the presence of the ground, just as in the case of the plane aerofoil, but the rate of increase becomes smaller as the thickness ratio increases. Further, by comparing the values of L/L_0 for the two aerofoils B and C, we see that the rate of increase of the lift due to the presence of the ground is greatly modified by the camber of the aerofoil, the rate of increase being decreased as the camber increases. The latter result is in agreement with the result of our investigations concerning the ground-effect on the lift of a circular arc aerofoil placed in a stream bounded by a plane rigid wall (**6**).

* The essentials of the method are described in W. F. Durand, *Aerodynamic Theory*, **2** (1936), 80–83.

† The value of C_L for the plane aerofoil has been calculated by the aid of the general formula as given by one of the present writers (**1**), assuming, as before, the value of the ratio l/H to be 3·486 and the angle of attack α to be $5^\circ\ 11'\ 45''$.

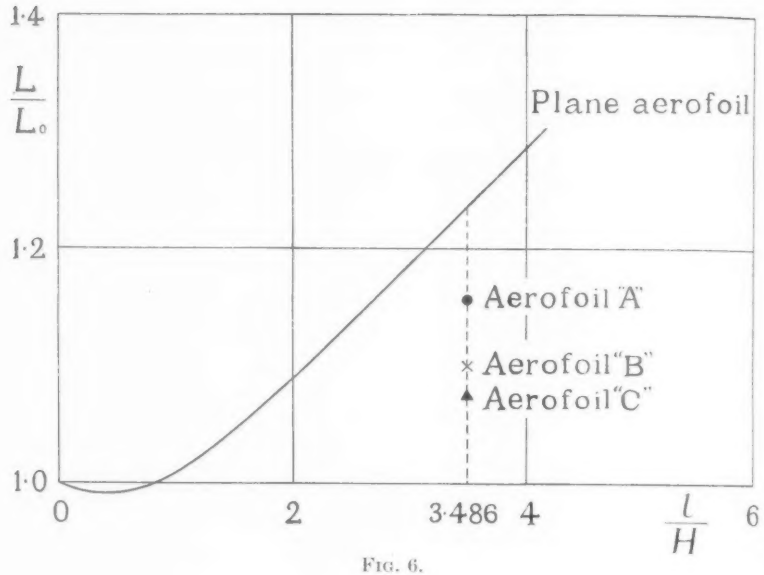
1·4
L/L₀
1·2
1·0
Plane aerofoil
Aerofoil "A"
Aerofoil "B"
Aerofoil "C"
0
2
3·486
4
l/H
6

FIG. 6.

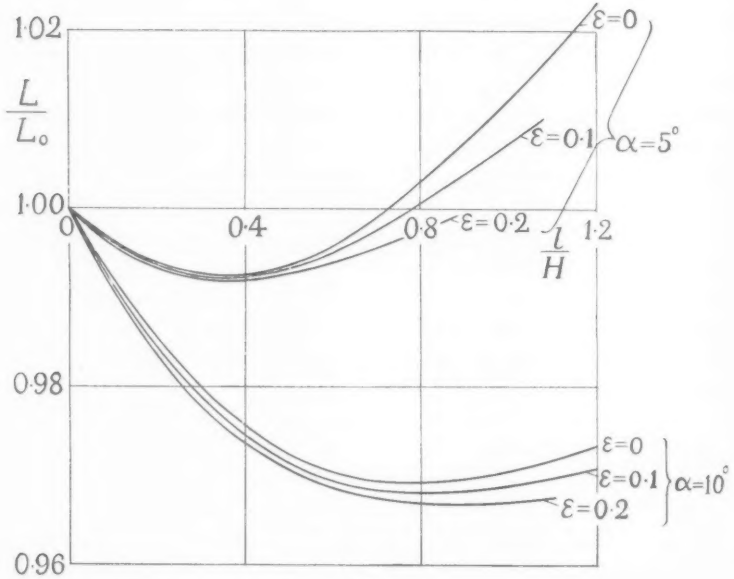
1·02
L/L₀
1·00
0·98
0·96
0
0·4
0·8
1·2
l/H
ε=0
ε=0·1
ε=0·2
α=5°
ε=0
ε=0·1
ε=0·2
α=10°

FIG. 7.

[*Note added January 1950*]

In a recent paper (**10**) Green has obtained the first three terms in the series expansion for the lift acting on the symmetrical Joukowski aerofoil of small thickness in the presence of a plane wall, and by comparing the results with those for a circular arc aerofoil he has conjectured that, for small values of the angle of attack, the effects of camber and thickness work mainly in opposite directions, so that the plane aerofoil might be expected to give a reasonable approximation to actual cases.

Quite recently Mr. H. Fujikawa has extended Green's calculations and obtained the first five terms in the series expansion for the lift acting on the symmetrical Joukowski aerofoil of small thickness in the presence of a plane wall. Fig. 7 shows, for comparison, the results of numerical calculations for three cases in which the thickness parameter ϵ of the aerofoil takes the values 0, 0·1, and 0·2 respectively, the corresponding thickness ratios being 0, 0·118, and 0·215 respectively. The values of the angle of attack have been taken to be 5° and 10°.

From this figure it will readily be seen that, in accordance with the results obtained in the present paper, the effect on the results for a plane aerofoil due to thickness acts in exactly the same direction as the effect due to camber.

REFERENCES

1. S. Tomotika, T. Nagamiya, and Y. Takenouti, 'The lift on a flat plate placed near a plane wall, with special reference to the effect of the ground upon the lift of a monoplane aerofoil', *Report Aeron. Res. Inst., Tokyo Imp. Univ.*, No. 97 (1933).
2. S. Tomotika, 'Further studies on the effect of the ground upon the lift of a monoplane aerofoil', ibid., No. 120 (1935).
3. S. Tomotika and I. Imai, 'The moment of the fluid pressure acting on a flat plate in a semi-infinite stream bounded by a plane wall, I. Case of lower boundary (The ground effect)', ibid., No. 153 (1937).
4. J. Bonder, 'Mouvement de deux cylindres dans le fluide parfait ainsi que les applications au vol à proximité du sol' (Polish, with French summary). *Comptes Rendus de la Société Polytechnique de Varsovie*, **4** (1925).
5. W. Müller, 'Abbildungstheoretische Grundlagen für das Problem des Tragflügels in Erdbodennähe', *Z.A.M.M.* **11** (1931), 231–6.
6. S. Tomotika, K. Tamada, and H. Umemoto, 'The lift and moment forces acting on a circular arc aerofoil in a stream bounded by a plane wall'. To appear in *Quart. Journ. Mech. and Applied Math.*
7. M. Lagally, 'Die reibungslose Strömung im Außengebiet zweier Kreise', *Z.A.M.M.* **9** (1929), 299–305.
8. J. Tannery and J. Molk, *Éléments de la théorie des fonctions elliptiques*, **4** (1902), 102.
9. —— —— ibid. 103.
10. A. E. Green, 'The two-dimensional aerofoil in a bounded stream', *Quart. J. of Math.* (Oxford), **18** (1947), 167–77.

THE PASSAGE OF TURBULENCE THROUGH WIRE GAUZES

By A. A. TOWNSEND (*Emmanuel College, Cambridge*)

[Received 29 August 1950]

SUMMARY

Measurements have been made of the turbulent intensities existing after the passage of isotropic turbulence through fine-mesh wire gauzes, and the results have been compared with the predictions of the theory of G. I. Taylor and G. K. Batchelor, who express the intensity reduction in terms of the pressure and refraction coefficients of the gauze. In agreement with the theory, the intensities of transverse components of the transmitted turbulence are considerably greater than that of the longitudinal component, but the degree of anisotropy is less than predicted. Observed reductions in total turbulent energy agree well with the predicted values. Upstream of the gauze, reductions of turbulent intensity are observed in very good agreement with theoretical predictions. It is concluded that the Taylor–Batchelor theory represents sufficiently accurately the motion at the gauze, but that turbulent energy transfer occurring within the zone of influence of the gauze leads to appreciable redistribution of energy between the turbulent velocity components. Outside this zone, energy transfer is comparatively weak, and the subsequent approach to isotropy is extremely slow.

Introduction

For many years it has been usual to place woven-wire gauzes in the settling-lengths of wind-tunnels with the object of reducing both the spatial variations of mean velocity due to flow around corner vanes and the intensity of the turbulent velocity fluctuations. The effectiveness of this procedure has been amply confirmed by experiment, but until recently no satisfactory theoretical treatment was available. L. Prandtl (**1**), who initiated the use of gauzes for the reduction of mean velocity fluctuations, gave an expression for the effect of gauzes on a steady stream in which the velocities along neighbouring stream-lines varied. In this work he took account only of the pressure coefficient of the gauze, but more recently A. R. Collar (**2**) has obtained a different relation. A more satisfactory theory has been developed by G. I. Taylor and G. K. Batchelor (**3**), who take into account the change in direction of the flow when the flow incident on the gauze is inclined to the normal. If the angle of incidence is not too large, this effect can be described by a 'refraction' coefficient, and this coefficient and the pressure coefficient both appear in the final equation for the reduction factor. It is shown that the equations given by Prandtl and Collar are special cases of the general equation, representing particular hypotheses about the 'refraction' coefficient. In all theories continuity of the velocity

component normal to the gauze is assumed. The theory can be extended to obtain expressions for the reduction of the intensity of isotropic turbulence in passing through a gauze, and Taylor and Batchelor compare their predictions with previously published measurements of the effect of gauzes on the background turbulence in wind-tunnels. These measurements were all made after passage of the turbulence through a large contraction of the tunnel, and not unexpectedly the agreement is poor. More recently G. B. Schubauer, W. G. Spangenberg, and P. S. Klebanoff (4) have published the results of measurements made immediately behind gauzes, but these results are also in poor agreement with the predictions of Taylor and Batchelor. In particular, the result that the attenuations of the down- and cross-stream components of the turbulence are not significantly different is at variance both with the theory and with some preliminary observations made in this laboratory some time ago. A more comprehensive set of measurements is now complete, and these results will be considered in relation to the Taylor–Batchelor theory of gauzes and to the properties of isotropic turbulence.

Notation

Consider Cartesian coordinates with Ox in the direction of the mean stream and origin in the plane of the gauze. The components of the instantaneous turbulent velocity fluctuation are denoted by u, v, w, with suffixes to indicate the values at particular parts of the field. Then, define

U the mean velocity,
θ the angle of incidence of the instantaneous flow,
ϕ the angle of emergence of the instantaneous flow,
$\alpha = \phi/\theta$,
ρ the fluid density,
Δp the pressure drop across the gauze at any point,
K the pressure coefficient of the gauze, defined by $\Delta p = \frac{1}{2}\rho U^2 K$.

Mean values are taken with respect to time at points fixed in space.

Results of the Taylor–Batchelor theory

In their treatment Taylor and Batchelor assume that viscosity plays no part in the phenomena except in the immediate neighbourhood of the gauze, and that the action of the gauze can be described in terms of the two parameters K and α, i.e. that the instantaneous pressure-drop across the gauze is

$$\Delta p = \tfrac{1}{2}K\rho(U+u)^2$$

and that the angles of incidence and emergence are related by

$$\phi = \alpha\theta.$$

It is also assumed that there are no dynamical changes in the turbulence while it is influenced by the presence of the gauze, such as would be caused by the ordinary processes of turbulent transfer and decay. On these assumptions, the action of a gauze on small disturbances is linear, and the effect on each single Fourier component of the velocity field may be computed separately. It turns out that the reduction in a Fourier component of the incident turbulence

$$u = A_1 e^{i[l(x-Ut)+my+nz]}$$

depends only on the direction of the wave-number vector (l, m, n). If spectral density functions F, G, H are defined such that

$F(l, m, n)\, dldmdn$ is the contribution to $\overline{u^2}$ of components of wave-numbers in the range l to $l+dl$, m to $m+dm$, n to $n+dn$,

$G(l, m, n)\, dldmdn$ is the contribution to $\overline{v^2}$ of components of wave-numbers in the range l to $l+dl$, m to $m+dm$, n to $n+dn$,

$H(l, m, n)\, dldmdn$ is the contribution to $\overline{w^2}$ of components of wave-numbers in the range l to $l+dl$, m to $m+dm$, n to $n+dn$,

then using the suffixes 1, 2, 3 to denote values respectively far upstream of the gauze, far downstream of the gauze, and immediately in front of the gauze, it is found that

$$F_2 = F_1 \frac{4\alpha^2\beta^2+(1+\alpha-\alpha K)^2}{4\beta^2+(1+\alpha+K)^2},$$

$$G_2+H_2 = (G_1+H_1)\left[\alpha^2+\beta^2 \frac{F_1}{G_1+H_1} \frac{(1+\alpha-\alpha K)^2-\alpha^2(1+\alpha+K)^2}{4\beta^2+(1+\alpha+K)^2}\right],$$

and

$$F_3 = F_1 \frac{(1+\alpha)^2}{4\beta^2+(1+\alpha+K)^2},$$

where

$$\beta^2 = l^2(m^2+n^2)^{-1}.$$

Knowing F_1, G_1, H_1, it is possible to compute the turbulent intensities and the mean squares of the spatial derivatives, and then to find the attenuation factors of these quantities:

$$\mu = \overline{u_2^2}/\overline{u_1^2}, \qquad \nu = (\overline{v_2^2}+\overline{w_2^2})/(\overline{v_1^2}+\overline{w_1^2}),$$

$$\mu' = \overline{\left(\frac{\partial u_2}{\partial x}\right)^2} \Big/ \overline{\left(\frac{\partial u_1}{\partial x}\right)^2}, \qquad \nu' = \left[\overline{\left(\frac{\partial v_2}{\partial x}\right)^2}+\overline{\left(\frac{\partial w_2}{\partial x}\right)^2}\right] \Big/ \left[\overline{\left(\frac{\partial v_1}{\partial x}\right)^2}+\overline{\left(\frac{\partial w_1}{\partial x}\right)^2}\right],$$

$$\mu_3 = \overline{u_3^2}/\overline{u_1^2}, \qquad \mu_3' = \overline{\left(\frac{\partial u_3}{\partial x}\right)^2} \Big/ \overline{\left(\frac{\partial u_1}{\partial x}\right)^2}.$$

If the incident turbulence is isotropic, it follows from the condition of incompressibility that

$$F_1 = (m^2+n^2)\Phi(l^2+m^2+n^2),$$
$$G_1 = (n^2+l^2)\Phi(l^2+m^2+n^2),$$
$$H_1 = (l^2+m^2)\Phi(l^2+m^2+n^2),$$

and, since the attenuation factor for any particular wave-number depends only on the direction of the wave-number vector and not on its magnitude, the total attenuation factors listed above are independent of the function* Φ. The computing of these factors is straightforward, but leads to rather lengthy algebraic expressions, and numerical results are given in Table 1. It is assumed that for $K > 0{\cdot}7$, $\alpha = 1{\cdot}1(1+K)^{-\frac{1}{2}}$, and that for $K < 0{\cdot}7$, $\alpha = (8-K)/(8+K)$, as found by Schubauer, Spangenberg, and Klebanoff.

TABLE I

K	α^2	μ	ν	μ'	ν'	μ_3	μ_3'
0·5	0·806	0·396	0·756	0·580	0·702	0·669	0·715
1	0·605	0·194	0·543	0·290	0·524	0·455	0·508
2	0·403	0·046	0·345	0·099	0·329	0·244	0·308
3	0·302	0·020	0·251	0·056	0·229	0·149	0·200
4	0·242	0·019	0·199	0·038	0·184	0·098	0·137
5	0·202	0·022	0·166	0·032	0·157	0·060	0·099

The obvious limitation of the theory is that it neglects the dynamic aspects of turbulent motion and assumes that the time necessary for completion of any of the processes of turbulent transfer and decay is very large compared with the time taken for a sample of turbulent fluid to pass through the zone of influence of the gauze. If L is the scale of the turbulent motion and u' is a typical velocity, then the condition is that

$$L/u' \gg D/U,$$

where D is the depth of the zone of influence. Since L and D are of the same order of magnitude, the condition becomes

$$u'/U \ll 1.$$

If u' and L refer to the energy-containing eddies, this condition is satisfied when the turbulent level is low. On the other hand, smaller eddies whose energy is derived from the large eddies have shorter 'reaction times', and may adjust themselves to the changed conformation of the turbulence sufficiently rapidly to make the overall effect of the gauze on them appreciably

* The paper of Taylor and Batchelor contains a contrary statement, but after publication the error was noticed by the authors. The factors computed are therefore of general validity for isotropic turbulence.

different from the theoretical prediction. These simple considerations lead to two necessary conditions for the validity of the theory, i.e.

(*a*) $u'/U \ll 1$,

(*b*) the eddies concerned shall not be too small compared with the energy-containing eddies.

Experimental arrangements

The measurements were made in the small wind-tunnel in the Cavendish Laboratory, which has a sufficiently low level of free-stream turbulence for this type of work. The greater part of the measurements were of the passage of approximately isotropic turbulence through gauzes of various solidities placed 79 cm. down-stream from the turbulence-producing grid. Apart from a small number of special measurements, the air-speeds were 480 cm. sec.$^{-1}$, 620 cm. sec.$^{-1}$, and 905 cm. sec.$^{-1}$, and the approximately isotropic turbulence was produced by passage of the air-stream through bi-plane grids of periodic spacing 2·54 cm. and 5·08 cm. and of spacing-diameter ratio 5·33.

The gauzes are of woven wire, fixed in light-alloy frames under sufficient tension to keep them reasonably flat. In the absence of incident turbulence, the flow down-stream of the gauzes changed from steady laminar flow at low wind-speeds to a three-dimensional periodic flow at intermediate speeds and finally to fully turbulent flow at higher speeds. Behind the higher resistance gauzes some spatial variation of mean velocity could be detected, approximately ± 3 per cent. from the mean for the highest resistance gauze. The effect of these variations on the transmitted turbulence is discussed below. The properties of the gauzes are given in Table II.

TABLE II

Gauze	*Mesh*	*Wire diameter*	*Solidity*	$\frac{U_c d^*}{\nu}$	*Pressure coefficient*		
					$U = 480$	$U = 620$	$U = 905$
	mm.	mm.					
A	0·635	0·234	0·60	26	3·4	3·2	3·1
B	0·508	0·152	0·51	48	2·31	2·08	1·87
C	0·705	0·173	0·43	50	1·44	1·32	1·21
D	1·59	0·254	0·294	53	0·582	0·535	0·506

Measurements were made of the mean squares of the down-stream velocity component, $\overline{u^2}$, and its derivative $\overline{(\partial u/\partial x)^2}$ in front of the gauze, and behind the gauze the quantities $\overline{u^2}$, $\overline{(\partial u/\partial x)^2}$, $\overline{v^2}$, $\overline{(\partial v/\partial x)^2}$ were measured. A few determinations of the spectrum functions of u and v were also made.

* The critical Reynolds number is based on the wire diameter d and the critical air velocity, U_c, at which the flow behind the gauze first becomes periodic. For an infinite cylinder, $U_c\, d/\nu = 40$ (Kovasznay **5**).

Standard techniques of hot-wire anemometry were used for all these measurements.

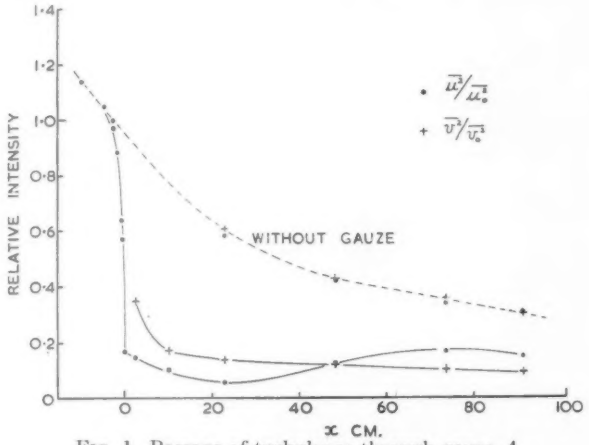

FIG. 1. Passage of turbulence through gauze A ($M = 5{\cdot}08$ cm., $U = 620$ cm. sec.$^{-1}$, $K' = 2{\cdot}94$).

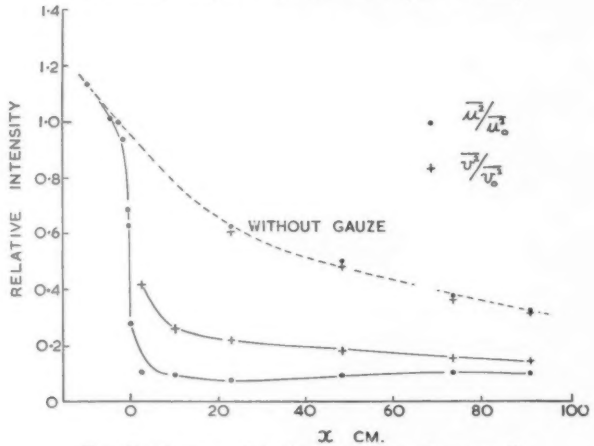

FIG. 2. Passage of turbulence through gauze B ($M = 5{\cdot}08$ cm., $U = 620$ cm. sec.$^{-1}$, $K' = 1{\cdot}70$).

Experimental results

The flow immediately behind the gauzes in the absence of incident turbulence changes from smooth steady flow to a regular periodic wake motion and then to fully turbulent flow as the wind-speed is increased. In all arrangements the scale of the wake motion behind the gauze was much smaller than the scale of the incident turbulence, and it seems likely that

the two motions are nearly independent, i.e. the intensity due to the transmitted turbulence can be obtained by subtracting the turbulent intensity due to the gauze alone from the total observed intensity. In this

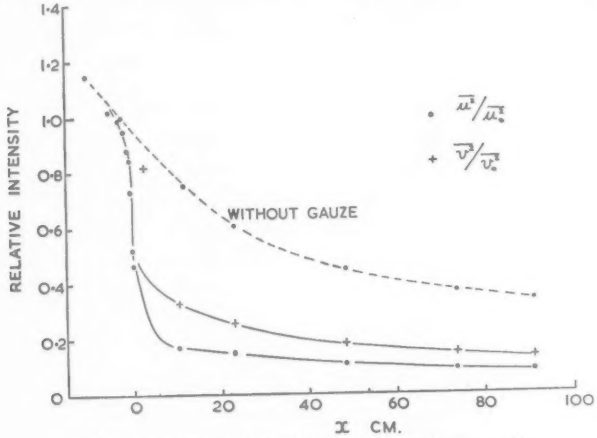

FIG. 3. Passage of turbulence through gauze C
($M = 5{\cdot}08$ cm., $U = 620$ cm. sec.$^{-1}$, $K' = 1{\cdot}12$).

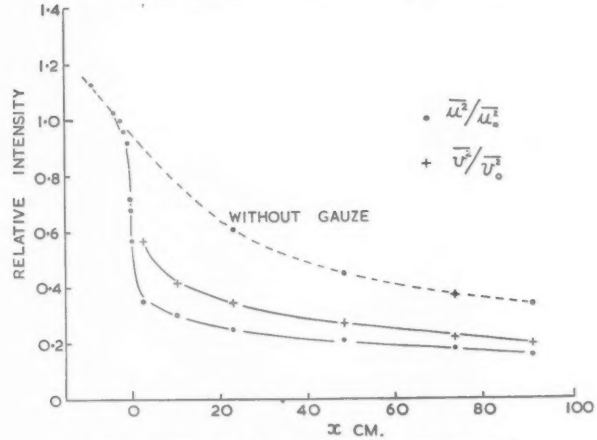

FIG. 4. Passage of turbulence through gauze D
($M = 5{\cdot}08$ cm., $U = 620$ cm. sec.$^{-1}$, $K' = 0{\cdot}47$).

way curves of the type shown in Figs. 1–4 were obtained, showing the variations of turbulent intensity on both sides of the gauze. It is noticeable that the two gauzes of high resistance produce far down-stream a large increase in the intensity of the down-stream velocity fluctuation, but only when an appreciable level of turbulence is incident on the gauze. This

phenomenon was observed by Schubauer, Spangenberg, and Klebanoff, and attributed to convection by the turbulent motion of the mean velocity pattern produced by local irregularities in the gauze. This explanation is consistent with the relative absence of any similar effect on the cross-stream component, but there is some evidence that the effect is an initial stage in the laminar instability of the mean velocity pattern, and that the turbulence provides an initial perturbation that is amplified. The two descriptions are identical in the initial stages of development, but the

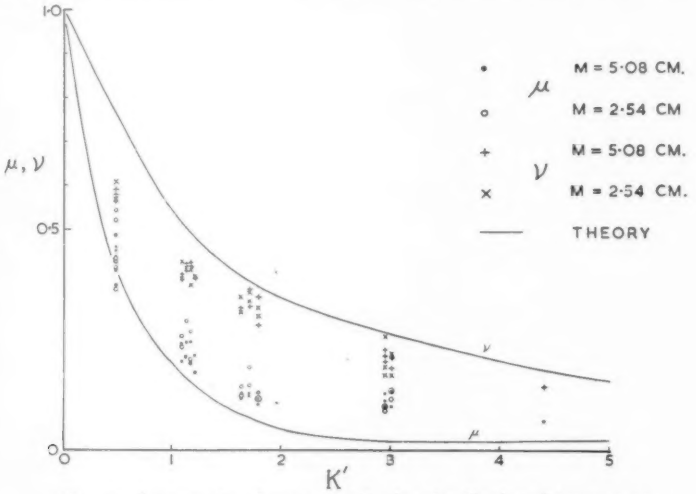

FIG. 5. Attenuation factors for the longitudinal and transverse velocity components.

occasional appearance of a small increase in the turbulent dissipation suggests that the instability hypothesis is more appropriate. For the practical problem of determining the reduction in intensity, the phenomenon can be disregarded if measurements are taken within 25 cm. of the gauze.

Fig. 5 shows the collected results for μ, the reduction factor for the longitudinal intensity, and ν, the reduction factor for the transverse intensity. The actual points represent the ratio of the intensity at a point behind the gauze to the intensity at the same point with the gauze removed, plotted against K', the differential pressure coefficient of the gauze. K' is defined by

$$\frac{d}{dU}(\Delta p) = \rho U K'$$

and is related to K by

$$K' = K\left(1 + \frac{1}{2}\frac{d(\log K)}{d(\log U)}\right).$$

This differential pressure coefficient is the one considered in the theory. Generally the values of ν are less than those predicted by the theory and the values of μ are greater. If values of $\frac{1}{3}(\mu+2\nu)$, the total attenuation of turbulent intensity, are compared with theoretical predictions the agreement is good for large values of K' but poor at small values (Fig. 6), where the observed factors are significantly less than those predicted.

The turbulence behind the gauze is distinctly anisotropic, but the re-

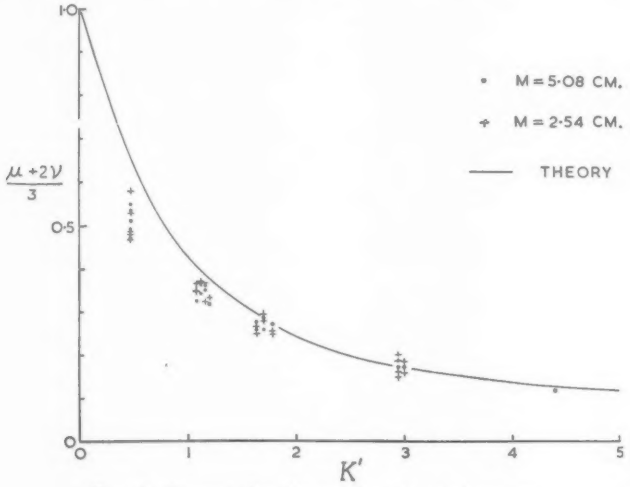

FIG. 6. Attenuation factors for the total energy.

covery of isotropy is very slow in the region accessible to observation (see Figs. 3–4). On the other hand, there is a rapid approach to local isotropy in the sense that, closely behind the gauze,

$$\overline{\left(\frac{\partial u}{\partial x}\right)^2} = \frac{1}{2}\overline{\left(\frac{\partial v}{\partial x}\right)^2},$$

within experimental error. This became evident in attempts to measure the attenuation factors for these quantities, i.e. μ' and ν'. The actual values of these attenuation factors change rapidly with distance of the point of observation from the gauze, but at any particular point the values of μ' and ν' were always equal within experimental error. Since in isotropic turbulence

$$\overline{\left(\frac{\partial u}{\partial x}\right)^2} = \frac{1}{2}\overline{\left(\frac{\partial v}{\partial x}\right)^2},$$

this must equally be true in the anisotropic turbulence behind the gauze.

Some trouble was taken to obtain measurements of turbulent intensities

on the up-stream side of the gauze, for it seems likely that the idealized theory should correspond most closely with practice in a region where the exact nature of the wake flow is unimportant. A hot-wire was mounted

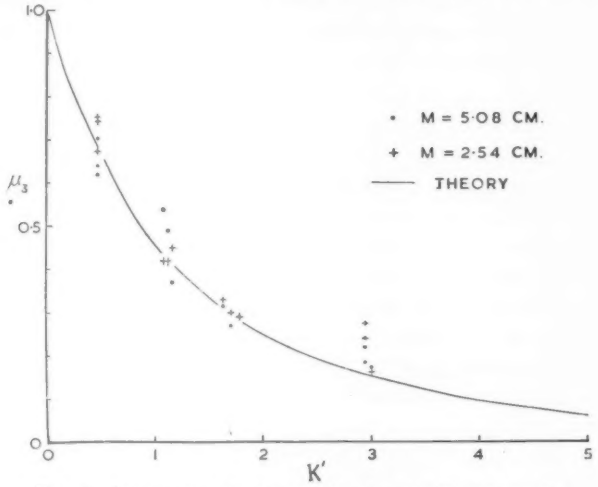

FIG. 7. Attenuation factors for the longitudinal intensity immediately upstream of the gauze.

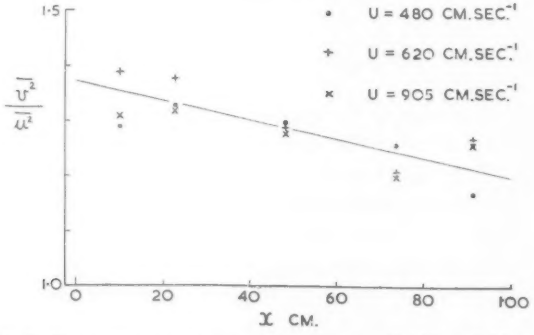

FIG. 8. Recovery of isotropy behind gauze D (M = 5·08 cm.).

on a holder that projected from the side of the wind-tunnel and could be rotated about an axis in the tunnel wall. By careful adjustment it was possible to measure $\overline{u^2}$ and $(\overline{\partial u/\partial x})^2$ at points within 8 cm. of the gauze. Both these quantities vary very rapidly close to the gauze, and much depends on the nerves of the experimenter who adjusts a delicate hot-wire to come within 1 mm. of the gauze with the knowledge that contact will break or damage the wire and so invalidate previous measurements. For

this reason measurements of μ_3' can be no more than upper limits to the true value, and only measurements of μ_3 are given in Fig. 8. These values are very close to the theoretical values, and while the results for μ_3' are very scattered their range is such that it is considered possible that experiments on a larger scale might verify the theory quite closely even in this respect. These results may be summarized.

(*a*) The reduction of turbulent intensity on the up-stream side of the gauze is described by the Taylor–Batchelor theory with adequate accuracy.

(*b*) The reduction of total turbulent intensity in passing through a gauze is consistent with the theory except for small values of K', when the observed reduction is greater than is predicted.

(*c*) As predicted by the theory, the turbulence emerging behind the gauze is anisotropic, with the intensities of the lateral components exceeding that of the longitudinal component. The degree of anisotropy is less than the theory predicts.

(*d*) The recovery of isotropy down-stream of the gauze is very slow, but local isotropy is valid within the range of observation in the sense that

$$\overline{\left(\frac{\partial u}{\partial x}\right)^2} = \frac{1}{2}\overline{\left(\frac{\partial v}{\partial x}\right)^2}.$$

Discussion

The experimental results outlined above bear on two distinct problems. The first and more practical problem is that of describing the passage of turbulence through a fine-mesh gauze, and it appears that the Taylor–Batchelor theory gives an accurate description of the behaviour up-stream of the gauze. Down-stream of the gauze the correspondence of theory and observation is not so close, and two sources of divergence may be distinguished. There is the excessive reduction of total turbulent intensity behind the gauzes of low resistance, and the tendency for the turbulence to be less anisotropic than the theory demands.

The excessive reduction of total turbulent intensity is unexpected, but it is possible that the results for the gauze of lowest resistance are influenced by the comparatively large mesh of this gauze. When flow behind the gauze is turbulent (as was true for gauze *D* at all wind-speeds), the possibility exists that gauze turbulence may act as an eddy viscosity to increase temporarily the energy dissipation of the transmitted turbulence, and so to increase the apparent reduction factor. Alternatively the passage through the gauze may distort the structure of the turbulence in such a way that the rate of energy dissipation becomes abnormally high for a short time. The first explanation is probably correct, at least for the gauze of lowest resistance.

The tendency for the transmitted turbulence to be less anisotropic than predicted is very natural, and, qualitatively, not surprising. What is surprising is that, after a short period of comparatively rapid interchange of energy between the velocity components, the ratio of the intensities becomes very nearly constant, and the once powerful tendency to isotropy

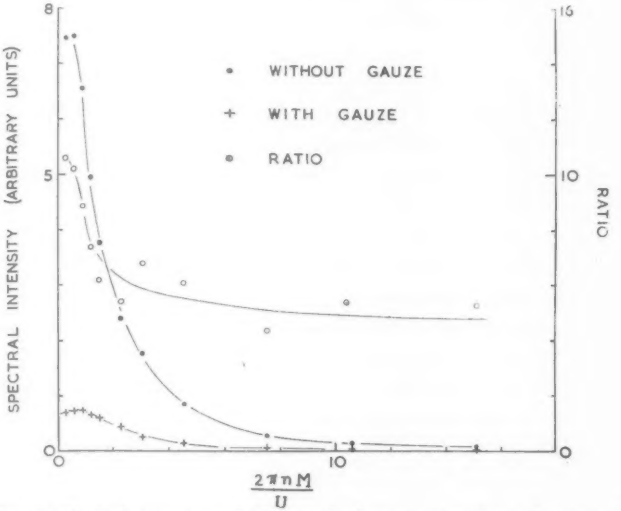

FIG. 9. Turbulent spectra before and after passage through gauze B ($M = 1{\cdot}27$ cm., $U = 526$ cm. sec.$^{-1}$, $K' = 1{\cdot}74$).

becomes a weak drift barely detectable (Figs. 3–4). Some explanation may be sought in the comparatively low Reynolds number of the turbulent flow down-stream of the gauze, and the initial rapid decrease of the ratio $\overline{v^2}/\overline{u^2}$ could be caused by adjustments of the smaller eddies in the direction of isotropy. That these adjustments occur, and occur rapidly, is shown by the validity of the local isotropy condition

$$\overline{\left(\frac{\partial u}{\partial x}\right)^2} = \frac{1}{2}\overline{\left(\frac{\partial v}{\partial x}\right)^2},$$

but the measurements behind the gauzes of highest resistance are difficult to reconcile with the notion that the initial approach to isotropy is purely concerned with the smaller eddies. For example, measurements of the spectrum of u in Fig. 9 show that the magnitude of the spectrum function at zero wave-number is reduced in the ratio 0·090. The theory predicts a ratio of 0·022, so even the large eddies determining this quantity have an initial rapid approach to isotropy. It is possible that flow behind the gauze

is not described by the theory at all, but this is improbable in view of the accurate confirmation of the predictions of total energy reduction. A more likely hypothesis is that, while the turbulence is in the zone of influence of the gauze, its configuration is such that interchange of energy between velocity components is very rapid. On this view, the initial rapid readjustment occurs only in the zone of influence of the gauze, and the subsequent slow approach to isotropy of the energy-containing eddies is typical of free turbulence.

This leads to the second problem, the nature of the processes which tend to establish isotropy in a field of homogeneous but anisotropic turbulence. It may be assumed that the turbulence behind a gauze is axisymmetric, which is the next simplest form of turbulence to isotropic, and details of the inertial transfer of energy between the velocity components might be obtained by measuring the approach to isotropy. The slowness of this approach makes it impossible to do anything quantitative by this method, but this slowness of recovery of isotropy is in general agreement with results of recent detailed studies of the rate of inertial redistribution of energy in the spectrum of isotropic turbulence (Stewart **6**, Stewart and Townsend **7**), and of the energy balance in turbulent wake flow (Townsend **8**). All this work tends to show that in free turbulent flows, i.e. flows not in any way confined by rigid boundaries, the customary image of feverish activity and instability of the energy-containing eddies is very far from the truth, and that these eddies are in fact highly permanent structures communicating energy preferentially to smaller eddies which contribute little to the total energy. This is clearly consistent with the present observations which show that only the smaller eddies have a reasonably strong tendency to isotropy. It would be very interesting to repeat and extend the work of MacPhail (**9**), who distorted a field of isotropic turbulence and observed the recovery of isotropy. Such an experiment avoids the difficulty of the present experiments, that an appreciable degree of anisotropy involves a large reduction in total turbulent energy.

REFERENCES

1. L. Prandtl, N.A.C.A. (U.S.A.) Tech. Mem. 726 (1933).
2. A. R. Collar, Brit. Aero. Res. Coun., R. and M. 1867 (1939).
3. G. I. Taylor and G. K. Batchelor, *Quart. J. Mech. and App. Math.* **2** (1949), 1–29.
4. G. B. Schubauer, W. G. Spangenberg, and P. S. Klebanoff, N.A.C.A. (U.S.A.) Tech. Note 2001 (1950).
5. L. S. G. Kovasznay, *Proc. Roy. Soc.* A, **198** (1949), 174–90.
6. R. W. Stewart, *Proc. Camb. Phil. Soc.* **47** (1951), 146–57.
7. —— and A. A. Townsend, *Phil. Trans.* (in the press).
8. A. A. Townsend, *Phil. Mag.* **41** (1950), 890–906.
9. D. C. MacPhail, Royal Aircraft Estab. Aero Rep. No. 1928 (1944).

THE ROUND LAMINAR JET

By H. B. SQUIRE

(*National Physical Laboratory, Teddington, Middlesex*)

[Received 28 December 1950]

SUMMARY

An exact solution of the equations of viscous fluid flow for axially-symmetric motion is derived. It is shown that this corresponds to the round laminar jet, or, alternatively, to the flow produced by the application of a force at a point in a viscous fluid. Some examples of the calculated streamlines are given. The effect of a source of heat at the point of application of the force is also considered.

1. Introduction

THE present paper discusses an exact solution of the Navier–Stokes equations for the flow of a viscous incompressible fluid for the case of axial symmetry. A special form of the stream function is assumed which corresponds to the component velocities being inversely proportional to the distance from the origin. The calculated flow turns out to be the exact solution for the flow in a round laminar jet emerging from an orifice at or near the origin; this flow has already been studied by Schlichting (ref. **1**, section 57) using the approximations of boundary layer theory. It is further shown that the flow may be regarded as that resulting from the application of a force applied at a point in a viscous fluid which is at rest at infinity. If, in addition to the force, a source of heat is introduced at the same point we obtain an idealized representation of a heated laminar jet.

From a mathematical viewpoint, the flow discussed here is the axially-symmetric analogue of the two-dimensional flow between non-parallel plane walls (ref. **1**, section 42, or ref. **2**). In both cases the velocities are inversely proportional to the distance from the origin and this condition could be regarded as the starting point of the analysis for each case.

The relation between laminar and turbulent jets is briefly considered in the appendix.

2. The equations of motion

We take spherical polar coordinates (r, θ, ϕ) with θ measured from the axis of the jet (Fig. 1). The velocity components are $(u, v, 0)$ measured in the directions of (r, θ, ϕ) respectively, and all quantities are independent of ϕ. The equation of continuity is (**1**, section 41)

$$\frac{1}{r^2}\frac{\partial}{\partial r}(r^2 u) + \frac{1}{r\sin\theta}\frac{\partial}{\partial \theta}(v\sin\theta) = 0,$$

and the equations of motion are

$$u\frac{\partial u}{\partial r}+\frac{v}{r}\frac{\partial u}{\partial \theta}-\frac{v^2}{r}=-\frac{1}{\rho}\frac{\partial p}{\partial r}+\nu\left(\nabla^2 u-\frac{2u}{r^2}-\frac{2}{r^2}\frac{\partial v}{\partial \theta}-\frac{2v\cot\theta}{r^2}\right),$$

$$u\frac{\partial v}{\partial r}+\frac{v}{r}\frac{\partial v}{\partial \theta}+\frac{uv}{r}=-\frac{1}{\rho r}\frac{\partial p}{\partial \theta}+\nu\left(\nabla^2 v+\frac{2}{r^2}\frac{\partial u}{\partial \theta}-\frac{v}{r^2\sin^2\theta}\right),$$

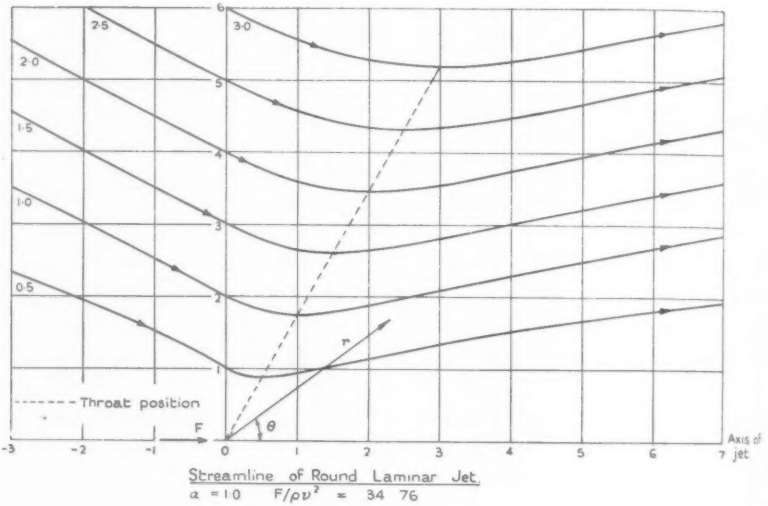

Streamline of Round Laminar Jet.
$\alpha = 10 \quad F/\rho\nu^2 = 34\ 76$

FIG. 1.

where p is the pressure, ρ is the density, ν is the kinematic viscosity, and

$$\nabla^2=\frac{1}{r^2}\frac{\partial}{\partial r}\left(r^2\frac{\partial}{\partial r}\right)+\frac{1}{r^2\sin\theta}\frac{\partial}{\partial \theta}\left(\sin\theta\frac{\partial}{\partial \theta}\right).$$

We shall assume that the stream function ψ has the form

$$\psi=\nu r f(\theta) \tag{1}$$

so that

$$\left.\begin{aligned} u&=\frac{1}{r^2\sin\theta}\frac{\partial\psi}{\partial\theta}=\frac{\nu}{r\sin\theta}f'(\theta)\\ v&=-\frac{1}{r\sin\theta}\frac{\partial\psi}{\partial r}=-\frac{\nu}{r\sin\theta}f(\theta)\end{aligned}\right\}. \tag{2}$$

Thus the velocity components are inversely proportional to r and hence

$$\nabla^2 u=\frac{1}{r^2\sin\theta}\frac{\partial}{\partial\theta}\left(\sin\theta\frac{\partial u}{\partial\theta}\right),$$

$$\nabla^2 v=\frac{1}{r^2\sin\theta}\frac{\partial}{\partial\theta}\left(\sin\theta\frac{\partial v}{\partial\theta}\right)=\frac{1}{r^2}\left(\frac{\partial^2 v}{\partial\theta^2}+\frac{\partial v}{\partial\theta}\cot\theta\right),$$

$$\frac{\partial u}{\partial r}=-\frac{u}{r},\qquad \frac{\partial v}{\partial r}=-\frac{v}{r},$$

and, from the equation of continuity,

$$u+\frac{\partial v}{\partial\theta}+v\cot\theta=0,$$

$$\frac{\partial u}{\partial\theta}+\frac{\partial^2 v}{\partial\theta^2}+\frac{\partial v}{\partial\theta}\cot\theta-v\,\mathrm{cosec}^2\theta=0.$$

Using these relations the equations of motion become

$$-\frac{u^2+v^2}{r}+\frac{v}{r}\frac{\partial u}{\partial\theta}=-\frac{1}{\rho}\frac{\partial p}{\partial r}+\frac{\nu}{r^2\sin\theta}\frac{\partial}{\partial\theta}\left(\sin\theta\frac{\partial u}{\partial\theta}\right), \tag{3}$$

$$\frac{v}{r}\frac{\partial v}{\partial\theta}=-\frac{1}{\rho r}\frac{\partial p}{\partial\theta}+\frac{\nu}{r^2}\frac{\partial u}{\partial\theta}. \tag{4}$$

From (4) we obtain the pressure by integration as

$$\frac{p-p_0}{\rho}=-\frac{v^2}{2}+\frac{\nu u}{r}+\frac{c_1}{r^2}, \tag{5}$$

where p_0 is the pressure at infinity, at which u and v vanish, c_1 is a constant of integration, and we exclude any other terms which depend on r only by consideration of (3). Hence, from (5) and (2),

$$\frac{1}{\rho}\frac{\partial p}{\partial r}=\frac{v^2}{r}-\frac{2\nu u}{r^2}-\frac{2c_1}{r^3}$$

and (3) becomes

$$-\frac{u^2}{r}+\frac{v}{r}\frac{\partial u}{\partial\theta}=\frac{\nu}{r^2}\left[2u+\frac{1}{\sin\theta}\frac{\partial}{\partial\theta}\left(\sin\theta\frac{\partial u}{\partial\theta}\right)\right]+\frac{2c_1}{r^3}. \tag{6}$$

Before substituting into (6) we change the variable to $\mu=\cos\theta$, so that $\sin\theta=\sqrt{(1-\mu^2)}$ and

$$\frac{1}{\sin\theta}\frac{d}{d\theta}=-\frac{d}{d\mu},$$

when equations (2) become

$$u=-\frac{\nu}{r}f'(\mu),\qquad v=-\frac{\nu}{r}\frac{f(\mu)}{\sqrt{(1-\mu^2)}}. \tag{7}$$

Substituting in (6) we obtain

$$[f'(\mu)]^2+f(\mu)f''(\mu)=2f'(\mu)+\frac{d}{d\mu}[(1-\mu^2)f''(\mu)]-2c_1. \tag{8}$$

Integration gives

$$ff'=2f+(1-\mu^2)f''-2c_1\mu-c_2, \tag{9}$$

where c_2 is a second constant of integration. Integrating again we get

$$f^2=4\mu f+2(1-\mu^2)f'-2(c_1\mu^2+c_2\mu+c_3), \tag{10}$$

where c_3 is a third constant of integration.

We now suppose that (10) has a solution of the form

$$f = \alpha(1+\mu)+\beta(1-\mu),$$

where α and β are arbitrary constants which depend on c_1, c_2, and c_3. (The existence of a solution of this type requires that one linear relation between c_1, c_2, and c_3 shall be satisfied.) Then a more general solution of (10) can be derived by standard methods to be

$$f = \alpha(1+\mu)+\beta(1-\mu)+2(1-\mu^2)\left[\frac{(1+\mu)^\beta}{(1-\mu)^\alpha}\right]\Big/\left[a - \int_1^\mu \frac{(1+\mu)^\beta}{(1-\mu)^\alpha}\,d\mu\right],$$

where a is a further constant of integration. For the remainder of the present paper we shall restrict consideration to the case $\alpha = \beta = 0$ for which this solution becomes†

$$f = \frac{2(1-\mu^2)}{a+1-\mu} = \frac{2\sin^2\theta}{a+1-\cos\theta}. \tag{11}$$

3. Description of the flow

The streamlines are given by

$$\psi = \nu r f(\mu) = \text{constant},$$

where $f(\mu)$ is given by (11). They all have the same shape for a given value of a, and are shown for $a = 1$, 10^{-1}, and 10^{-2} in Figs. 1–3.

The stream tubes have a minimum area or throat at the station which is given by $\mu = \cos\theta = (1+a)^{-1}$, and this direction is indicated in Figs. 1–3.

We can interpret the solution as a jet issuing from a nozzle which coincides with one of the streamlines as far as its throat; it must be assumed, however, that a special frictional boundary condition is satisfied on the walls of this nozzle. In the central part of the jet the flow is very similar to Schlichting's approximate solution which can be obtained by assuming the pressure to be constant, by neglecting the first term on the right-hand side of equations (6), (8), (9), and by supposing that $(1-\mu) \ll 1$. In place of (11) we should obtain

$$f(\mu) = \frac{4(1-\mu)}{a+(1-\mu)}, \tag{11a}$$

valid for $(1-\mu) \ll 1$, $a \ll 1$.

There is, however, a more fundamental interpretation of the solution. This is obtained by supposing that the flow is generated by the continuous application of a force F at the origin acting in the direction of the resulting jet. The magnitude of this force can be evaluated by integrating the rate

† This also corresponds to $c_1 = c_2 = c_3 = 0$.

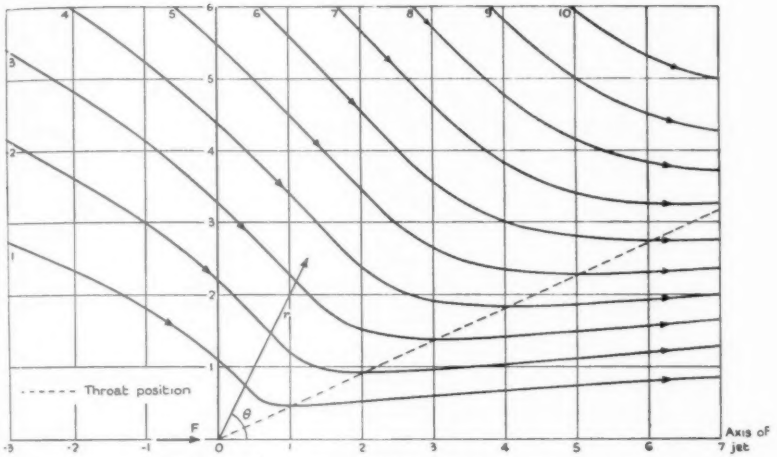
Throat position
F
θ
Axis of jet
Streamlines of Round Laminar Jet.
$a = 10^{-1}$ $F/\rho\nu^2 = 3{\cdot}140 \times 10^2$

FIG. 2.

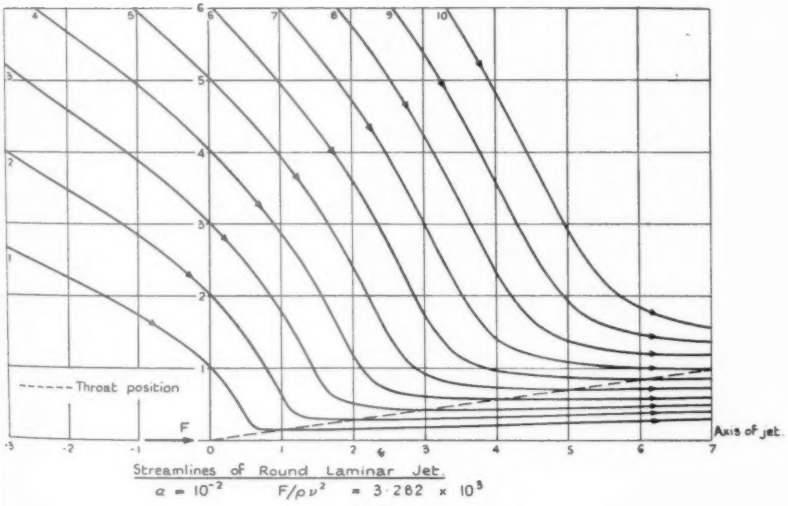
Throat position
F
Axis of jet.
Streamlines of Round Laminar Jet.
$a = 10^{-2}$ $F/\rho\nu^2 = 3{\cdot}282 \times 10^3$

FIG. 3.

of transfer of momentum across a sphere $r = \text{const.}$ due to the pressure and kinetic momenta and to the viscous stress. We obtain the result

$$\frac{F}{2\pi\rho\nu^2} = \frac{32(a+1)}{3a(a+2)} + 8(1+a) - 4(1+a)^2 \log[(a+2)/a]. \tag{12}$$

The most important contribution for $a \ll 1$ comes from the jet momentum. The following numerical values were obtained:

a	1·0	10^{-1}	10^{-2}
$F/\rho\nu^2$	$3{\cdot}476 \times 10$	$3{\cdot}140 \times 10^2$	$3{\cdot}282 \times 10^3$

It is interesting to note the importance of the non-dimensional quantity $[\text{force}/\rho\nu^2]$ in the present problem.

4. Temperature field of a heat source at the origin

Suppose that, in addition to the force F, we have a heat source of strength Q at the origin, such that its effect on the velocity and density distributions may be neglected except very near the origin. This system can be realized experimentally by a hot jet with a small orifice at or near the origin. Then the temperature at any point in the field satisfies the equation (**1**, chap. 14)

$$u\frac{\partial T}{\partial r} + \frac{v}{r}\frac{\partial T}{\partial \theta} = \kappa\nabla^2 T, \tag{13}$$

where T represents the excess temperature above the temperature of the fluid at a large distance and κ is the thermometric conductivity. We put

$$T = \frac{1}{r}g(\theta), \tag{14}$$

so that, with ∇^2 as in section 2,

$$\nabla^2 T = \frac{1}{r^2 \sin\theta}\frac{\partial}{\partial\theta}\left(\sin\theta\,\frac{\partial T}{\partial\theta}\right).$$

Changing the variable to $\mu = \cos\theta$ and substituting for the velocity components from (7), equation (13) becomes

$$f'(\mu)g(\mu) + f(\mu)g'(\mu) = \frac{1}{\sigma}\frac{d}{d\mu}[(1-\mu^2)g'(\mu)],$$

where $\sigma = \nu/\kappa$ is the Prandtl number of the fluid. On integration we obtain

$$\sigma fg = (1-\mu^2)g',$$

the constant of integration vanishing since $f = 0$ on the axis of the jet $\mu = 1$. Substituting for f from (11) we get

$$\frac{g'}{g} = \frac{2\sigma}{a+1-\mu},$$

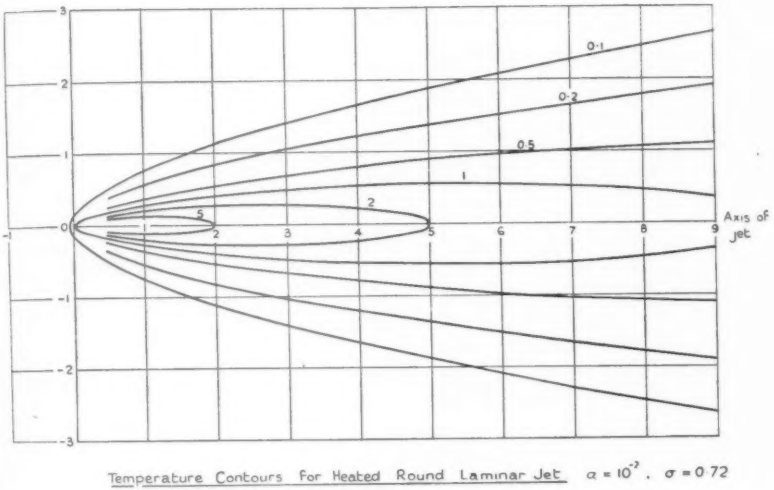

FIG. 4.

the solution of which is

$$g(\mu) = A\left(\frac{a}{a+1-\mu}\right)^{2\sigma}, \tag{15}$$

where A is a constant which depends on the source strength. The source strength Q is determined from the heat flux across a sphere of radius r, the quantity of heat crossing unit area in unit time being $\rho c_p v_n T$, where v_n is the velocity normal to the area and c_p is the specific heat of the fluid at constant pressure. In this way we obtain the formula

$$\frac{Q}{2\pi\rho c_p \nu} = A\int_{-1}^{1} f'(\mu)g(\mu)\,d\mu,$$

and, with $f(\mu)$ and $g(\mu)$ given by (11) and (15),

$$\frac{Q}{4\pi\rho c_p \nu} = A\left[\left(\frac{a+2}{2\sigma+1}\right)\left\{1-\left(\frac{a}{a+2}\right)^{2\sigma+1}\right\}-\left(\frac{a}{2\sigma-1}\right)\left\{1-\left(\frac{a}{a+2}\right)^{2\sigma-1}\right\}\right].$$

For $a \ll 1$,

$$\frac{Q}{4\pi\rho c_p \nu} = \frac{2A}{2\sigma+1}$$

approximately, and then, from (14) and (15),

$$T = \frac{(2\sigma+1)Q}{8\pi\rho c_p \nu r}\left(\frac{a}{a+1-\mu}\right)^{2\sigma}. \tag{16}$$

Fig. 4 gives the temperature contours for $a = 0{\cdot}01$, corresponding to the velocity contours of the jet shown in Fig. 3, taking $\sigma = 0{\cdot}72$ (the value for air), and

$$\frac{(2\sigma+1)Q}{8\pi\rho c_p \nu} = A = 10.$$

We may note that for $a \ll 1$, $1-\mu \ll 1$, the radial velocity distribution, given by (7) and (8), is

$$u = \frac{\nu}{ar}\left(\frac{a}{a+1-\mu}\right)^2.$$

Comparing this with (16) we see that the temperature and radial velocity distributions are similar within the jet for $\sigma = 1$.

Acknowledgement

The work described above was carried out in the Aerodynamics Division of the National Physical Laboratory, and it is published on the recommendation of the Aeronautical Research Council and by permission of the Director of the Laboratory.

APPENDIX

The Relation between Laminar and Turbulent Jets

Though very different in detail, the flow in a turbulent jet bears a general resemblance to the flow in a laminar jet. As will be seen from the analysis below, the turbulent jet is an example of turbulent flow for which the eddy viscosity may be treated as a constant throughout the jet, at least as far as the main features are concerned.

We first determine the value of a which corresponds to the turbulent jet, from the observed rate of spread of the jet. Experiments (**3**, **4**) show that the stations at which the velocity is one-half the velocity on the axis at the same cross-section lie on a cone of semi-angle 5°. From the theory of the laminar jet given above we obtain this observed rate of spread if we take $a = 0{\cdot}0092$. Hence the flow in the jet, and more particularly the flow outside the jet, will resemble that shown in Fig. 3 for which $a = 0{\cdot}01$. If ϵ is the eddy viscosity of the turbulent jet then, from (12) with $a = 0{\cdot}0092$,

$$\frac{F}{2\pi\rho\epsilon^2} = 476.$$

Also if the jet is formed by a uniform stream of velocity U_0 coming out of an orifice of diameter d the applied force F is equal to the jet thrust so that

$$F = \tfrac{1}{4}\pi\rho U_0^2 d^2,$$

and hence

$$\epsilon = 0{\cdot}0162 U_0 d.$$

This equation gives the value of the eddy viscosity of the turbulent jet in terms of the exit conditions.

The mean velocities for the turbulent jet can be calculated from equation (7) if ν is replaced by ϵ. It is shown in (3) that the velocity distribution calculated for a laminar jet is in good agreement with measurements made with a turbulent jet.

REFERENCES

1. S. Goldstein (ed.), *Modern Developments in Fluid Dynamics* (Oxford, 1938).
2. L. Rosenhead, *Proc. Roy. Soc.* A, **175** (1940), 436–67.
3. J. Hinze and B. van der Hegge Zijnen, *Applied Scientific Research*, A, **1** (1949), 435–61.
4. H. B. Squire, *Aircraft Engineering*, **22** (1950), 62–67.

THE EFFECT OF FRICTION ON SURGES IN LONG PIPE-LINES

By A. M. BINNIE (*Trinity College, Cambridge*)

[Received 16 January 1951]

SUMMARY

A pressure fluctuation occurs in a pipe-line when the velocity of the liquid in it is altered by means of a valve. A method of calculating these surges in a gravity pipe-line is described for the two cases when the exit velocity is reduced to zero (i) instantaneously and (ii) at a uniform rate. Allowance is made for the effect of friction, which is assumed to be proportional to the velocity, but the method may be used to provide an approximate result when the friction loss follows some other relation. Dimensionless quantities are employed, and the working is expressed in terms of a single characteristic number k, which depends upon the properties of the pipe-line and of the liquid in it. The method holds good unless k is too large. For the two cases, numerical results are given for a small and a large value of k, and they are compared with those derived by the graphical method of solution.

1. Introduction

When a valve controlling the flow of liquid in a pipe-line is moved, a pressure surge occurs which may have serious consequences. Hitherto the prediction of these surges has commonly proceeded on the assumption that friction effects are negligible. If the pipe-line is long, this supposition is doubtful, but the matter has received no great attention, and few reliable experimental results have been published. However, a report issued by the Joint Surge Conference (**1**) now makes available a full account of the pressure fluctuations observed in very long oil pipe-lines by means of modern electrical gauges linked together by wireless. Of particular interest are the results obtained with gravity pipe-lines when the control valve at exit was shut either suddenly or in such a way that the velocity near the valve was reduced at a uniform rate to zero in a known time. A graphical analysis is given, which (as explained in reference **2**) is based on the work of Allievi, Bergeron, and Schnyder; this allows for friction, but supposes that it is concentrated at a finite number of points. In the present paper this limitation is removed, and a way of calculating the surges is described, the friction being distributed uniformly along the pipe-line. The labour involved is trivial compared with that of carrying out the experiments. In general, the method will not hold good until the motion ceases, but it will usually be applicable at least to the first surge in which, of course, the greatest pressure is developed.

The same idealizing assumptions are made as in the graphical method. The liquid, the pipe, and its surroundings are taken to possess perfect and linear elasticity so that the velocity of a pressure wave is constant. The reflections at the open and the closed ends of the pipe-line are also perfect, and the motion is regarded as one-dimensional, the velocity over a cross-section being uniform. The only loss of energy which is taken into account is the same as that shown up in steady flow by a fall in pressure along the pipe-line. The particle velocity is supposed small; therefore the product terms in the equation of motion may be neglected. The surges under consideration are analytically similar to those in an electric cable, and the two problems mentioned above are solved by operational methods developed from Heaviside's classical work.

2. General theory of the waves

To avoid complications arising from the varying gradients of actual pipe-lines, we consider the arrangement depicted in Fig. 1. The uniform pipe-

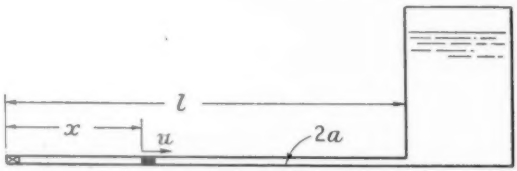

FIG. 1. Arrangement of pipe-line.

line, of length l and internal radius a, is assumed to be horizontal; it is supplied from a large reservoir, and the flow is controlled by means of a valve at outlet. The displacement and mean velocity at a cross-section distant x from the valve are denoted by ξ and u, which are connected with time t by the relation

$$u = \frac{\partial \xi}{\partial t}. \tag{2.1}$$

We also have that

$$s = -\frac{\partial \xi}{\partial x}, \tag{2.2}$$

$$\rho = \rho_0(1+s), \tag{2.3}$$

$$P = c^2 \rho_0 s, \tag{2.4}$$

where s is the condensation, ρ is the density, c is the velocity of sound, and P is the pressure measured from a zero where the density is ρ_0.

The dynamical equation for an element of unit length (Fig. 1) is

$$\frac{\partial u}{\partial t} = X - \frac{1}{\rho}\frac{\partial P}{\partial x} = X - \frac{c^2}{\rho_0}\frac{\partial \rho}{\partial x}, \tag{2.5}$$

where X is the extraneous force per unit of mass. No information is available by means of which X can be determined when u is varying, and we must be content to employ the value which obtains under steady conditions. In steady laminar flow the tangential stress at the wall is $4\mu u/a$, where μ is the viscosity, and it acts over an area $2\pi a$. The mass of the element is $\rho\pi a^2$, hence

$$X = -\frac{8\nu}{a^2}u = -Ku, \quad \text{say}, \tag{2.6}$$

where ν is the kinematic viscosity. When the initial motion is turbulent, the friction loss varies approximately as u^2, and even with the simple index 2 the ensuing equations become too complicated to be of service. To avoid this difficulty, the factor in (2.6), by which u is multiplied, will be adjusted to give the correct loss of head at the pipe exit under the steady conditions which prevail before the valve is moved. This procedure seems the best that can be adopted, and it is reasonable in view of the uncertainty mentioned above. We then find with the aid of (2.3) that (2.5) becomes

$$\frac{\partial u}{\partial t} = -Ku - c^2\frac{\partial s}{\partial x}. \tag{2.7}$$

Since numerical work will be required later, it is desirable to remove dimensional factors from the equations. This can be effected by writing

$$x = lx', \qquad \xi = l\xi', \qquad u = cu', \qquad t = \frac{l}{c}t', \qquad k = \frac{l}{c}K, \qquad P = c^2\rho_0 P', \tag{2.8}$$

in (2.1), (2.2), (2.4), and (2.7), which then become

$$u' = \frac{\partial \xi'}{\partial t'}, \tag{2.9}$$

$$s = -\frac{\partial \xi'}{\partial x'}, \tag{2.10}$$

$$P' = s, \tag{2.11}$$

$$\frac{\partial u'}{\partial t'} = -ku' - \frac{\partial s}{\partial x'}. \tag{2.12}$$

Only one number k remains, and this may be termed the characteristic number of the pipe-line and the liquid in it. Hereafter the dashes will be suppressed, and all quantities, including the boundary conditions which will be introduced, will carry non-dimensional significance.

To determine the consequence of the closure of the valve, it is necessary to form the differential equation for ξ. This is done by substituting (2.9) and (2.10) in (2.12) with the result

$$\frac{\partial^2 \xi}{\partial x^2} - k\frac{\partial \xi}{\partial t} - \frac{\partial^2 \xi}{\partial t^2} = 0. \tag{2.13}$$

3. Instantaneous closure of the valve

We suppose that before the valve is shut the steady velocity throughout the pipe-line is $u = -U$, the variations in velocity due to the changing condensation along the pipe-line being negligible. The condensation at the inlet to the pipe-line is denoted by S, which remains constant throughout all the ensuing changes in u. Then from (2.10) and (2.12)

$$\xi = -Sx+kUx-\tfrac{1}{2}kUx^2, \tag{3.1}$$

an expression which is arranged to give $s = S$ at $x = 1$ and $\xi = 0$ at $x = 0$. This equation and

$$\frac{\partial \xi}{\partial t} = -U \tag{3.2}$$

are the conditions to be satisfied at $t = 0$.

If the Laplace transformation be defined by

$$\bar{y}(p) = \int_0^\infty e^{-pt} y(t)\, dt, \tag{3.3}$$

the subsidiary equation corresponding to (2.13) and subject to (3.1) and (3.2) is

$$\frac{d^2\bar{\xi}}{dx^2} - q^2\bar{\xi} = U-(p+k)(-Sx+kUx-\tfrac{1}{2}kUx^2), \tag{3.4}$$

where

$$q^2 = p(p+k). \tag{3.5}$$

The solution of (3.4) is

$$\bar{\xi} = A\sinh qx + B\cosh qx - \frac{U}{p^2} + \frac{-Sx+kUx-\tfrac{1}{2}kUx^2}{p}, \tag{3.6}$$

A and B being constants to be determined from the boundary conditions. After the valve is shut, the displacement there remains zero and the condensation at inlet retains its value S. Hence for $t > 0$,

$$\bar{\xi} = 0 \quad \text{at } x = 0, \tag{3.7}$$

and, from (2.10),

$$\frac{d\bar{\xi}}{dx} = -\frac{S}{p} \quad \text{at } x = 1. \tag{3.8}$$

On inserting these conditions into (3.6) we find that

$$\bar{s} = -\frac{d\bar{\xi}}{dx} = \frac{Uq}{p^2}\frac{\sinh q(1-x)}{\cosh q} + \frac{S-kU+kUx}{p}. \tag{3.9}$$

Now

$$\begin{aligned}\frac{\sinh q(1-x)}{\cosh q} &= e^{-qx}(1-e^{-2q(1-x)})(1+e^{-2q})^{-1} \\ &= e^{-qx}-e^{-q(2-x)}-e^{-q(2+x)}+e^{-q(4-x)}+\ldots,\end{aligned} \tag{3.10}$$

and from Carslaw and Jaeger's analysis (**3**) of electric transmission lines it can be deduced that the inverse transform of

$$\frac{q}{p^2}e^{-qx}$$

is $$[e^{-\frac{1}{2}kt}I_0\{\tfrac{1}{2}k(t^2-x^2)^{\frac{1}{2}}\}+k\int_x^t e^{-\frac{1}{2}k\tau}I_0\{\tfrac{1}{2}k(\tau^2-x^2)^{\frac{1}{2}}\}\,d\tau]H(t-x), \qquad (3.11)$$

in which Heaviside's unit function

$$\left.\begin{aligned} H(t-T) &= 0 \quad (t \leqslant T)\\ &= 1 \quad (t > T)\end{aligned}\right\}, \qquad (3.12)$$

and I_0 denotes the Bessel function of the first kind. Thus we find from (3.9) and (3.10) that

$$\begin{aligned} P = s = U\Bigg(&\left[e^{-\frac{1}{2}kt}I_0\{\tfrac{1}{2}k(t^2-x^2)^{\frac{1}{2}}\}+k\int_x^t e^{-\frac{1}{2}k\tau}I_0\{\tfrac{1}{2}k(\tau^2-x^2)^{\frac{1}{2}}\}\,d\tau\right]H(t-x)-\\ &-\left[e^{-\frac{1}{2}kt}I_0\{\tfrac{1}{2}k(t^2-(2-x)^2)^{\frac{1}{2}}\}+k\int_{2-x}^t e^{-\frac{1}{2}k\tau}I_0\{\tfrac{1}{2}k(\tau^2-(2-x)^2)^{\frac{1}{2}}\}\,d\tau\right]\times\\ &\cdot\times H(t-(2-x))-\ldots+\ldots\Bigg)+(S-kU+kUx). \qquad (3.13)\end{aligned}$$

It will be noticed that the final term represents the pressure which prevails before the valve is shut.

A check can be applied to (3.13) by ascertaining the value of P when $t\to\infty$. Carslaw and Jaeger (**3**) proved that, when $t\to\infty$, (3.11) tends to

$$\left(\frac{k}{R}\right)^{\frac{1}{2}}e^{-(kR)^{\frac{1}{2}}x}, \qquad (3.14)$$

where R is a constant which in the present problem tends to zero. Writing for brevity $\alpha=(kR)^{\frac{1}{2}}$, we see that the Bessel terms in (3.13) reduce to

$$\frac{Uk}{\alpha}(e^{-\alpha x}-e^{-\alpha(2-x)}-e^{-\alpha(2+x)}+e^{-\alpha(4-x)}+\ldots). \qquad (3.15)$$

The alternate terms form two geometric series; and when these are summed (3.15) becomes

$$\frac{Uk}{\alpha}\left(\frac{e^{-\alpha x}}{1+e^{-2\alpha}}-\frac{e^{-\alpha(2-x)}}{1+e^{-2\alpha}}\right)=Uk\frac{e^{-\alpha x}}{1+e^{-2\alpha}}\frac{1-e^{-\alpha(2-2x)}}{\alpha}. \qquad (3.16)$$

When $\alpha\to 0$, (3.16) tends to

$$Uk(1-x), \qquad (3.17)$$

therefore, from (3.13), $P\to S$ as it should.

To avoid the troublesome integrals in (3.13) we can expand the Bessel functions and take

$$I_0(z) = 1+\frac{z^2}{4}+\frac{z^4}{64}, \tag{3.18}$$

using only the first three terms. The numerical results set out in section 5 make it clear that $\frac{1}{2}k$ may be expected to be substantially less than unity, and normally we shall not need to consider values of t exceeding 3 or 4, thus the argument of the Bessel function is unlikely to be much in excess of unity. Correct to four figures, the value of $I_0(1)$ obtained from (3.18) is 1·266, which is the same as that given in tables, hence the accuracy of the approximation (3.18) should be ample for practical purposes. It is simpler to insert (3.18) into both parts of (3.11), rather than in the integral alone; and when this is done, the result is

$$[e^{-\frac{1}{2}kx}\{\tfrac{15}{4}+\tfrac{7}{8}kx+\tfrac{1}{16}k^2x^2\}-e^{-\frac{1}{2}kt}\{\tfrac{11}{4}-\tfrac{3}{32}k^2x^2+\tfrac{1}{1024}k^4x^4+ \\ +kt(\tfrac{7}{8}-\tfrac{1}{64}k^2x^2)+k^2t^2(\tfrac{5}{32}-\tfrac{1}{512}k^2x^2)+\tfrac{1}{64}k^3t^3+\tfrac{1}{1024}k^4t^4\}]H(t-x). \tag{3.19}$$

The exponential terms can, if desired, be expanded to yield a formula expressed solely in powers of kx and kt, but for numerical work it is easier to employ (3.19) as it stands, in the later terms x being replaced by $2-x$, $2+x$, $4-x$, etc.

A crude approximation, causing an immediate error of rather more than 1 per cent. when z is unity, is to employ merely the first two terms in (3.18). The expression corresponding to (3.19) is then

$$[e^{-\frac{1}{2}kx}\{3+\tfrac{1}{2}kx\}-e^{-\frac{1}{2}kt}\{2-\tfrac{1}{16}k^2x^2+\tfrac{1}{2}kt+\tfrac{1}{16}k^2t^2\}]H(t-x). \tag{3.20}$$

The maximum pressure developed in the pipe-line may readily be obtained. The most heavily loaded part is at the valve, and we see from (3.13) and (3.19) that for $x = 0$, $0 \leqslant t \leqslant 2$,

$$P = U\{\tfrac{15}{4}-e^{-\frac{1}{2}kt}(\tfrac{11}{4}+\tfrac{7}{8}kt+\tfrac{5}{32}k^2t^2+\tfrac{1}{64}k^3t^3+\tfrac{1}{1024}k^4t^4)\}+(S-kU). \tag{3.21}$$

When the exponential term is expanded, (3.21) becomes

$$P = U\{1+\tfrac{1}{2}kt-\tfrac{1}{16}k^2t^2+\tfrac{1}{96}k^3t^3-\tfrac{5}{3072}k^4t^4\}+(S-kU). \tag{3.22}$$

Thus, as we expect, the initial pressure-rise above the working pressure is U. The pressure continues to increase until $t = 2$ when

$$P = U\{1-\tfrac{1}{4}k^2+\tfrac{1}{12}k^3-\tfrac{5}{192}k^4\}+S, \tag{3.23}$$

therefore the maximum pressure-rise above the static pressure is diminished by the fraction

$$\tfrac{1}{4}k^2-\tfrac{1}{12}k^3+\tfrac{5}{192}k^4, \tag{3.24}$$

compared with the rise calculated on the assumption that friction is entirely negligible. Thus friction has no first-order effect.

The attenuation of the vertically-fronted wave as it travels up the pipe-line may be followed by putting $t = x$ in (3.11), which yields

$$P = Ue^{-\frac{1}{2}kx}. \tag{3.25}$$

Hence, on arrival for the first time at the upper end of the pipe-line, the wave has been reduced in magnitude to $e^{-\frac{1}{2}k}$ times its initial value.

4. Exit velocity falling uniformly to zero in time t_0

We now consider the consequences of shutting the valve in such a way that the velocity in the pipe-line close to the valve falls to zero at a uniform rate in time t_0. Since the initial conditions are unchanged, (3.6) holds good; but of the two boundary conditions (3.7) and (3.8), the former needs alteration. For $t \geqslant 0$, $x = 0$, we take

$$\xi = U\left(\frac{t^2}{2t_0} - t\right) - \frac{U}{2t_0}(t-t_0)^2 H(t-t_0), \tag{4.1}$$

which satisfies the required conditions

$$\left.\begin{array}{lll} t = 0, & & \xi = 0 \\ 0 \leqslant t \leqslant t_0, & & u = \dfrac{\partial \xi}{\partial t} = -U\left(1 - \dfrac{t}{t_0}\right) \\ t \geqslant t_0, & & u = 0 \end{array}\right\}; \tag{4.2}$$

hence

$$\bar{\xi} = U\left\{\frac{1}{p^3 t_0}(1 - e^{-pt_0}) - \frac{1}{p^2}\right\}. \tag{4.3}$$

From (3.6), (3.8), and (4.3) we then have

$$\bar{s} = -\frac{d\bar{\xi}}{dx} = \frac{U}{t_0}\frac{q}{p^3}(1 - e^{-pt_0})\frac{\sinh q(1-x)}{\cosh q} + \frac{S - kU + kUx}{p}. \tag{4.4}$$

The substitution (3.10) will again be used; therefore we want the inverse transforms of

$$\frac{q}{p^3}e^{-qx} \quad \text{and} \quad \frac{qe^{-pt_0}}{p^3}e^{-qx}.$$

The former can be obtained by means of the integration theorem from the inverse transform of $qp^{-2}e^{-qx}$, and on integrating, between the limits t and x, that part of (3.19) which lies within square brackets, we arrive at the expression

$$\left[\frac{e^{-\frac{1}{2}kx}}{k}\left\{-\tfrac{55}{4} - \tfrac{63}{8}kx - \tfrac{19}{16}k^2x^2 - \tfrac{1}{16}k^3x^3 + kt(\tfrac{15}{4} + \tfrac{7}{8}kx + \tfrac{1}{16}k^2x^2)\right\} + \right.$$
$$+ \frac{e^{-\frac{1}{2}kt}}{k}\left\{\tfrac{55}{4} - \tfrac{9}{32}k^2x^2 + \tfrac{1}{512}k^4x^4 + kt(\tfrac{33}{8} - \tfrac{3}{64}k^2x^2) + \right.$$
$$\left.\left. + k^2t^2(\tfrac{19}{32} - \tfrac{1}{256}k^2x^2) + \tfrac{3}{64}k^3t^3 + \tfrac{1}{512}k^4t^4\right\}\right] H(t-x). \tag{4.5}$$

If we apply the process to (3.20) we find

$$\left[\frac{e^{-\frac{1}{2}kx}}{k}\{-7-\tfrac{9}{2}kx-\tfrac{1}{2}k^2x^2+kt(3+\tfrac{1}{2}kx)\}+\right.$$
$$\left.+\frac{e^{-\frac{1}{2}kt}}{k}\{7-\tfrac{1}{8}k^2x^2+\tfrac{3}{2}kt+\tfrac{1}{8}k^2t^2\}\right]H(t-x). \quad (4.6)$$

In both (4.5) and (4.6) the constants inside the curly brackets are equal in magnitude and opposite in sign. To avoid the difficulty which arises in finding a small difference between two large quantities, it is essential for purposes of computation to expand the exponential terms. Equations (4.5) and (4.6) then become

$$\frac{1}{k}\left[(-kx+\tfrac{3}{4}k^2x^2-\tfrac{1}{6}k^3x^3+\tfrac{5}{384}k^4x^4-\tfrac{7}{184320}k^6x^6)+\right.$$
$$+kt(1-kx+\tfrac{3}{16}k^2x^2-\tfrac{5}{3072}k^4x^4)+k^2t^2(\tfrac{1}{4}-\tfrac{1}{64}k^2x^2+\tfrac{1}{4096}k^4x^4)+$$
$$+k^3t^3(-\tfrac{1}{48}+\tfrac{1}{512}k^2x^2)+k^4t^4(\tfrac{1}{384}-\tfrac{1}{4096}k^2x^2)-$$
$$\left.-\tfrac{1}{30720}k^5t^5+\tfrac{7}{184320}k^6t^6\right]H(t-x), \quad (4.7)$$

and

$$\frac{1}{k}[(-kx+\tfrac{3}{4}k^2x^2-\tfrac{1}{6}k^3x^3+\tfrac{5}{384}k^4x^4)+kt(1-kx+\tfrac{3}{16}k^2x^2)+$$
$$+k^2t^2(\tfrac{1}{4}-\tfrac{1}{64}k^2x^2)-\tfrac{1}{48}k^3t^3+\tfrac{1}{384}k^4t^4]H(t-x). \quad (4.8)$$

As many terms as possible are given, subject to the proviso that none requires alteration if additional terms in the expansion of the Bessel function are employed. Both (4.7) and (4.8) reduce to zero when t is put equal to x.

To determine the other inverse transform we make use of the fact that, if $\bar{y}(p)$ is the transform of $y(t)H(t-x)$, $e^{-pt_0}\bar{y}(p)$ is the transform of

$$y(t-t_0)H(t-t_0-x).$$

Hence in (4.7) or (4.8) $(t-t_0)$ is substituted for t, both in the unit function and in the remainder of the expression. In effect, no additional calculation of the terms typified by (4.7) is required; for a fixed position on the pipeline, the values already found are used again with the times increased by t_0. Thus the determination of P follows the same lines as in section 3, it being necessary to evaluate a succession of terms associated with $H(t-x)$, $H(t-t_0-x)$, $H(t-(2-x))$, $H(t-t_0-(2-x))$, etc.

For $x = 0$, the coefficient of $H(t-x)$ in (4.7) and (4.8) is

$$t+\tfrac{1}{4}kt^2-\tfrac{1}{48}k^2t^3+\ldots. \quad (4.9)$$

Thus as far as $t = 2$ or $t = t_0$, whichever is the smaller, the initial pressure-rise does not follow a line that is exactly straight. Its gradient increases unless kt is very great, and then the approximation, which has been used, is known to be defective.

5. Numerical results

As examples of the methods set out in the two preceding sections, four tests have been considered which are fully described in the report (1) previously mentioned. For the conditions obtaining in these tests the pressure fluctuations at the valve ($x = 0$) have been calculated. The details of the two pipe-lines and of the oil that they conveyed are given in Table 1.

TABLE 1. *Details of the pipe-lines and of the oils*

	McCamey 4-*in.* *Tests* 23, 22B	*Wink–Monahans* 6-*in.* *Tests* 51, 50
Pipe internal radius, a ft.	0·1677	0·2526
Pipe length, l ft.	2232	108800
Kinematic viscosity, ν ft.^{2}/sec.	$5{\cdot}62\times10^{-4}$	$0{\cdot}47\times10^{-4}$
Density, ρ_0 lb./ft.^{3}	56·4	52·2
Wave velocity, c ft./sec.	4010	4000
k, obtained from (2.8) and (2.6)	0·0892	0·160

In the two experiments on the McCamey pipe-line the Reynolds number was below the critical, hence k as determined from (2.8) and (2.6) was employed. For the other pipe-line, however, the flow was turbulent and the value of k required adjustment.

(i) *Instantaneous closure*

For the McCamey pipe-line the value of k in Table 1 was checked by means of the results of test 23. From the well-known formula for the pressure drop in laminar flow it was deduced that at a steady velocity 1·03 ft./sec. the drop should be 4·45 lb./sq. in. This is in agreement with the observation that the difference between the static and running pressures at the valve was $121-117 = 4$ lb./sq. in. Accordingly, with the above value of k, the terms typified by (3.19) were evaluated at time intervals of $\frac{1}{2}$, giving the ratio of the pressure P_1 (measured above the static pressure) to U. The calculations were pursued as far as $t = 6{\cdot}5$ where $\frac{1}{2}kt$ was only 0·290, hence the approximation made in (3.18) should have no appreciable consequences. The results are shown by the broken line in Fig. 2, to which the ordinary rectangular diagram for frictionless motion has been added as a full line for purposes of comparison. After the initial jump equal to unity at $t = 0$, the broken line rises as more and

more of the oil is brought to rest and the friction head is reduced. Owing to the dissipation of energy which continues during the process of compression, the line fails to reach the ordinate 1·0 at $t = 2$ by an amount given by (3.24), which is here too small to be distinguishable in the figure.

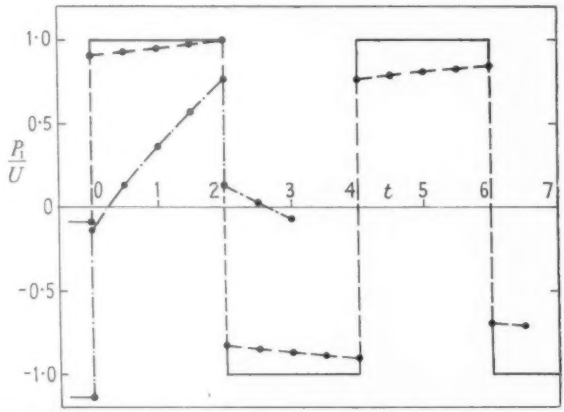

FIG. 2. Pressure fluctuations at valve. Instantaneous closure. ——$k = 0$(frictionless); — — $k = 0{\cdot}0892$; —·— $k = 1{\cdot}14$.

At $t = 2$ the wave reflected from the open end arrives, and since the static pressure is taken to be sufficient to prevent bouncing, the pressure suddenly becomes negative. At this instant the whole of the oil column is moving towards the reservoir; therefore, owing to friction, the pressure in it is greater, i.e. the tension is less, at the valve than at the reservoir. As the tension wave retreats from the valve and brings the oil to rest, this friction effect is progressively reduced. Thus between $t = 2$ and $t = 4$ the tension at the valve increases. The fluctuations continue in the same manner with slowly diminishing discontinuities.

In contrast, the friction loss in the Wink–Monahans pipe-line was very great. In test 51 with a steady velocity 1·09 ft./sec. the loss was 56 lb./sq. in., whereas that given by the laminar flow formula is 7·87 lb./sq. in. The value of k in Table 1 was therefore increased in the ratio of these figures, giving $k = 1{\cdot}14$ as the value to be employed in the computations. The results are shown by the dash-dot line in Fig. 2. Here the friction is so large that the initial rise of unity is insufficient to bring the pressure up to the static pressure, and the maximum pressure, which occurs at $t = 2$, is 25 per cent. below the frictionless value. The ensuing sudden fall is too feeble to reduce the pressure below zero until a further lapse of time. The calculations were terminated at $t = 3$ when $\frac{1}{2}kt = 1{\cdot}71$, which is as far as the approximation should be pushed.

(ii) *Closure in time* $t_0 = 1$

As examples of the theory explained in section 4, the terms typified by (4.7) have been evaluated for both pipe-lines for $t_0 = 1$. The value of x being fixed, a useful check on the computations occurs in the following way. When we are considering the term involving say $H(t-(2-x))$, $(2-x)$ is

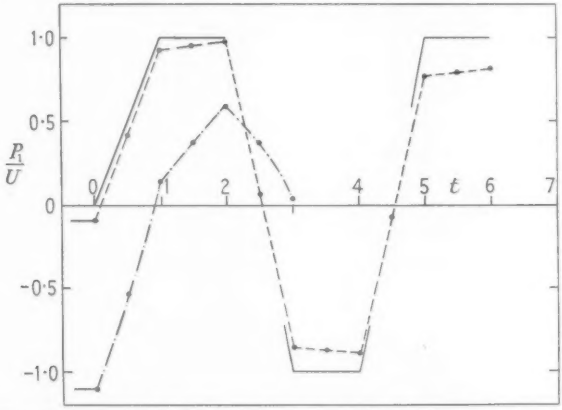

FIG. 3. Pressure fluctuations at valve. Closure in time $t_0 = 1$.
—— $k = 0$ (frictionless); — — $k = 0{\cdot}0892$; —·— $k = 1{\cdot}10$.

substituted for x inside the square brackets in (4.7) or (4.8). These expressions vanish when t is put equal to $(2-x)$, as will be seen both from the algebra and from the obvious physical fact that the pressure change at the nose of the reflected wave is zero.

For the McCamey pipe-line $k = 0{\cdot}0892$ has again been taken. The result is shown in Fig. 3, which is drawn with the same notation of lines as in Fig. 2. The initial pressure-rise steepens very slightly as it proceeds, and after $t = 1$ the pressure continues to increase as in Fig. 2. The effect of friction upon the maximum pressure attained at $t = 2$ is now more pronounced, and at this point a visible difference exists between the full and the broken lines.

For the Wink–Monahans pipe-line it was desired to make a comparison with test 50. In this the initial steady velocity was 1·05 ft./sec., which was somewhat less than in test 51. The corresponding value of k, obtained by the same method as before, was 1·10, and this was used in the calculations, yielding the dash-dot line in Fig. 3. Although k is less, friction has again a larger effect, amounting to a reduction of 41 per cent. at $t = 2$.

(iii) *Comparison with the graphical method*

In the report the results of the graphical method are plotted as isolated points on reproductions of the pressure-gauge readings. For tests 23 and

22B on the McCamey pipe-line and tests 51 and 50 on the Wink–Monahans pipe-line these points have been transferred to Figs. 4, 5, 6, and 7, where they are shown surrounded by circles. To these figures the results (with

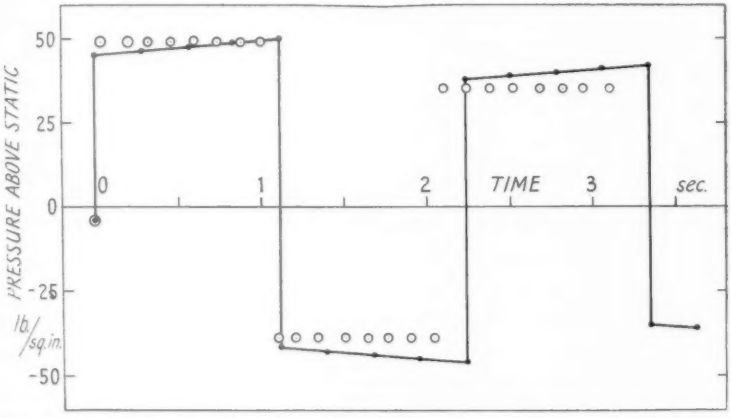

FIG. 4. McCamey pipe-line (test 23). Instantaneous closure at 1·03 ft./sec.
⊙ ⊙ ⊙ by graphical method; —— by calculation.

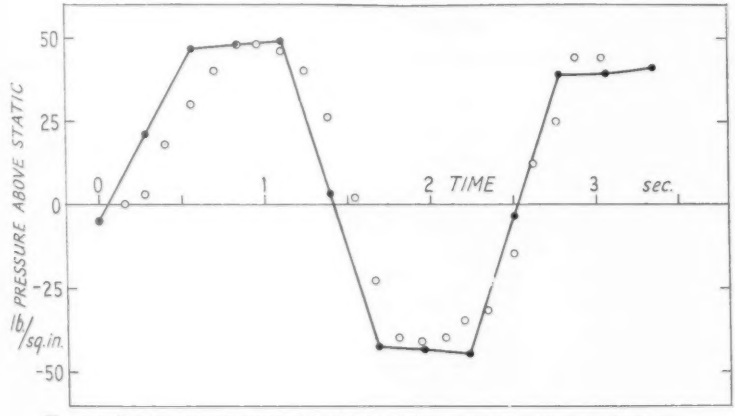

FIG. 5. McCamey pipe-line (test 22B). Closure in time l/c at 1·03 ft./sec.
⊙ ⊙ ⊙ by graphical method; —— by calculation.

friction) displayed in Figs. 2 and 3 have been added in full lines after transformation to the dimensional quantities appropriate to the tests. In Fig. 4 it appears that in the graphical method no attempt was made to obtain the sloping part of the diagram; moreover, one end of each discontinuity is omitted. Nevertheless, the two methods agree in yielding the same maximum pressure, and this is true also of Fig. 5.

For the Wink–Monahans pipe-line (Figs. 6 and 7) with its heavy friction, the discrepancies are more serious, and again the discontinuities resulting from sudden closure are blurred in the graphical method. An explanation

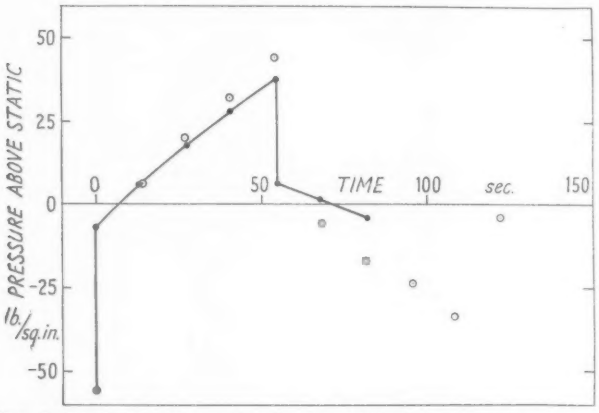

FIG. 6. Wink–Monahans pipe-line (test 51). Instantaneous closure at 1·09 ft./sec. ⊙ ⊙ ⊙ by graphical method; —— by calculation.

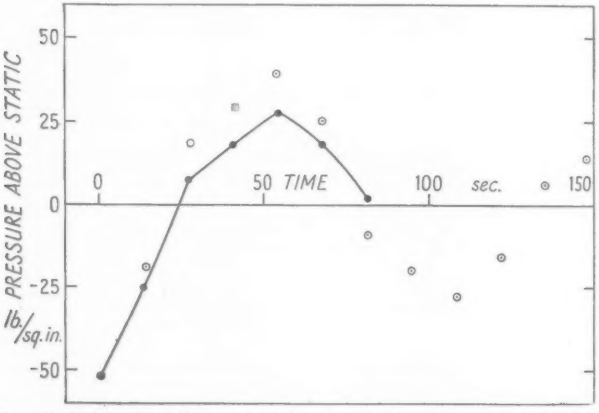

FIG. 7. Wink–Monahans pipe-line (test 50). Closure in time l/c at 1·05 ft./sec. ⊙ ⊙ ⊙ by graphical method; —— by calculation.

can be put forward of the fact that the graphical method yields a larger maximum pressure, the difference being more marked when closure is gradual. The friction–loss relation which was employed does not seem to be explicitly stated in the report, but to judge from a worked example it almost certainly was taken to vary as the square of the velocity throughout

every test. On the other hand, a loss proportional simply to the velocity is assumed in this paper. Thus, as the velocity falls after the closure of the valve, the friction loss in the graphical method diminishes more rapidly, leading to a higher maximum pressure. Clearly this effect should be more marked when the oil is brought gradually to rest; no doubt it is too slight to be noticeable in the McCamey tests, in which friction was so small. It would be out of place in a computational paper to discuss the experimental observations in detail. But it may be remarked that, whereas in tests 23 and 22B the graphical method satisfactorily predicted the maximum pressure, in tests 51 and 50 it led to a considerable over-estimate and the other method is more accurate.

The report also gives details of a test on the Wink–Monahans pipe-line, in which the velocity was raised to 4·38 ft./sec. by means of a pump. Under these severe conditions the effective value of k is so large that the approximation (3.18) cannot provide an accurate result for the maximum pressure. No doubt this case could be met by employing more terms, but only at the cost of considerable labour. Evidently it will not be possible to claim that the general problem with laminar flow has been solved completely until tables of the integral in (3.11) are available.

REFERENCES

1. Joint Surge Conference, Final Report 1949, Middle East Pipelines Ltd., 293 Regent Street, London, W. 1.
2. E. G. Chilton, Shell Development Co. Engineering Report No. ETDT–103, Appendix II. See also R. W. Angus, *Proc. Inst. Mech. Eng.* **136** (1937), 245.
3. H. S. Carslaw and J. C. Jaeger, *Operational Methods in Applied Mathematics* (Oxford, 1948).

Note added 13 February 1951

The problem treated in this paper has been examined also by M. Ludwig (*Amer. Soc. Mech. Eng.*, Preprint No. 50–SA–26, 1950).

ON THE HALF-PLANE DIFFRACTION PROBLEM

By F. G. FRIEDLANDER (*The University, Manchester*)

[Received 22 November 1950]

SUMMARY

The diffraction of an arbitrary two-dimensional disturbance by a semi-infinite plane screen is considered. It is shown that the solution, at all points of space, can be obtained by a modification of the method developed by Hadamard for Cauchy's problem. The diffraction of the disturbance represented by Hadamard's 'elementary solution' is discussed, and a remarkably simple expression for the diffracted disturbance is found; its Laplace transform is shown to agree with the Green's functions derived from Sommerfeld's two-valued solutions of the wave equation.

1. THE diffraction of two-dimensional waves—both infinite harmonic wave trains and aperiodic disturbances—by a semi-infinite plane screen has been treated by various authors since Sommerfeld derived an exact solution for the case of an incident plane harmonic wave train. Various methods of attack, ranging from Sommerfeld's many-valued solutions of the wave equation to the reduction of the problem to an integral equation of the Wiener–Hopf type, have been employed. In the present paper it is shown that the problem can be solved by a modification of the method developed by Hadamard for Cauchy's problem.

We shall consider the two-dimensional wave equation

$$\frac{\partial^2 u}{\partial t^2} - \frac{\partial^2 u}{\partial x^2} - \frac{\partial^2 u}{\partial y^2} = f(x, y, t), \tag{1.1}$$

where x, y are Cartesian coordinates, t is the time (on a suitable scale), $f(x, y, t)$ is a known function, and u is a variable whose physical significance depends on the problem under consideration; e.g. for sound waves u may be the pressure, and for electromagnetic waves it may be a component of the Hertz vector. It is more convenient to consider two auxiliary problems, which may be formulated as follows.

Let $p(x, t)$ and $q(x, t)$ be defined for $x \geqslant 0$, and be identically zero for $t \leqslant \sigma(x)$, where $|\sigma'(x)| \leqslant 1$;† they must also satisfy certain conditions of regularity which will be mentioned later. In the 'space-time' (x, y, t) the union of the influence domains of the points $(x, 0, \sigma(x))$ is bounded by a characteristic C_1 which is the envelope of the characteristic half-cones

$$t = \sigma(x') + \{(x-x')^2 + y^2\}^{\frac{1}{2}} \quad (0 \leqslant x' < \infty).$$

† $p(x, t)$ and $q(x, t)$ may be considered, jointly, as a disturbance propagating along the half-plane. The condition $|\sigma'(x)| \leqslant 1$ means that the velocity of the front of this disturbance does not exceed the velocity of wave propagation.

It is easily shown that if a point (x, y, t) is above† C_1, then the points (x', y', t') which lie above C_1, and for which

$$t' \leqslant t - \{(x-x')^2 + (y-y')^2\}^{\frac{1}{2}},$$

are a bounded set of points. We then consider

PROBLEM I. *To find a function $u_1(x, y, t)$, regular except on $y = 0$, $x \geqslant 0$, satisfying* (1.1) *and*

(*a*) $$\lim_{y=0} \frac{\partial u_1}{\partial y} = q(x, t) \quad (x \geqslant 0); \tag{1.2}$$

(*b*) $$u_1 = 0 \quad \text{on } C_1; \tag{1.3}$$

(*c*) $$x \frac{\partial u_1}{\partial x} + y \frac{\partial u_1}{\partial y} \to 0 \quad \text{as } x^2 + y^2 \to 0. \tag{1.4}$$

PROBLEM II. *To find a function $u_2(x, y, t)$, regular except on $y = 0$, $x \geqslant 0$, satisfying* (1.1) *and*

(*a*) $$\lim_{y=0} u_2 = p(x, t) \quad (x \geqslant 0); \tag{1.5}$$

(*b*) *condition* (1.3); (*c*) *condition* (1.4).

By a trivial modification of the proof of the well-known uniqueness theorem, it can be shown that the solutions of both these problems, if they exist, are unique (**1**). (The condition (1.4) excludes certain diverging cylindrical waves, infinite at $x = y = 0$.)

Now let $u_0(x, y, t)$ be a solution of (1.1) which vanishes on and below a characteristic C_0 which intersects $(y = 0, x \geqslant 0)$ in a curve $t = \sigma(x)$ (then necessarily $|\sigma'(x)| \leqslant 1$). If we define C_1 by means of this curve as above, and put

$$p(x, t) = -[u_0]_{y=0}, \qquad q(x, t) = -\left[\frac{\partial u_0}{\partial y}\right]_{y=0} \quad (x \geqslant 0), \tag{1.6}$$

then the functions

$$u_3 = u_0 + u_1, \qquad u_4 = u_0 + u_2 \tag{1.7}$$

satisfy the boundary conditions

$$\left[\frac{\partial u_3}{\partial y}\right]_{y=0} = 0, \qquad [u_4]_{y=0} = 0 \quad (x \geqslant 0). \tag{1.8}$$

Thus they are the solutions of the diffraction problems for the semi-infinite screen $(y = 0, x \geqslant 0)$, the incident wave being u_0, and the boundary conditions $\partial u/\partial y = 0$ and $u = 0$ on the screen, respectively.

† The t-axis is to be thought of as drawn vertically upwards, so that 'above' is equivalent to 'later' and 'below' is equivalent to 'earlier'.

2. Let S be a closed surface of space-time, (l_1, l_2, l_0) the direction cosines of its inward normal, and du/dv the transversal derivative defined by

$$\frac{du}{dv} = l_0 \frac{\partial u}{\partial t} - l_1 \frac{\partial u}{\partial x} - l_2 \frac{\partial u}{\partial y}. \tag{2.1}$$

If u satisfies (1.1) and v satisfies the homogeneous wave equation

$$\frac{\partial^2 v}{\partial t^2} - \frac{\partial^2 v}{\partial x^2} - \frac{\partial^2 v}{\partial y^2} = 0, \tag{2.2}$$

then, by a modification of the divergence theorem,

$$\int \left(u \frac{dv}{dv} - v \frac{du}{dv} \right) dS = - \int fv \, dT, \tag{2.3}$$

where dS is the surface element of S, dT the volume element $dxdydt$, the surface integral is taken over S, and the volume integral over the interior of S. This equation is in the first instance only valid if u and v are sufficiently regular in and on S; but Hadamard has shown that it can be used even when S contains portions on which, for example, v is 'fractionally' infinite, provided that the integrals are interpreted as 'finite parts' of divergent integrals, in the sense defined by Hadamard (**2**).

Let (x, y, t) be a fixed point of space-time situated above C_1, and (x', y', t') be a variable point. The elementary solution of (2.2) is

$$v = \{(t-t')^2 - (x-x')^2 - (y-y')^2\}^{-\frac{1}{2}}. \tag{2.4}$$

It can be considered as a 'retrograde' wave whose wave fronts constitute the characteristic C,

$$t' = t - \{(x-x')^2 + (y-y')^2\}^{\frac{1}{2}}. \tag{2.5}$$

With it, a retrograde diffracted wave is associated whose wave fronts constitute a characteristic C_d,

$$t' = t - (x^2+y^2)^{\frac{1}{2}} - (x'^2+y'^2)^{\frac{1}{2}}, \tag{2.6}$$

(see Fig. 1). Put

$$x = r\cos\theta, \qquad y = r\sin\theta, \qquad x' = r'\cos\theta', \qquad y' = r'\sin\theta', \tag{2.7}$$

$$R = \{(x'-x)^2 + (y'-y)^2\}^{\frac{1}{2}} = \{r^2 + r'^2 - 2rr'\cos(\theta'-\theta)\}^{\frac{1}{2}}. \tag{2.8}$$

We shall take, in the first instance, $y > 0$, so that $0 < \theta < \pi$. The equations of C and of C_d become

$$t' = t - R, \qquad t' = t - r' - r \tag{2.9}$$

respectively, and it is obvious that, for $0 < \theta < \pi$, C_d is below C except for $\theta' = \theta + \pi$, when they touch along a generator.

3. The surfaces C, C_d, for $0 < \theta' \leqslant \theta + \pi$, together with $(y' = 0, x' \geqslant 0)$ and C_1, delimit a bounded domain of space-time to which we shall now

apply (2.3), taking v to be the elementary solution (2.4). In order to do so, we first introduce two auxiliary characteristics C', C'_d, given by

$$t' = t-(R^2+\epsilon)^{\frac{1}{2}}, \qquad t' = t-(r^2+\epsilon)^{\frac{1}{2}}-r' \tag{3.1}$$

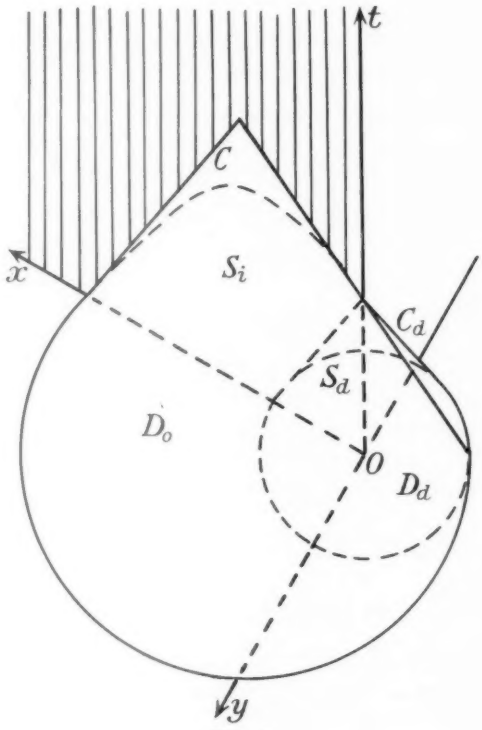

FIG. 1.

respectively, where ϵ is afterwards made to tend to zero, and apply (2.3) to the domain bounded by C', C'_d ($y' = 0$, $x' \geqslant 0$), C_1, and a surface S_η defined by

$$t' = t-\eta, \qquad R \leqslant (\eta^2-\epsilon)^{\frac{1}{2}} \quad (\eta > \epsilon^{\frac{1}{2}}).$$

The contribution of this surface S_η to the surface integral as $\epsilon \to 0$ first and then $\eta \to 0$ is evaluated exactly as in Hadamard's treatment of Cauchy's problem and turns out to be (neglecting fractional infinities in ϵ)

$$-2\pi u(x, y, t). \tag{3.2}$$

The surface C_1 makes no contribution to the surface integral; for in either problem, $u = 0$ on C_1, and as C_1 is a characteristic, the transversal to C_1 is also tangential to C_1, so that also $du/dv = 0$ on C_1.

On $(y = 0,\ x \geqslant 0)$, the transversal derivative is $-\partial/\partial y$ and so its contribution to the surface integral is, as $\epsilon \to 0$,

$$-\int\!\!\int^{*} \left[u\,\frac{\partial v}{\partial y'} - v\,\frac{\partial u}{\partial y'}\right]_{y'=0+0} dx'dt',$$

where the asterisk indicates that this is to be interpreted as a 'finite part', and the domain of integration is bounded by

$$t' = \sigma(x'), \qquad t' = t-r-x', \qquad t' = t-\{(x-x')^2+y^2\}^{\frac{1}{2}}.$$

Putting $$\lim_{y=+0} u = p(x,t), \qquad \lim_{y=+0} \frac{\partial u}{\partial y} = q(x,t) \quad (x \geqslant 0), \tag{3.3}$$

and $$R_0 = \{(x-x')^2+y^2\}^{\frac{1}{2}}, \tag{3.4}$$

this can be written as

$$-\int_0^{*\infty} dx' \int_{t-r-x'}^{t-R_0} \left\{\frac{q(x',t')}{\{(t-t')^2-R_0^2\}^{\frac{1}{2}}} + \frac{yp(x',t')}{\{(t-t')^2-R_0^2\}^{\frac{3}{2}}}\right\} dt', \tag{3.5}$$

where the upper limit ∞ has been used for convenience; as in fact $p(x',t')$ and $q(x',t')$ vanish for $t' \leqslant \sigma(x')$, the domain of integration is finite.

The contribution of C' is of the form $A(\epsilon)\epsilon^{-\frac{1}{2}}$, where $A(\epsilon)$ tends to a limit as $\epsilon \to 0$, and hence its finite part is zero.

4. It only remains to consider the contribution from C'_d. On C'_d we can write

$$dS\,\frac{d}{d\nu} = -r'\,dr'd\theta'\left(\frac{\partial}{\partial t'} - \frac{\partial}{\partial r'}\right).$$

Also, if for the moment we distinguish functions evaluated on C'_d by enclosing them in square brackets, it follows from (3.1) that

$$\frac{\partial}{\partial r'}[u] = \left[\frac{\partial u}{\partial r'}\right] - \left[\frac{\partial u}{\partial t'}\right], \qquad \frac{\partial}{\partial r'}[v] = \left[\frac{\partial v}{\partial r'}\right] - \left[\frac{\partial v}{\partial t'}\right].$$

Hence the contribution from C'_d to the surface integral is

$$I = \int_0^{\theta+\pi} d\theta' \int_0^{\infty} \left\{[u]\,\frac{\partial}{\partial r'}[v] - [v]\,\frac{\partial}{\partial r'}[u]\right\} r'\,dr', \tag{4.1}$$

where the upper limit ∞ has again been introduced for convenience, $[u]$ vanishing when r' is so large that the corresponding point of C'_d lies below C_1. In view of this, and of condition (1.4), a partial integration transforms (4.1) into

$$I = \int_0^{\theta+\pi} d\theta' \int_0^{\infty} [u]\left\{2r'\,\frac{\partial}{\partial r'}[v] + [v]\right\} dr'.$$

Substituting the value of $[v]$, which by (2.4) and (3.1) is

$$[v] = \{\epsilon+2r'(r^2+\epsilon)^{\frac{1}{2}}+2rr'\cos(\theta-\theta')\}^{-\frac{1}{2}},$$

and putting $\theta' = \pi+\theta-\phi$, this becomes

$$I = \int_0^{\pi+\theta} d\phi \int_0^{\infty} \frac{\epsilon\bar{u}(v', \pi+\theta-\phi, t-(v^2+\epsilon)^{\frac{1}{2}}-r')}{\{\epsilon+2r'(r^2+\epsilon)^{\frac{1}{2}}-2rr'\cos\phi\}^{\frac{3}{2}}}\, dr', \tag{4.2}$$

where

$$\bar{u}(r, \theta, t) = u(r\cos\theta, r\sin\theta, t). \tag{4.3}$$

The behaviour of the kernel of the integral in (4.2) is singular as $\epsilon \to 0$; it tends to zero with ϵ if both $r' \neq 0$ and $\phi \neq 0$, but at the same time

$$\lim_{\epsilon=0} \int_0^{\pi+\theta} \frac{\epsilon\, d\phi}{\{\epsilon+2r'(r^2+\epsilon)^{\frac{1}{2}}-2rr'\cos\phi\}^{\frac{3}{2}}} = \left(\frac{r}{r'}\right)^{\frac{1}{2}} \frac{1}{r+r'}. \tag{4.4}$$

Hence it can be shown—assuming that u is continuous—that

$$\lim_{\epsilon=0} I = \int_0^{\infty} \frac{\bar{u}(r', \pi+\theta, t-r-r')}{r+r'} \left(\frac{r}{r'}\right)^{\frac{1}{2}} dr'. \tag{4.5}$$

The detailed proof—which is not difficult—will be omitted, but we shall establish (4.4). If the range of integration in the integral in (4.4) is divided into $(0, \eta)$ and $(\eta, \pi+\theta)$, where $\eta > 0$, then the contribution from $(\eta, \pi+\theta)$ tends to zero with ϵ for fixed η. We need therefore only consider

$$\begin{aligned} J &= \int_0^{\eta} \frac{\epsilon\, d\phi}{\{\epsilon+2r'(r^2+\epsilon)^{\frac{1}{2}}-2rr'\cos\phi\}^{\frac{3}{2}}} \\ &= \int_0^{2\sin\frac{1}{2}\eta} \frac{\epsilon\, d\psi}{(1-\frac{1}{4}\psi^2)^{\frac{1}{2}}\{\epsilon+2r'(r^2+\epsilon)^{\frac{1}{2}}-2rr'+rr'\psi^2\}^{\frac{3}{2}}}, \end{aligned}$$

where $\cos\phi = 1-\frac{1}{2}\psi^2$.

Clearly

$$J^* \leqslant J \leqslant J^* \sec\tfrac{1}{2}\eta,$$

where

$$\begin{aligned} J^* &= \int_0^{2\sin\frac{1}{2}\eta} \frac{\epsilon\, d\psi}{\{\epsilon+2r'(r^2+\epsilon)^{\frac{1}{2}}-2rr'+rr'\psi^2\}^{\frac{3}{2}}} \\ &= \frac{\epsilon}{\epsilon+2r'(r^2+\epsilon)^{\frac{1}{2}}-2rr'} \frac{2\sin\frac{1}{2}\eta}{\{\epsilon+2r'(r^2+\epsilon)^{\frac{1}{2}}-2rr'+4rr'\sin^2\frac{1}{2}\eta\}^{\frac{1}{2}}}. \end{aligned}$$

Thus

$$\lim_{\epsilon=0} J^* = \frac{1}{r+r'}\left(\frac{r}{r'}\right)^{\frac{1}{2}},$$

and letting finally $\eta \to 0$, we obtain (4.4).

Collecting our results, (3.2), (3.5), and (4.5), we obtain now

$$2\pi u(x,y,t) = -\int_0^{*\infty} dx' \int_{t-r-x'}^{t-R_0} \left\{ \frac{q(x',t')}{\gamma_0^{\frac{1}{2}}} + \frac{yp(x',t')}{\gamma_0^{\frac{3}{2}}} \right\} dt' -$$

$$-\int_0^{\infty} \frac{\tilde{u}(r',\theta+\pi,t-r-r')}{r+r'} \left(\frac{r}{r'}\right)^{\frac{1}{2}} dr' + \iiint \frac{f_1(x',y',t')}{\gamma^{\frac{1}{2}}}\, dx'dy'dt', \quad (4.6)$$

where $$\gamma = (t-t')^2 - R^2, \qquad \gamma_0 = (t-t')^2 - R_0^2, \quad (4.7)$$

the volume integral is taken over

$$t-r-r' \leqslant t' \leqslant t-R, \qquad 0 \leqslant \theta' \leqslant \pi+\theta,$$

and f_1 is equal to f above C_1, and zero below C_1.

5. Again, let (2.3) be applied to a domain bounded by C_d, C_1 and by $\theta' = \eta$, $\theta' = 2\pi-\eta$, v being still the elementary solution (2.4). As $\eta \to 0$, this domain tends to $\mathscr{D}_d$. The contributions of $\theta' = \eta$, $\theta' = 2\pi-\eta$ tend, as $\eta \to 0$, to terms of the same type as (3.5), with p, q replaced, respectively, by

$$p^*(x,t) = [u]_{y=-0}^{y=+0}, \qquad q^*(x,t) = \left[\frac{\partial u}{\partial y}\right]_{y=-0}^{y=+0}, \quad (5.1)$$

and the limits of the inner integral replaced by $(-\infty, t-r-x')$. As (x,y,t) is outside the domain, there is no term corresponding to (3.2). As for the contribution of C_d, it is calculated as above; but as the sense of the transversal must be reversed, its sign must be changed, and as the integral corresponding to (4.2) must be taken over $(0, 2\pi)$, the result (4.5) must be multiplied by 2. Hence after division by 2 the resulting equation is

$$0 = -\tfrac{1}{2}\int_0^{*\infty} dx' \int_{-\infty}^{t-r-x'} \left\{ \frac{q^*(x',t')}{\gamma_0^{\frac{1}{2}}} + \frac{yp^*(x',t')}{\gamma_0^{\frac{3}{2}}} \right\} dt' +$$

$$+\int_0^{\infty} \frac{\tilde{u}(r',\theta+\pi,t-r-r')}{r+r'} \left(\frac{r}{r'}\right)^{\frac{1}{2}} dr' + \iiint \frac{f_1(x',y',t')}{2\gamma^{\frac{1}{2}}}\, dx'dy'dt' \quad (5.2)$$

where the volume integral is taken over $t' \leqslant t-r-r'$, $0 \leqslant \theta' \leqslant 2\pi$.

If this equation is added to (4.6), the contributions from C_d cancel, and we obtain the following equation, which must necessarily be satisfied by any solution of the wave equation which is sufficiently regular to ensure

the validity of the various limiting operations by which it has been obtained:

$$2\pi u(x,y,t) = \iiint_{\mathscr{D}_0} \frac{f_1(x',y',t')}{\gamma^{\frac{1}{2}}}\,dx'dy'dt' + \tfrac{1}{2}\iiint_{\mathscr{D}_d} \frac{f_1(x',y',t')}{\gamma^{\frac{1}{2}}}\,dx'dy'dt' -$$

$$-\,{\iint_{\mathscr{S}_i}}^{*} \left\{\frac{q(x',t')}{\gamma_0^{\frac{1}{2}}} + \frac{yp(x',t')}{\gamma_0^{\frac{3}{2}}}\right\} dx'dt' - \tfrac{1}{2}{\iint_{\mathscr{S}_d}}^{*} \left\{\frac{q^*(x',t')}{\gamma_0^{\frac{1}{2}}} + \frac{yp^*(x',t')}{\gamma_0^{\frac{3}{2}}}\right\} dx'dt' \tag{5.3}$$

where $\mathscr{D}_0$, $\mathscr{D}_d$, $\mathscr{S}_i$, $\mathscr{S}_d$ are defined by

$$\left.\begin{array}{ll} \mathscr{D}_0: & t-r-r' \leqslant t' \leqslant t-R, \quad 0 \leqslant \theta' \leqslant \pi+\theta; \\ \mathscr{D}_d: & -\infty < t' \leqslant t-r-r', \quad 0 \leqslant \theta' \leqslant 2\pi; \\ \mathscr{S}_i: & y=0, \quad 0 \leqslant x' < \infty, \quad t-r-x' \leqslant t' \leqslant t-R_0; \\ \mathscr{S}_d: & y=0, \, 0 \leqslant x' < \infty, \quad -\infty < t' \leqslant t-r-x'. \end{array}\right\} \tag{5.4}$$

This result holds for $y > 0$; if $y < 0$, the sign of the surface integrals must be reversed, and in the definition of $\mathscr{D}_0$, θ and θ' must be replaced by $2\pi-\theta$, $2\pi-\theta'$ respectively.

Now let $$\bar{v} = \bar{\gamma}^{-\frac{1}{2}} = \{(t-t')^2-(x-x')^2-(y+y')^2\}^{-\frac{1}{2}} \tag{5.5}$$

be the elementary solution relative to the point $(x, -y, t)$ which is the image of (x, y, t) in $y = 0$, put

$$\bar{R} = \{(x-x')^2+(y+y')^2\}^{\frac{1}{2}} = \{r^2+r'^2-2rr'\cos(\theta+\theta')\}^{\frac{1}{2}}, \tag{5.6}$$

and let $\mathscr{D}_r$ be defined by

$$\mathscr{D}_r: \qquad t-r-r' \leqslant t' \leqslant t-\bar{R}, \quad 0 \leqslant \theta' \leqslant \pi-\theta, \tag{5.7}$$

for $y > 0$ (see Fig. 2); if $y < 0$, θ and θ' must again be replaced by $2\pi-\theta$, $2\pi-\theta'$ in the definition of $\mathscr{D}_r$. Applying (2.3) to $\mathscr{D}_r$ with $\bar{v}$ instead of v, and to $\mathscr{D}_d$ with $\frac{1}{2}\bar{v}$ instead of v, and adding the resulting equations, we obtain, after a calculation similar to the one which has just been carried out, that

$$0 = \iiint_{\mathscr{D}_r} \frac{f_1(x',y',t')}{\bar{\gamma}^{\frac{1}{2}}}\,dx'dy'dt' + \tfrac{1}{2}\iiint_{\mathscr{D}_d} \frac{f_1(x',y',t')}{\bar{\gamma}^{\frac{1}{2}}}\,dx'dy'dt' -$$

$$-\,{\iint_{\mathscr{S}_i}}^{*} \left\{\frac{q(x',t')}{\gamma_0^{\frac{1}{2}}} - \frac{yp(x',t')}{\gamma_0^{\frac{3}{2}}}\right\} dx'dt' - \tfrac{1}{2}{\iint_{\mathscr{S}_d}}^{*} \left\{\frac{q^*(x',t')}{\gamma_0^{\frac{1}{2}}} - \frac{yp^*(x',t')}{\gamma_0^{\frac{3}{2}}}\right\} dx'dt'. \tag{5.8}$$

The left-hand side is zero as neither $\mathscr{D}_r$ nor $\mathscr{D}_d$ contains the point $(x, -y, t)$.

6. We can now deduce the solutions of problems I and II from (5.3) and (5.8). In problem I, q is given and so, by (5.1), $q^* = 0$. Hence, adding (5.3) and (5.8), we obtain

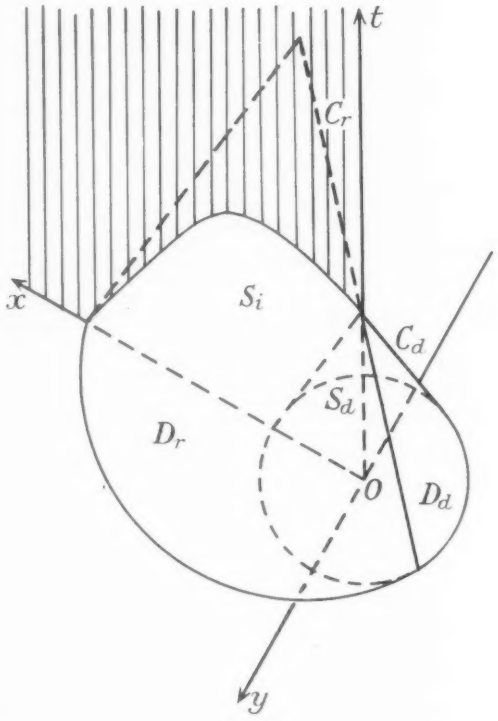

FIG. 2.

$$u_1(x,y,t) = -\frac{\operatorname{sgn} y}{\pi} \iint_{\mathscr{D}_i} \frac{q(x',t')}{\gamma_0^{\frac{1}{2}}}\, dx'dt' +$$

$$+\frac{1}{2\pi} \iiint_{\mathscr{D}_i+\mathscr{D}_r+\mathscr{D}_d} V_1(x,y,t;x',y',t') f_1(x',y',t')\, dx'dy'dt', \quad (6.1)$$

where V_1 is defined by

$$V_1 = \frac{1}{\gamma^{\frac{1}{2}}} \text{ in } \mathscr{D}_i; \qquad V_1 = \frac{1}{\gamma^{\frac{1}{2}}} + \frac{1}{\bar{\gamma}^{\frac{1}{2}}} \text{ in } \mathscr{D}_r; \qquad V_1 = \frac{1}{2}\left(\frac{1}{\gamma^{\frac{1}{2}}} + \frac{1}{\bar{\gamma}^{\frac{1}{2}}}\right) \text{ in } \mathscr{D}_d, \quad (6.2)$$

$\mathscr{D}_i$ being the domain of points belonging to $\mathscr{D}_0$ but not to $\mathscr{D}_r$, and it will be recalled that $f_1 = f$ above C_1 and $f_1 = 0$ below C_1.

In problem II, p is given and hence $p^* = 0$; subtracting (5.8) from (5.3), we obtain therefore

$$u_2(x,y,t) = -\frac{|y|}{\pi}\overset{*}{\iint_{\mathscr{D}_i}}\frac{p(x',t')}{\gamma_0^{\frac{1}{2}}}\,dx'dt' + \\ + \frac{1}{2\pi}\iiint_{\mathscr{D}_i+\mathscr{D}_r+\mathscr{D}_d} V_2(x,y,t;x',y',t')f_1(x',y',t')\,dx'dy'dt', \quad (6.3)$$

where

$$V_2 = \frac{1}{\gamma^{\frac{1}{2}}} \text{ in } \mathscr{D}_i; \qquad V_2 = \frac{1}{\gamma^{\frac{1}{2}}} - \frac{1}{\bar{\gamma}^{\frac{1}{2}}} \text{ in } \mathscr{D}_r; \qquad V_2 = \frac{1}{2}\left(\frac{1}{\gamma^{\frac{1}{2}}} - \frac{1}{\bar{\gamma}^{\frac{1}{2}}}\right) \text{ in } \mathscr{D}_d. \quad (6.4)$$

The solutions of problems I and II, if they exist, are necessarily of the forms (6.1), (6.3) respectively. To make the argument rigorous, we should now establish the existence of these solutions by verifying that the expressions (6.1), (6.3) for u_1 and u_2 satisfy the wave equation and the respective boundary conditions. The calculations involved are lengthy, and of some complexity, and will be omitted. If the homogeneous wave equation is considered, so that $f = 0$ and the volume integrals in (6.1), (6.3) are absent, no particular difficulty is encountered. To verify that the wave equation is, for example, satisfied by

$$-\frac{\operatorname{sgn} y}{\pi}\iint_{\mathscr{D}_i}\frac{q(x',t')}{\gamma_0^{\frac{1}{2}}}\,dx'dt'$$

it is permissible, according to Hadamard, to differentiate under the integral sign, provided that the resulting integrals are interpreted as 'finite parts', and that any fractional infinities arising from differentiation with respect to the variable limits are omitted. (The expressions for the second-order derivatives also contain finite line integrals; these, however, cancel on substitution in the wave equation.) This process is valid only if the finite parts of divergent integrals occurring in the formal expressions for the second-order derivatives have a meaning. A sufficient condition for this is that q should possess partial derivatives of the first order satisfying Lipschitz conditions. But if q is, for example, singular on a curve in the (x,t)-plane, the expression for u_1 may still be valid; such cases are best examined as they arise.

As for the boundary condition at $y = 0$, $x \geqslant 0$, the verification is exactly as in the case of the boundary $y = 0$, $-\infty < x < \infty$. It is analogous to the treatment of a double layer in the theory of potential.

The volume integral is more troublesome. The singularity near $x' = x$, $y' = y$, $t' = t$ occurs in the solution of Cauchy's problem, and is dealt with in Hadamard's book. However, formal differentiation gives integrals with singularities at $\theta' = \pi \pm \theta$, $t' = t - r - r'$, $r' \geqslant 0$, to which the method of the 'finite part' cannot be applied directly. I have not carried out the calculation in this case, but there is little doubt that it would lead to the requisite verification.

The solution (6.3) can be considered in a similar manner. It must be noted, however, that as the surface integral is now a 'finite part', a sufficient condition for the validity of the solution is that the partial derivatives of the second order of p should exist and satisfy Lipschitz conditions.

7. A little consideration will show that the process by which (6.1) and (6.3) have been obtained is equivalent to taking the function v in (2.3) to be V_1, defined by (6.2), or V_2, defined by (6.4), respectively. These functions therefore play the role of Green's functions for these problems, and by reciprocity the solutions of the associated diffraction problems for an incident wave generated by an instantaneous point source can be obtained. In fact, suppose that $p = q = 0$, and let $f(x, y, t)$ tend to the singular function

$$f(x, y, t) = \delta(x - x_0)\delta(y - y_0)\delta(t), \tag{7.1}$$

where δ denotes Dirac's δ-function. The limiting values of (6.1) and (6.3) are then the solutions of the diffraction problems with an incident wave

$$\left.\begin{aligned} u_0 &= \{t^2 - (x-x_0)^2 - (y-y_0)^2\}^{-\frac{1}{2}} && (t > \{(x-x_0)^2 + (y-y_0)^2\}^{\frac{1}{2}}) \\ &= 0 && (t < \{(x-x_0)^2 + (y-y_0)^2\}^{\frac{1}{2}}) \end{aligned}\right\} \tag{7.2}$$

for the boundary conditions $\partial u/\partial y = 0$ and $u = 0$, at $y = 0$, $x \geqslant 0$, respectively. Let, for example, $y_0 \geqslant 0$ and put

$$\left.\begin{aligned} \rho &= \{(x-x_0)^2 + (y-y_0)^2\}^{\frac{1}{2}}, \qquad \bar{\rho} = \{(x-x_0)^2 + (y+y_0)^2\}^{\frac{1}{2}} \\ x_0 &= r_0 \cos\theta_0, \qquad y_0 = r_0 \sin\theta_0 \quad (0 < \theta_0 < \pi) \end{aligned}\right\} \tag{7.3}$$

$$\left.\begin{aligned} \bar{u}_0 &= (t^2 - \bar{\rho}^2)^{-\frac{1}{2}} && (t > \bar{\rho}) \\ &= 0 && (t < \bar{\rho}) \end{aligned}\right\}. \tag{7.4}$$

Let the domains $\mathscr{D}_i^0$, $\mathscr{D}_r^0$, $\mathscr{D}_d^0$ be defined by

$$\left.\begin{aligned} \mathscr{D}_i^0\text{:} \quad & \begin{cases} 0 < \theta \leqslant \pi - \theta_0, & \rho < t < \bar{\rho} \\ \pi - \theta_0 \leqslant \theta < \pi_0 + \theta, & \rho < t < r_0 + r \end{cases} \\ \mathscr{D}_r^0\text{:} \quad & 0 < \theta < \pi - \theta_0, \qquad \bar{\rho} < t < r_0 + r \\ \mathscr{D}_d^0\text{:} \quad & 0 < \theta < 2\pi, \qquad r_0 + r < t \end{aligned}\right\}. \tag{7.5}$$

Then it follows from (6.1) and (6.3) that the solutions of these 'elementary' diffraction problems are

$$\left.\begin{aligned} &u = u_0 \text{ in } \mathscr{D}_i^0; && u = u_0 \pm \bar{u}_0 \text{ in } \mathscr{D}_r^0; \\ &u = \tfrac{1}{2}(u_0 \pm \bar{u}_0) \text{ in } \mathscr{D}_d^0; && u = 0 \text{ at all other points,} \end{aligned}\right\} \tag{7.6}$$

with the upper sign for problem I and the lower sign for problem II. (If the origin in Figs. 1 and 2 is moved to $(0, 0, t)$, the sense of the t-axis is reversed, and x, y are replaced by x_0, y_0, then these figures represent $\mathscr{D}_i^0 + \mathscr{D}_r^0$ and $\mathscr{D}_d^0$, and $\mathscr{D}_r^0$, $\mathscr{D}_d^0$, respectively.)

These results are remarkable, both because of their simplicity, and because of the discontinuity on the 'diffraction characteristic'

$$t = r_0 + r.$$

In either case the discontinuity is compatible with the wave equation, or rather with the generalized continuity equation

$$\int \frac{du}{dv}\, dS = 0,$$

which follows from (2.1) by taking $v = 1, f = 0$, as the square of the saltus satisfies the intensity law of geometrical optics (3). Mathematically, the discontinuity is probably due to the singular behaviour of the elementary solution (6.5) on its wave front. Its physical meaning is obscure, but it must be remembered that (6.5) represents an instantaneous infinitely long line source. For a source which is not instantaneous, the discontinuity disappears.

8. Finally, it may be of some interest to compare the results obtained here with some of the results obtained by different methods. In the first place, consider (7.6). It is to be expected that the Laplace transform of this solution is the Green's function of the half-plane for the equation

$$\frac{\partial^2 U}{\partial x^2} + \frac{\partial^2 U}{\partial y^2} = s^2 U. \tag{8.1}$$

Let (x, y) be a point of the shadow, so that $\pi + \theta_0 < \theta < 2\pi$. Then, by (7.5), (7.6),

$$u = \tfrac{1}{2}(u_0 + \bar{u}_0) \quad (t > r + r_0); \qquad u = 0 \quad (t < r + r_0). \tag{8.2}$$

The Laplace transform of this function is

$$\frac{1}{2} \int_{r+r_0}^{\infty} \frac{e^{-st}}{(t^2 - \rho^2)^{\frac{1}{2}}}\, dt \pm \frac{1}{2} \int_{r+r_0}^{\infty} \frac{e^{-st}}{(t^2 - \bar{\rho}^2)^{\frac{1}{2}}}\, dt$$

Putting $t^2 = \rho^2+\nu^2$ in the first, and $t^2 = \bar{\rho}^2+\nu^2$ in the second of these integrals, we obtain the expression

$$U = \frac{1}{2}\int_{2\nu(rr_0)^{\frac{1}{2}}|\cos\{(\theta-\theta_0)/2\}|}^{\infty} \frac{e^{-s(\rho^2+\nu^2)^{\frac{1}{2}}}}{(\rho^2+\nu^2)^{\frac{1}{2}}}\,d\nu \pm \frac{1}{2}\int_{2\nu(rr_0)^{\frac{1}{2}}|\cos\{(\theta+\theta_0)/2\}|}^{\infty} \frac{e^{-s(\bar{\rho}^2+\nu^2)}}{(\bar{\rho}^2+\nu^2)^{\frac{1}{2}}}\,d\nu, \quad (8.3)$$

with the upper sign again for the boundary condition $\partial U/\partial y = 0$ on $y = 0$, $x \geqslant 0$, and the lower sign for the boundary condition $U = 0$ on $y = 0$, $x \geqslant 0$. This, however, is equivalent to the Green's functions deduced from Sommerfeld's integral (**4**, equation (42)); it is easily verified that at points not in the shadow, the corresponding expressions are obtained by taking the Laplace transform of (7.6).

Next, let us consider the homogeneous wave equation, i.e. take $f = 0$. Then, if we let $y \to \pm 0$ in (6.1) we obtain, for $x > 0$,

$$\lim_{y=\pm 0} u_1 = \mp\frac{1}{\pi}\int_0^{\infty} dx' \int_{t-x-x'}^{t-|x-x'|} \frac{q(x',t')\,dt'}{\{(t-t')^2-(x-x')^2\}^{\frac{1}{2}}}, \quad (8.4)$$

which is equivalent to a result which has been obtained by Evvard (**5**) and Ward (**6**).

In the homogeneous case, $-u_1(x,-y,t)$ satisfies the same boundary conditions as $u_1(x,y,t)$, as well as the wave equation, and so by the uniqueness theorem

$$u_1(x,y,t) = -u_1(x,-y,t),$$

so that u_1 is an odd function of y. In particular, it vanishes on $y = 0$, $x < 0$, and so by (1.7) the function u_3, which is the solution of the diffraction problem for an incident wave u_0 with the boundary condition $\partial u/\partial y = 0$ on the screen, satisfies the boundary corditions

$$u = u_0 \quad (y = 0,\ x < 0); \qquad \partial u/\partial y = 0 \quad (y = 0,\ x > 0). \quad (8.5)$$

Similarly, u_2 is an even function of y and its derivative vanishes on $y = 0$, $x < 0$. Hence, if the wave-front characteristic of u_0 is of a suitable type, u_3 may be defined, for example, in $y < 0$ as the solution of a problem of type II, with u given, and equal to u_0, on $y = 0$, $x < 0$. This formulation of the diffraction problem has been used by Fox (**7**), who has obtained the value of u on $y = 0$, $x > 0$ from an integral equation. His result can also be deduced from (6.3), by considering the limiting value of the surface integral as $y \to 0$ for $x < 0$ (since (6.3) applies to problem II in the unmodified form).

Let us first calculate for this purpose

$$J = -\frac{|y|}{\pi}\int_{t-r-x'}^{*t-R_0} \frac{dt'}{\{(t-t')^2-R_0^2\}^{\frac{1}{2}}} = -\frac{|y|}{\pi}\int_{R_0}^{*r+x'} \frac{d\tau}{(\tau^2-R_0^2)^{\frac{1}{2}}}. \quad (8.6)$$

By definition, this is the limit of

$$-\frac{|y|}{\pi}\int_{R_0+\epsilon}^{r+x'}\frac{d\tau}{(\tau^2-R_0^2)^{\frac{3}{2}}}+\frac{A}{\epsilon^{\frac{1}{2}}},$$

as $\epsilon\to 0$, where A is chosen so as to cancel the fractional infinity. From this it follows that

$$J=\frac{|y|}{\pi R_0^2}\frac{r+x'}{\{2x'(r+x)\}^{\frac{1}{2}}}=\frac{1}{\pi}\left(\frac{r-x}{2x'}\right)^{\frac{1}{2}}\frac{r+x'}{(x-x')^2+y^2},$$

and hence, as $y\to 0$ and so $r\to -x$ (for $x<0$),

$$\lim_{y=0}J=\frac{1}{\pi}\left(\frac{|x|}{x'}\right)^{\frac{1}{2}}\frac{1}{x'-x}. \tag{8.7}$$

Now we can write (6.3) for $f=0$ as

$$u_2=\int_0^\infty p(x',t-R_0)J\,dx'+\frac{|y|}{\pi}\int_0^\infty dx'\int_{t-r-x'}^{t-R_0}\frac{p(x',t-R_0)-p(x',t')}{\{(t-t')^2-R_0^2\}^{\frac{3}{2}}}\,dt'.$$

Assuming that p satisfies a Lipschitz condition, and is bounded, it is easily shown that the second integral tends to zero with y, and that the passage to the limit under the integral sign in the first term is legitimate, so that

$$\lim_{y=0}u_2=\frac{1}{\pi}\int_0^\infty\frac{p(x',t+x-x')}{x'-x}\left(\frac{|x|}{x'}\right)^{\frac{1}{2}}dx'\quad(x<0), \tag{8.8}$$

which is equivalent to the result obtained by Fox (**7**, Appendix B).

REFERENCES

1. See e.g. F. G. Friedlander, 'Note on the geometrical optics of diffracted wave fronts', *Proc. Camb. Phil. Soc.* **45** (1949), 395–404.
2. J. Hadamard, *Lectures on Cauchy's Problem*, 117–214 (Yale, 1923).
3. F. G. Friedlander, 'On the solutions of the wave equation with discontinuous derivatives', *Proc. Camb. Phil. Soc.* **38** (1943), 378–82.
4. J. C. Gunn, 'Linearized supersonic aerofoil theory', *Phil. Trans.* A, **240** (1947), 327–73.
5. J. C. Evvard, *Distribution of Wave Drag and Lift in the Vicinity of Wing Tips at Supersonic Speeds*, Nat. Adv. Comm. for Aeronautics (U.S.A.), Technical Note No. 1382 (1947).
6. G. N. Ward, 'Supersonic flow past thin wings, I. General theory', *Quart. J. Mech. and Applied Math.* **2** (1949), 136–52, eq. (31).
7. E. N. Fox, 'The diffraction of sound pulses by an infinitely long strip', *Phil. Trans.* A, **241** (1948), 71–103.

A NEW RELAXATION TREATMENT OF FLOW WITH AXIAL SYMMETRY

By L. C. WOODS (*Engineering Laboratory, Oxford*)

[Received 16 January 1951]

SUMMARY

In this paper methods are developed for the calculation of incompressible and compressible flow under conditions of axial symmetry. Relaxation is used to solve new forms of the flow equations. In these equations ϕ, the velocity potential, and ψ, Stokes's stream function, for the incompressible flow, are the independent variables.

The radial distance, r, is the dependent variable in the incompressible flow equation, and this feature renders the method especially suitable for the design of axially symmetric ducts. A typical design problem is calculated as an example at the end of the paper.

$\mathrm{Log}(1/q)$, where q is the velocity, is the dependent variable in the compressible flow equation, which can only be solved after the incompressible flow solution has been found.

Nomenclature

r radial distance measured from axis of symmetry.
x distance measured parallel to axis of symmetry.
u, v velocity components in the x and r directions respectively.
(q, θ) velocity vector in polar coordinates.
(ϕ, ψ) the incompressible flow plane, in which ϕ is the velocity potential, and ψ is Stokes's stream function.
n, m mesh size in ϕ and ψ directions respectively.
$f = r^2$.
$L = \log(1/q)$.
ρ density.
M local Mach number.
a local velocity of sound.
ζ vorticity.
α angle between the incompressible flow vector and the compressible flow vector.

1. Introduction

THIS paper extends the methods of references **1** and **2** to the flow of an inviscid fluid with axial symmetry. Even for incompressible flow, the equation of motion is too difficult to solve except by a relaxation treatment. Relaxation and 'squaring' treatments of similar problems of axial symmetry have been given (**3**, **4**) but they have all been based on equations

in which x and r have been the independent variables. This has the disadvantage of requiring 'irregular stars' in the relaxation mesh near curved boundaries. The method of the present paper avoids this difficulty by taking ϕ and ψ as the independent variables. For the incompressible flow r is taken to be the dependent variable, a procedure which permits the direct design of ducts.

The design problem is essentially the calculation of r on the duct boundary such that a specified pressure distribution is achieved. When working in the (x, r)-plane with ϕ (or ψ) as the dependent variable, the relaxation pattern involves r, which is, of course, unknown on the boundary in the design problem. (However, a 'trial and error' method of design in the (x, r)-plane has been developed (**5**).) Interchanging the roles of (x, r) and (ϕ, ψ) avoids the difficulty, and the design can be carried out directly. As an example of the method a design problem is worked out in section 7.

For compressible flow L $(\log(1/q))$ is taken to be the dependent variable in the (ϕ, ψ)-plane. The method is very similar to that developed previously for two-dimensional flow (**2**).

2. Incompressible flow

By definition we have

$$\phi_x = u = \frac{1}{r}\psi_r, \qquad \phi_r = v = -\frac{1}{r}\psi_x, \tag{1}$$

while Laplace's equation for ϕ and ψ can be written

$$\psi_{xx} - \frac{\psi_r}{r} + \psi_{rr} = 0, \qquad \phi_{xx} + \frac{\phi_r}{r} + \phi_{rr} = 0, \tag{2}$$

where suffixes denote partial derivatives. Now

$$\frac{\partial(\phi, \psi)}{\partial(x, r)} = \phi_x\psi_r - \phi_r\psi_x = r(u^2 + v^2) = rq^2,$$

and therefore

$$x_\phi = \frac{\psi_r}{rq^2}, \qquad x_\psi = -\frac{\phi_r}{rq^2}, \qquad r_\phi = -\frac{\psi_x}{rq^2}, \qquad r_\psi = \frac{\phi_x}{rq^2}, \tag{3}$$

where suffixes denote partial derivatives.

From (1) and (3) we find

$$x_\phi = rr_\psi, \qquad x_\psi = -\frac{r_\phi}{r}, \tag{4}$$

and hence

$$\frac{\partial}{\partial\phi}\left(\frac{1}{r}\frac{\partial r}{\partial\phi}\right) + \frac{\partial}{\partial\psi}\left(r\frac{\partial r}{\partial\psi}\right) = 0, \tag{5}$$

and

$$\frac{\partial}{\partial\phi}\left(\frac{1}{r}\frac{\partial x}{\partial\phi}\right) + \frac{\partial}{\partial\psi}\left(r\frac{\partial x}{\partial\psi}\right) = 0. \tag{6}$$

If we write
$$f = r^2 \tag{7}$$
equation (5) becomes
$$\frac{\partial}{\partial\phi}\left(\frac{1}{f}\frac{\partial f}{\partial\phi}\right)+\frac{\partial^2 f}{\partial\psi^2}=0. \tag{8}$$

Equation (6) is of no value as it involves both dependent variables, but equation (8) is relatively simple. A relaxation treatment of (8) is given in the next section.

From (4) it follows that
$$\begin{aligned} dx &= rr_\psi\,d\phi-(r_\phi/r)\,d\psi \\ &= \tfrac{1}{2}\{f_\psi\,d\phi-(f_\phi/f)\,d\psi\}, \end{aligned} \tag{9}$$
which enables $x = x(\phi,\psi)$ to be calculated directly from the $f = f(\phi,\psi)$ solution of equation (8).

Further, from (1) and (3),
$$q = (r_\phi^2+r^2(r_\psi)^2)^{-\frac{1}{2}}, \qquad \theta = \tan^{-1}\left(\frac{r_\phi}{rr_\psi}\right);$$
i.e.
$$q = 2(f_\phi^2/f+(f_\psi)^2)^{-\frac{1}{2}}, \quad \theta = \tan^{-1}\left(\frac{f_\phi}{f^{\frac{1}{2}}f_\psi}\right), \tag{10}$$
and so the velocity vector (q,θ) can be directly calculated from the f field.

3. Relaxation solution

Fig. 1 shows four typical rectangles of the ϕ,ψ mesh. The points a, b, c, and d bisect the intervals 0–2, 0–3, 0–4, and 0–1 respectively. The difference equation corresponding to (8) can be written†
$$\left(\frac{m}{n}\right)^2\left(\frac{f_1-f_0}{f_d}-\frac{f_0-f_3}{f_b}\right)+(f_2+f_4-2f_0) = X_0 = 0. \tag{11}$$

For an arbitrary arrangement of the f field, X (residual of the relaxation process) will not generally be zero. From (11) we find the 'influence coefficients'
$$\left.\begin{aligned} &\frac{\partial X_0}{\partial f_{2,4}} = 1, \qquad \frac{\partial X_0}{\partial f_0} = -\left\{2+\left(\frac{m}{n}\right)^2\left(\frac{1}{f_d}+\frac{1}{f_b}\right)\right\} \\ &\frac{\partial X_0}{\partial f_1} = \left(\frac{m}{n}\right)^2\Big/f_d, \qquad \frac{\partial X_0}{\partial f_3} = \left(\frac{m}{n}\right)^2\Big/f_b \end{aligned}\right\}. \tag{12}$$

For most practical problems $\dfrac{\partial f}{\partial\phi} \ll \dfrac{\partial f}{\partial\psi}$ and so it is sufficient to interpolate for f_d and f_b using
$$f_b = \tfrac{1}{2}(f_3+f_0), \qquad f_d = \tfrac{1}{2}(f_1+f_0).$$

Since f is usually large compared with $\partial f/\partial\phi$ and $\partial^2 f/\partial\phi^2$, a close approximation to equation (8) is
$$\frac{\partial^2 f}{\partial\psi^2} = 0,$$

† See Appendix for an alternative method.

i.e. $$\frac{\partial f}{\partial \psi} = \text{const.}, \quad \text{on} \quad \phi = \text{const.}, \tag{13}$$

and the corresponding difference equation is

$$f_2 + f_4 = 2f_0.$$

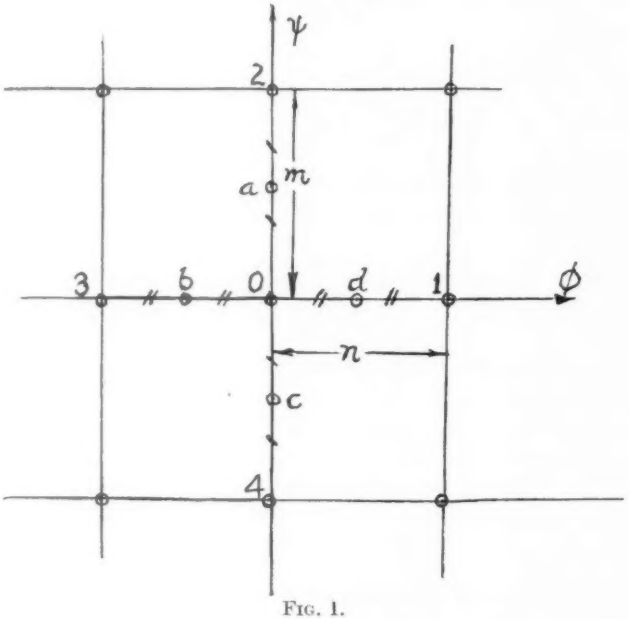

FIG. 1.

From the last of equations (3) we find that equation (13) implies that $u/q^2 = \text{const.}$, on $\phi = \text{const}$. Now the linear theory of axial symmetric flow assumes that $v = 0, q = u = \text{const.}$, on ϕ (i.e. in this case, x) = const. and so the approximation (13) is equivalent to assuming the linear theory, and is a useful starting assumption for the f field.

4. Boundary conditions

Normally either r or q will be specified on a boundary as a function of x. We shall assume for the moment that we have been able to find q or r as functions of ϕ. Then with $r = r(\phi)$ there is no difficulty, while with $q = q(\phi)$ we proceed as follows.

Suppose the line 3–0–1 in Fig. 1 is the boundary, then from (10)

$$\frac{16m^2}{q_0^2} = \left(\frac{m}{n}\right)^2 \frac{(f_1 - f_3)^2}{f_0} + (f_2 - f_4)^2, \tag{14}$$

i.e. $$f_2 = f_4 + 2\left\{\frac{4m^2}{q_0^2} - \left(\frac{m}{n}\right)^2 \frac{(f_1 - f_3)^2}{4f_0}\right\}^{\frac{1}{2}}. \tag{15}$$

Using this in (11) we have for a boundary point

$$X_0 = \left(\frac{m}{n}\right)^2\left(\frac{f_1-f_0}{f_d}+\frac{f_3-f_0}{f_b}\right)+2f_4+2\left\{\frac{4m^2}{q_0^2}-\left(\frac{m}{n}\right)^2\frac{(f_1-f_3)^2}{f_0}\right\}^{\frac{1}{2}}-2f_0, \tag{16}$$

and since usually $(f_1-f_3)^2/4f_0$ is $\ll 4m^2/q_0^2$, the approximate influence coefficients

$$\frac{\partial X_0}{\partial f_4}=2, \qquad \frac{\partial X_0}{\partial f_1}=\left(\frac{m}{n}\right)^2\Big/f_d, \qquad \frac{\partial X_0}{\partial f_3}=\left(\frac{m}{n}\right)^2\Big/f_b,$$

$$\frac{\partial X_0}{\partial f_0}=-\left\{2+\left(\frac{m}{n}\right)^2\left(\frac{1}{f_b}+\frac{1}{f_d}\right)\right\}, \tag{17}$$

can be used. Any errors introduced by this approximation are detected when (16) is used to recalculate residuals as a check at the end of the calculation.

On lines $\phi = \text{const.}$ at a sufficient distance upstream and downstream the linear theory will enable fairly accurate boundary conditions to be established.

Now it remains to show how we can arrive at $q = q(\phi)$ from $q = q(x)$. Using the linear theory we can deduce an approximate $\phi = \phi(x)$, and hence an approximate $q = q(\phi)$ to start with. The f field is then relaxed with these approximate boundary conditions. Next we integrate along the boundary, $\psi = \text{const.}$, using a difference equation form of (9), i.e., referring to Fig. 1,

$$x_1-x_3=\left(\frac{n}{m}\right)\tfrac{1}{2}(f_2-f_4).$$

Substituting the value of f_2 from (11) we have

$$x_1-x_3=\left(\frac{n}{m}\right)\left\{(f_0-f_4)-\frac{1}{2}\left(\frac{m}{n}\right)^2\left(\frac{f_1-f_0}{f_d}+\frac{f_3-f_0}{f_b}\right)\right\}, \tag{18}$$

from which we find immediately $x = x(\phi)$.

Using this in $q = q(x)$ we find a new and more accurate relation $q = q(\phi)$, the relaxation is carried out with these more accurate boundary values, and so on. This iterative process converges rapidly.

5. Compressible flow

In this section incompressible values will be distinguished by a suffix '0'.

We have the following equations

Continuity:
$$\frac{\partial(\rho u r)}{\partial x}+\frac{\partial(\rho v r)}{\partial r}=0. \tag{19}$$

Bernoulli:
$$q\,dq=-a^2\,d\rho/\rho. \quad \text{i.e. } dL=\frac{d\rho}{M^2\rho}. \tag{20}$$

Vorticity:
$$\frac{\partial v}{\partial x}-\frac{\partial u}{\partial r}=\zeta. \tag{21}$$

(19) can be written

$$\rho r\left(\frac{\partial u}{\partial x}+\frac{\partial v}{\partial r}\right)+\rho v = -ur\frac{\partial \rho}{\partial x}-vr\frac{\partial \rho}{\partial r}.$$

Therefore, using (20),

$$r\left(\frac{\partial u}{\partial x}+\frac{\partial v}{\partial r}\right)+v = -rM^2\left(u\frac{\partial L}{\partial x}+v\frac{\partial L}{\partial r}\right).$$

Writing $u = q\cos\theta$ and $v = q\sin\theta$, this equation becomes

$$r\left(-\sin\theta\frac{\partial\theta}{\partial x}-\cos\theta\frac{\partial L}{\partial x}+\cos\theta\frac{\partial\theta}{\partial r}-\sin\theta\frac{\partial L}{\partial r}\right)+\sin\theta$$

$$= -rM^2\left(\cos\theta\frac{\partial L}{\partial x}+\sin\theta\frac{\partial L}{\partial r}\right) = r\lambda', \text{ say.} \quad (22)$$

Also (21) can be written

$$r\left(\cos\theta\frac{\partial\theta}{\partial x}-\sin\theta\frac{\partial L}{\partial x}+\sin\theta\frac{\partial\theta}{\partial r}+\cos\theta\frac{\partial L}{\partial r}\right) = \frac{r\zeta}{q}. \quad (23)$$

From (22) and (23) we find

$$r\left(-\frac{\partial L}{\partial x}+\frac{\partial\theta}{\partial r}\right)+\cos\theta\sin\theta = r\left(\lambda'\cos\theta+\frac{\zeta}{q}\sin\theta\right), \quad (24)$$

and

$$r\left(-\frac{\partial\theta}{\partial x}-\frac{\partial L}{\partial r}\right)+\sin^2\theta = r\left(\lambda'\sin\theta-\frac{\zeta}{q}\cos\theta\right). \quad (25)$$

We now transform to the (ϕ,ψ) plane using

$$\frac{\partial}{\partial x} \equiv u_i\frac{\partial}{\partial\phi}-rv_i\frac{\partial}{\partial\psi}, \quad \text{and} \quad \frac{\partial}{\partial r} \equiv v_i\frac{\partial}{\partial\phi}+ru_i\frac{\partial}{\partial\psi},$$

which follow from (1), then after some calculation (24) and (25) yield

$$-\frac{\partial L}{\partial\phi}+r\frac{\partial\theta}{\partial\psi} = \lambda_1\cos\alpha+\frac{\zeta}{qq_i}\sin\alpha, \quad (26)$$

$$\frac{\partial\theta}{\partial\phi}+r\frac{\partial L}{\partial\psi} \equiv -\lambda_1\sin\alpha+\frac{\zeta}{qq_i}\cos\alpha, \quad (27)$$

where

$$\lambda_1 = -M^2\left(\cos\alpha\frac{\partial L}{\partial\phi}+\sin\alpha\frac{\partial L}{\partial\psi}\right)-\frac{\sin\theta}{rq_i}. \quad (28)$$

Cross differentiation of (26) and (27) yields

$$\frac{\partial}{\partial\psi}\left(r\frac{\partial L}{\partial\psi}\right)+\frac{\partial}{\partial\phi}\left(\frac{1}{r}\frac{\partial L}{\partial\phi}\right) = -\frac{\partial}{\partial\phi}\left\{\frac{1}{r}\left(\lambda_1\cos\alpha+\frac{\zeta}{qq_i}\sin\alpha\right)\right\}-$$

$$-\frac{\partial}{\partial\psi}\left\{\lambda_1\sin\alpha-\frac{\zeta}{qq_i}\cos\alpha\right\}, \quad (29)$$

$$\frac{\partial}{\partial\phi}\left(\frac{1}{r}\frac{\partial\theta}{\partial\phi}\right)+\frac{\partial}{\partial\psi}\left(r\frac{\partial\theta}{\partial\psi}\right) = -\frac{\partial}{\partial\phi}\left\{\frac{1}{r}\left(\lambda_1\sin\alpha-\frac{\zeta}{qq_i}\cos\alpha\right)\right\}+$$

$$+\frac{\partial}{\partial\psi}\left\{\lambda_1\cos\alpha+\frac{\zeta}{qq_i}\sin\alpha\right\}, \quad (30)$$

which correspond to equations (24) and (25) of reference **1** for two-dimensional motion.

If we ignore α, the error introduced will be small for subsonic flow, and further, if the vorticity is zero, (29) becomes

$$\frac{\partial}{\partial\psi}\left(r\frac{\partial L}{\partial\psi}\right)+\frac{\partial}{\partial\phi}\left(\frac{1}{r}\frac{\partial L}{\partial\phi}\right)=\frac{\partial}{\partial\phi}\left(\frac{M^2}{r}\frac{\partial L}{\partial\phi}\right)+\frac{\partial}{\partial\phi}\left(\frac{\sin\theta_i}{q_i r^2}\right). \tag{31}$$

If (8) and (10) have been solved, r, q_i, and $\sin\theta_i$ will be known as functions of ϕ and ψ, and hence (31) can be solved by relaxation.

A finite difference equation representing (31) is easily found. Referring to Fig. 1, we find that

$$r_a(L_2-L_0)-r_c(L_0-L_4)+\frac{1}{r_d}(L_1-L_0)-\frac{1}{r_b}(L_0-L_3)$$
$$=\left(\frac{M^2}{r}\right)_d(L_1-L_0)-\left(\frac{M^2}{r}\right)_b(L_0-L_3)+\left(\frac{\sin\theta}{q_i r^2}\right)_d-\left(\frac{\sin\theta}{q_i r^2}\right)_b,$$

and thus

$$\left(\frac{1-M^2}{r}\right)_d L_1+r_a L_2+\left(\frac{1-M^2}{r}\right)_b L_3+r_c L_4$$
$$=\left\{r_a+r_c+\left(\frac{1-M^2}{r}\right)_d+\left(\frac{1-M^2}{r}\right)_b\right\}L_0+\left(\frac{\sin\theta}{q_i r^2}\right)_d-\left(\frac{\sin\theta}{q_i r^2}\right)_b, \tag{32}$$

is a suitable difference equation representing (31).

The special case $r=0$ requires some attention. On $r=0$,

$$\frac{\partial L}{\partial\psi}=0,\quad \theta=0,\quad \frac{\partial r}{\partial\psi}=-\frac{\partial(r,x)}{\partial(\phi,\psi)}\frac{\partial\phi}{\partial x}=\frac{u_i}{rq_i^2}=0,$$

and

$$\frac{\partial r}{\partial\phi}=\frac{\partial(r,x)}{\partial(\phi,\psi)}\frac{\partial\psi}{\partial x}=\frac{v_i}{q_i^2}=0.$$

Substituting these special values in the expanded form of (31) we find

$$\frac{\partial^2 L}{\partial\phi^2}=\frac{\partial}{\partial\phi}\left(M^2\frac{\partial L}{\partial\phi}\right). \tag{33}$$

6. The boundary conditions

If R is the radius of curvature of the profile in the (x,r)-plane, and n is the direction normal to the profile boundary, then

$$\frac{\partial q}{\partial n}=\frac{q}{R}.$$

Hence,

$$\frac{\partial L}{\partial n}=-\frac{1}{R},$$

and since

$$\frac{\partial\psi}{\partial n}=q_i r,$$

then
$$\frac{\partial L}{\partial \psi} = -\frac{1}{Rq_i r}. \tag{34}$$

The boundary conditions are, of course, not specified for the (ϕ, ψ)-plane, but if the incompressible flow has been determined the relationship between the (x, r) and (ϕ, ψ) planes will be known, and hence the boundary conditions can be immediately deduced for the (ϕ, ψ) plane.

7. Example: the design of a contraction

The problem of this section arose in connexion with the design of a general-purpose wind tunnel which may shortly be erected in New Zealand. The problem was the design of a contraction ratio of 6·83 with a linear pressure gradient along the wall. Adverse pressure gradients were to be avoided if possible. The ratio of contraction length to the radius at the largest end was to be about 3·6. Air velocities were small enough to permit the assumption that flow was incompressible.

The solution is shown in Fig. 2. The curve ABC is that deduced by the theory of sections 3 and 4. It deviates considerably from the curve predicted by the linear theory. At first the contraction was started at the point B, where $\phi = 0$, but to give a more gentle lead into the contraction and to avoid too serious an adverse pressure gradient on the straight tunnel wall preceding the point B, the wall was 'relaxed' back to the point A so that constant pressure was maintained in the section AB. A very slight adverse pressure gradient still survives in the section AD, and in fact this will not disappear until the contraction is of infinite length. In other words, it is not possible to avoid an adverse pressure gradient in a contraction of finite length. This becomes evident when equation (14) is applied to a point such as F in Fig. 2. It is clear that $AG > EF$, i.e. from (14) $q_A < q_F$, therefore the pressure at A is greater than the pressure at F, and so there is an adverse pressure gradient along AD. Mr. W. Rainbird of Cranfield first drew the author's attention to this point. There must similarly be an adverse pressure gradient in the section CF. It will be noticed that the pressure curve has been rounded off at B and C to avoid a discontinuity in the gradient. Table 1 gives the coordinates of the contraction.

TABLE 1

Coordinates of the Contraction

r	16·00	16·00	15·54	14·83	12·96	11·15	10·15	9·17	8·56	8·14
x	0	10·4	22·9	29·0	34·4	38·0	40·6	44·6	48·4	51·8
ϕ		−1	$-\frac{1}{2}$	$-\frac{1}{4}$	0	$\frac{1}{4}$	$\frac{1}{2}$	1	$1\frac{1}{2}$	2

r	7·58	7·18	6·90	6·68	6·50	6·35	6·23	6·14	6·12	6·12
x	57·9	63·3	68·2	72·8	77·1	81·2	85·1	88·9	92·7	96·4
ϕ	3	4	5	6	7	8	9	10	11	12

Linear theory
Left hand section of duct
Right hand section of duct
Very slight adverse pressure gradient
Pressure Ratio
ψ=1
φ=-1
A
B
C
D
E
F
G
H

The calculations were made as follows

1. An approximate solution was found from the linear theory.

If the velocity at the inlet to the contraction is unity then, to give a linear pressure gradient, the velocity at a point x, in the contraction of length X, must be given by

$$q^2 = 1+\frac{x}{X}(k^2-1),$$

where k is the contraction ratio, and the origin is taken at the entrance to the contraction. Now

$$\phi = \int_0^X v\,dx = \int_0^X \left\{1+\frac{x}{X}(k^2-1)\right\}^{\frac{1}{2}} dx = \frac{2}{3}\frac{X}{k^2-1}\left\{\left(1+\frac{x}{X}(k^2-1)\right)^{\frac{3}{2}}-1\right\}. \tag{35}$$

When $x = X, \qquad \phi = \frac{2}{3}X(k^2-1)^{\frac{1}{2}}.$

Suppose that at $x = 0$, $r = r_0$, then $X = 3{\cdot}6r_0$ (specified ratio $X/r_0 = 3{\cdot}6$), i.e.

$$\phi = \tfrac{2}{3}\times 3{\cdot}6\times(6{\cdot}83^2-1)^{\frac{1}{2}}r_0 \doteq 16{\cdot}2r_0.$$

Now ψ on the boundary is given by

$$\psi_b = \int_0^{r_0} r\,dr = \tfrac{1}{2}r_0^2.$$

Hence, $\qquad \psi_b/\phi = r_0/32{\cdot}4;$ e.g. if $r_0 = 16$, $\psi_b/\phi = \frac{1}{2}$.

Suppose that there are 10 divisions of ϕ in the contraction, then there must be 5 divisions of ψ. These divisions are shown in Fig. 2, and the above argument shows why 16 was selected as the value of r_0.

Regardless of the nature of the pressure gradient, the linear theory yields

$$q_x r_x^2 = q_0 r_0^2,$$

i.e.
$$r_x = r_0/q_x^{\frac{1}{2}}, \tag{36}$$

and it was from this equation that the dotted line in Fig. 2 was calculated.

2. Using (35) we have
$$\phi = \phi(x), \tag{37}$$

and hence from the given pressure distribution, $p = p(x)$, we can deduce a relationship $q^2 = q^2(\phi)$ to use in equation (16). Further, from (36) and (37) we find approximate boundary values of f

$$f = f(\phi) = f\{\phi(x)\} = r^2 = r_0^2/q.$$

Equation (13) shows that we merely need to fill in the values of f along each equipotential line so that the gradient is linear, with $f = 0$ on $\psi = 0$, and $f = f(\phi)$ on $\psi = \psi_b$, to obtain a fair approximation to the f field.

3. The residuals are now calculated and the relaxation carried out. A point to notice here is that if the equipotentials are correctly spaced for a reasonably small mesh size (to avoid large errors in the neglected terms of

the exact difference equation) near the small end of the contraction, they will be far too largely spaced at the large end (see Fig. 2). This can be easily remedied by inserting extra equipotentials at the large end so that in equation (11) $m > n$. The mesh actually used is shown in Fig. 2.

4. Next equation (18) was used to integrate along the boundary to yield a new $x = x(\phi)$.

5. Steps 2 to 4 were repeated twice, after which no significant change occurred in the boundary conditions, and the f field was thus 'settled'.

6. Difference equations representing (9) and (10) were then used on the f field to complete the solution.

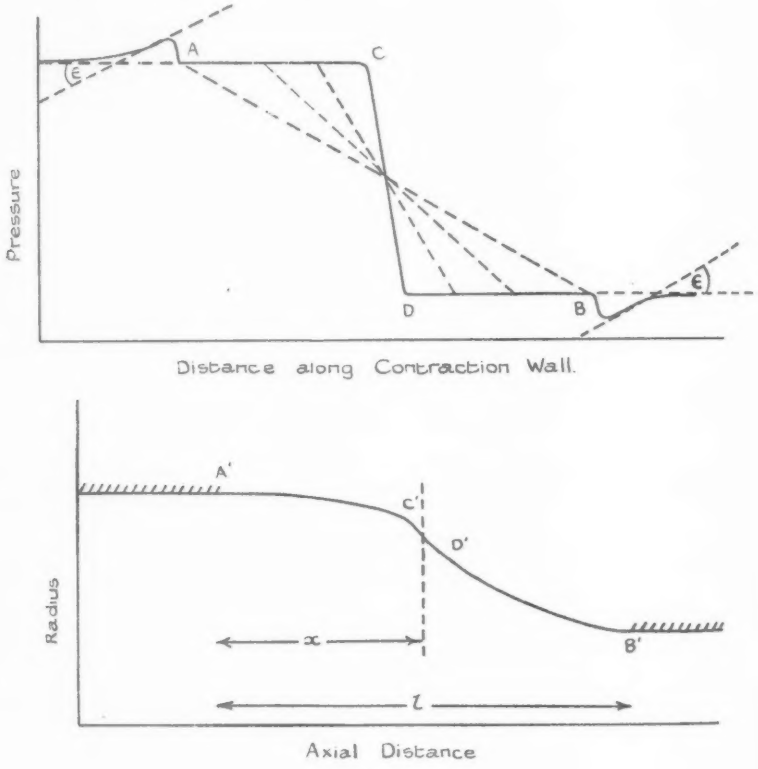

FIG. 3.

8. Design for minimum length of contraction ratio

It is of some interest to be able to design a contraction so that, given the contraction ratio and the maximum permissible adverse pressure gradient (ϵ), the contraction is of minimum length l. Referring to Fig. 3 we have to

determine the pressure curve AB so that, given ϵ, l is a minimum. This is a difficult problem, but it could be solved by relaxation. Consider the linear gradient family shown in Fig. 3. The experience gained with the problem of section 7 leads the author to believe that of this family the one labelled $ACDB$ (CD extends over one mesh interval only) would result in the shortest value of l. Theoretically the gradient of CD could be made infinite but, as in the corresponding two-dimensional problem, this would result in an infinite spiral at CD (θ becomes infinite at a discontinuity of $\log(1/q)$) which would be impracticable. If it is true that $ACDB$ (with CD vertical) is the optimum curve of the linear gradient family, then it appears that the significant point for minimum length is that the constant gradient portions, AC and DB, should be as long as possible. It also appears that $ACDB$ is the optimum curve for *all* possible families. A series of calculations by the method of this paper could prove or disprove this point. If $ACDB$ proved to be the optimum curve, then it would be necessary to carry out a further series of calculations to establish the optimum value of x/l at which CD is to be placed. At values of x/l other than this optimum it is likely that the adverse pressure gradient at one end of the contraction would not reach the permissible maximum ϵ.

Appendix

Since this paper was written a simplification of the relaxation treatment of equation (8) has occurred to the author. This equation can be written

$$\frac{\partial^2 \log(f)}{\partial \phi^2} + \frac{\partial^2 f}{\partial \psi^2} = 0. \tag{38}$$

Then with the same order of error term as for the difference equation (11) we can write (38) (see Fig. 1) in the form

$$\left(\frac{m}{n}\right)^2 \{\log(f_1) + \log(f_3) - 2\log(f_0)\} + \{f_2 + f_4 - 2f_0\} = X_0,$$

i.e.

$$\left(\frac{m}{n}\right)^2 \log(f_1 f_3 / f_0^2) + f_2 + f_4 - 2f_0 = X_0, \tag{39}$$

and the influence coefficients become

$$\frac{\partial X_0}{\partial f_{2,4}} = 1, \qquad \frac{\partial X_0}{\partial f_{1,3}} = \left(\frac{m}{n}\right)^2 \Big/ f_{1,3}, \qquad \frac{\partial X_0}{\partial f_0} = -2\left\{1 + \left(\frac{m}{n}\right)^2 \Big/ f_0\right\}. \tag{40}$$

The residuals are now calculated from (39) and relaxed using equations (40). Equations (39) and (40) have obvious advantages over (11) and (12). They are simpler and avoid the use of the intermediate points b and d.

With this modification, (16) and (18) become

$$X_0 = \left(\frac{m}{n}\right)^2 \log(f_1 f_3 / f_0^2) + 2(f_4 - f_0) + 2\left\{\frac{4m^2}{q_0^2} - \left(\frac{m}{n}\right)^2 \frac{(f_1 - f_3)^2}{f_0}\right\}^{\frac{1}{2}}, \tag{41}$$

and

$$x_1 - x_3 = \frac{n}{m}\left\{(f_0 - f_4) - \frac{1}{2}\left(\frac{m}{n}\right)^2 \log(f_1 f_3 / f_0^2)\right\}, \tag{42}$$

respectively.

REFERENCES

1. L. C. Woods, *The Design of an Aerofoil Profile to give a Specified Velocity Distribution at a Given Stream Mach Number*, A.R.C. 12,922—F.M. 1412 (Nov. 1949).
2. —— *A New Relaxation Treatment of the Compressible Two-dimensional Flow about an Aerofoil with Circulation*, A.R.C. 13,034—F.M. 1429 (March 1950).
3. R. V. Southwell, *Relaxation Methods in Theoretical Physics* (Oxford, 1946).
4. A. Thom, *Arithmetical Solution of Problems in Steady Viscous Flow*. R. & M. 1475 (May 1932).
5. G. K. Batchelor and F. S. Shaw, *A Consideration of the Design of Wind Tunnel Contractions*. Report ACA. 4 (March 1944).

APPLICATION OF RELAXATION TO THE ROTATIONAL FIELD OF FLOW BEHIND A BOW SHOCK WAVE

By A. R. MITCHELL (*Mathematics Department, United College, The University, St. Andrews*)

[Received 6 February 1951]

SUMMARY

A development of the relaxation technique due to R. V. Southwell for evaluating subsonic isentropic regions of compressible flow in two dimensions is used to evaluate mixed subsonic-supersonic regions where the flow is rotational.

The new technique is employed to determine the complete field downstream of the bow shock wave formed when a parallel supersonic flow of Mach number 1·8 impinges on a blunt-nosed two-dimensional obstacle. The vorticity is calculated everywhere in the field and it is found that the stream-line starting at the point of maximum vorticity on the bow shock wave is a locus of high vorticity in the rotational field downstream of the shock wave.

1. Introduction

Two attempts have been made so far to obtain a numerical solution of the field of flow behind a shock wave. Emmons (**1**) developed a method of relaxation, applicable to subsonic regions only, which he used to evaluate the rotational subsonic field of flow behind an arbitrarily placed shock in a hyperbolic channel. Maccoll and Codd (**2**) investigated the important practical problem of a supersonic flow of Mach number 1·5 streaming past a flat-nosed obstacle, the position of the bow shock wave having been obtained from photographs. They examined the subsonic region behind the shock wave by a relaxation method, the solution being based on the assumptions that the flow was irrotational and that the sonic line started at the obstacle corner and intersected the stream-lines at right angles.

In the present paper Southwell's relaxation method (**3**) for evaluating subsonic irrotational regions in two dimensions, as extended to cover supersonic regions by Rutherford and the present author (**4**), is further extended to evaluate mixed subsonic-supersonic regions where the flow is rotational. The new technique is then used to determine the entire field downstream of the bow shock wave formed when a uniform parallel flow of Mach number 1·8 impinges on a square-nosed two-dimensional obstacle.

Several attempts have been made to obtain an analytical solution in the hodograph plane of the two-dimensional field of flow behind a bow shock wave. These investigations, reviewed by Guderley (**5**) and Busemann (**6**), all deal with free stream supersonic Mach numbers close to $M = 1$. This restriction on Mach number permits the assumption of approximately

isentropic conditions behind the shock, and so Chaplygin's form of the compressible flow differential equation in the hodograph plane is used.

In a very recent paper Goldstein and Lighthill (**7**) gave some indication of the difficulties likely to be encountered in using the hodograph plane to obtain analytical solutions of flows with vorticity present. In the simple example of the flow of an incompressible stream with uniform shear past a circular cylinder, the hodograph plane was shown to be a Riemann surface of six sheets.

2. The fundamental equations

For the two-dimensional steady motion of a rotational non-viscous compressible fluid with uniform conditions at infinity, the stream-function ψ must satisfy (**8**)

$$\frac{\partial}{\partial x}\left(\frac{1}{\rho}\frac{\partial \psi}{\partial x}\right)+\frac{\partial}{\partial y}\left(\frac{1}{\rho}\frac{\partial \psi}{\partial y}\right)+\frac{p}{\mathscr{R}}\frac{\partial S}{\partial \psi}=0. \tag{1}$$

In this formula ρ, p, and S denote the density, pressure, and entropy respectively, while $\mathscr{R}$ is the gas constant. After some reduction this equation may be written in the form

$$\nabla^2(\chi\psi)-\psi\nabla^2\chi+\frac{p}{\mathscr{R}\chi}\frac{\partial S}{\partial \psi}=0, \tag{2}$$

where $\chi=\rho^{-1}$.

In the flow behind a shock, the conditions, although adiabatic, are not necessarily isentropic. However, the entropy maintains a constant value along each stream-line, and so Bernoulli's equation for the rth stream-line downstream of the shock may be written

$$\left(\frac{u}{c_s}\right)^2=\frac{2}{\gamma-1}\left\{1-\frac{p}{\rho}\frac{(\rho_s)_r}{(p_s)_r}\right\},$$

where u is the speed, γ denotes the ratio of the specific heats, and c_s is the speed of sound at a point of stagnation; also $(\rho_s)_r$ and $(p_s)_r$ are the values of the stagnation density and pressure respectively on the rth stream-line downstream of the shock. The pressure may be eliminated by using the adiabatic gas law

$$\frac{p}{\rho^\gamma}=\frac{p_s}{\rho_s^\gamma}e^{(S_r-S_0)/c_v}=k_r=\frac{(p_s)_r}{(\rho_s)_r^\gamma}, \tag{3}$$

where S_0, p_s, and ρ_s are the entropy, stagnation pressure, and density on all stream-lines upstream of the shock, and S_r and k_r are the entropy and adiabatic gas constant on the rth stream-line downstream of the shock. Bernoulli's equation thus becomes

$$\left(\frac{u}{c_s}\right)^2=\frac{2}{\gamma-1}\left\{1-\left(\frac{\rho}{(\rho_s)_r}\right)^{\gamma-1}\right\},$$

which may be written in the form

$$\frac{2}{\gamma-1}\left\{1-\left(\frac{\chi}{(\chi_s)_r}\right)^{2(1-\gamma)}\right\}=\frac{\chi^4}{c_s^2}\left\{\left(\frac{\partial\psi}{\partial x}\right)^2+\left(\frac{\partial\psi}{\partial y}\right)^2\right\}. \tag{4}$$

(2) and (4) are the fundamental equations for the flow behind a shock wave.

It will be advantageous to write these equations in the non-dimensional forms

$$\nabla^2(\chi\psi)-\psi\nabla^2\chi+\frac{p}{\mathscr{R}\chi}\frac{1}{\gamma\nu_r^2}\frac{\partial S}{\partial\psi}=0 \tag{5}$$

and

$$\frac{2}{\gamma-1}\{1-\chi^{2(1-\gamma)}\}=\nu_r^2\chi^4\left\{\left(\frac{\partial\psi}{\partial x}\right)^2+\left(\frac{\partial\psi}{\partial y}\right)^2\right\}. \tag{6}$$

To obtain these equations, some significant linear dimension h pertaining to the problem under consideration is chosen, and the flow parameter on the rth stream-line behind the shock is expressed as

$$\nu_r=\frac{G}{(\rho_s)_r c_s h},$$

in which G is the mass flow per second under free stream conditions. With a slight change of notation, χ, ψ, p, x, y now stand for the non-dimensional quantities $\chi/(\chi_s)_r$, ψ/G, $p/(p_s)_r$, x/h, y/h. Eliminating the pressure by means of (3), (5) becomes

$$\nabla^2(\chi\psi)-\psi\nabla^2\chi+\frac{1}{\gamma\nu_r^2\chi^{(2\gamma+1)}}\frac{1}{\mathscr{R}}\frac{\partial S}{\partial\psi}=0. \tag{7}$$

Thus the fundamental equations (2) and (4) take the non-dimensional forms (6) and (7).

Before the last two equations can be used to evaluate the flow, it is necessary to obtain the values of ν_r and $(\partial S/\partial\psi)/\mathscr{R}$ on every stream-line downstream of the shock. As a consequence of the fact that G/h and c_s have the same values on both sides of the shock, the flow parameter ratio for the rth stream-line is given by

$$\frac{\nu_r^2}{\nu^2}=\frac{\rho_s^2}{(\rho_s)_r^2},$$

where ν is the flow parameter on all stream-lines upstream of the shock. Now using the gas laws

$$c_s^2=\frac{\gamma p_s}{\rho_s}=\frac{\gamma(p_s)_r}{(\rho_s)_r},\qquad \frac{p_s}{\rho_s^\gamma}=k=\frac{p_1}{\rho_1^\gamma},$$

and

$$\frac{(p_s)_r}{(\rho_s)_r^\gamma}=k_r=\frac{p_2}{\rho_2^\gamma},$$

where the suffixes 1 and 2 indicate quantities at the shock on the upstream

and downstream sides of the rth stream-line respectively, the flow parameter ratio becomes

$$\frac{\nu_r^2}{\nu^2} = \left(\frac{p_2}{p_1}\right)^{2/(\gamma-1)} \left(\frac{\rho_1}{\rho_2}\right)^{2\gamma/(\gamma-1)},$$

or in terms of the ratio p_2/p_1 only,

$$\frac{\nu_r^2}{\nu^2} = \left(\frac{p_2}{p_1}\right)^{2/(\gamma-1)} \left[\frac{(\gamma-1)(p_2/p_1)+(\gamma+1)}{(\gamma+1)(p_2/p_1)+(\gamma-1)}\right]^{2\gamma/(\gamma-1)}. \tag{8}$$

It will be shown in section 4 how (8) together with the standard shock-wave data can be used to evaluate ν_r and $(\partial S/\partial\psi)/\mathscr{R}$ on stream-lines downstream of the shock in the problem of this paper.

3. The relaxation method

In order to use the method of relaxation, the field to be examined is covered with a regular network. In the problem considered in this paper

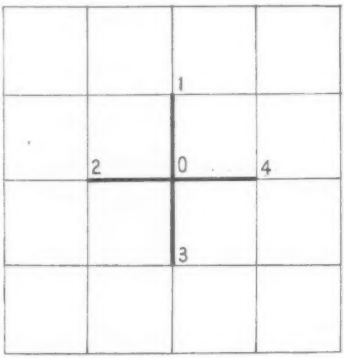

FIG. 1

a square network is used. The relaxation method and the use of patterns to eliminate residuals are discussed fully in (**3**) and need only be summarized here. In all calculations the value 1·4 has been taken for γ.

The finite difference approximations to (6) and (7) for a square net of non-dimensional mesh size a are, in the manner of (**3**),

$$R_0 \equiv \chi_0^{-4} - \chi_0^{-2(1+\gamma)} = (\gamma-1)\frac{(\nu_r^2)_0}{a^2}\left\{\psi_0^2 + \tfrac{1}{4}\sum_{i=1}^{4}\psi_i(\psi_i - 2\psi_0)\right\} \tag{9}$$

and

$$F_0 \equiv \sum_{i=1}^{4}\chi_i(\psi_i-\psi_0) + \frac{a^2}{\gamma(\nu_r^2)_0\,\chi_0^{(2\gamma+1)}}\frac{1}{\mathscr{R}}\left(\frac{\partial S}{\partial\psi}\right)_0 = 0, \tag{10}$$

where the suffixes 0, 1, 2, 3, 4 are as shown (Fig. 1). Thus for a given ψ-distribution, using (9), R_0 and hence χ_0 can be calculated at every node of the network. Equation (10) will then enable the residual F_0 to be evaluated

at every node of the field. Modification of the original ψ-distribution with a view to eliminating these residuals is carried out either by trial and error or by a relaxation pattern.

In the present case the changes in δF_j ($j = 0, 1, 2, 3, 4$) consequent on

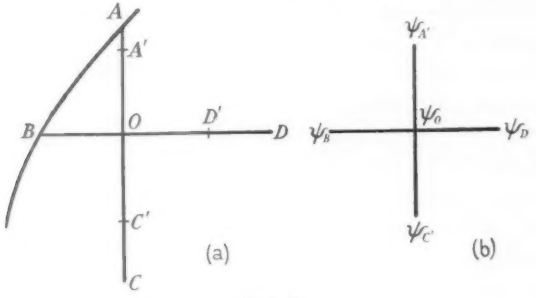

FIG. 2

an assumed modification $\delta\psi_0$ of ψ_0 are given by the relaxation pattern formulae,

$$\delta F_0 = -\left[\sum_{i=1}^{4} \frac{(\gamma-1)(v_r^2)_i}{2a^2}\{f'(R)\}_i(\psi_0-\psi_i)^2 + \right.$$
$$\left. + \sum_{i=1}^{4}\chi_i + \frac{(2\gamma+1)(\gamma-1)}{2\gamma\chi_0^{2(\gamma+1)}}\frac{1}{\mathscr{R}}\left(\frac{\partial S}{\partial\psi}\right)_0\{f'(R)\}_0\Big(4\psi_0-\sum_{i=1}^{4}\psi_i\Big)\right]\delta\psi_0 \tag{11}$$

and

$$\delta F_j = \left[\chi_0+\frac{(\gamma-1)(v_r^2)_0}{2a^2}\{f'(R)\}_0(\psi_0-\psi_j)\Big(4\psi_0-\sum_{i=1}^{4}\psi_i\Big)-\right.$$
$$\left.-\frac{(2\gamma+1)(\gamma-1)}{2\gamma\chi_j^{2(\gamma+1)}}\frac{1}{R}\left(\frac{\partial S}{\partial\psi}\right)_j\{f'(R)\}_j(\psi_0-\psi_j)\right]\delta\psi_0 \quad (j = 1, 2, 3, 4), \tag{12}$$

where, as in (**4**), $\qquad f'(R) = \dfrac{\chi^5}{4\{(\gamma+1)\chi^{2(1-\gamma)}/2-1\}}$.

These formulae are also obtained in the manner of (**3**). They are, however, only approximately true, as it was assumed in their derivation that $(\partial S/\partial\psi)_0$ and $(v_r^2)_0$ did not vary with the increment $\delta\psi_0$ of ψ_0. The consequent inaccuracy in the relaxation pattern formulae is unimportant except in the neighbourhood of the speed of sound, where a trial-and-error method of residual elimination must be used on another account, detailed in section 4 of the present paper.

Because of the curved nature of the bow shock wave, which is a boundary of the region examined in the problem of this paper, the field contains several irregular stars. The evaluation of such nodes is discussed in (**3**).

The method found to be most suitable in the present problem is illustrated. O is an irregular star (Fig. 2 (a)). The four associated points are A, B, C, and D, where $OB < OA < OC = OD = a$, the non-dimensional mesh size. A', C', and D' are such that $OA' = OC' = OD' = OB = b$, say, where b is non-dimensional. The stream-function ψ is known at A, B, C, D, and O, and so by interpolation the value of ψ is found at A', C', and D'. Thus the irregular star centred on O has been replaced by a regular node of a square net of non-dimensional size b (Fig. 2 (b)).

4. The problem to be solved

The particular problem described in this paper is that of a uniform parallel stream of Mach number $M = 1{\cdot}8$ ($\nu = 0{\cdot}40$) flowing past a square-nosed two-dimensional obstacle. The shape of the bow shock wave was obtained from a photograph made in the N.P.L. (**9**), and the extent of the field considered is from the axis of symmetry to the first stream-line which is not appreciably deflected by the shock. At such a stream-line the shock angle should be approximately the Mach angle $\sin^{-1}(1/1{\cdot}8)$. It is required to find the complete pattern downstream of this shock.

With a view to applying the methods of the preceding section, the significant linear dimension h, which was introduced in order to obtain non-dimensional quantities, was chosen to be five semi-widths of the square-nosed obstacle. The first stream-line not appreciably deflected by the shock is at a distance $10h$ from the axis of symmetry. The shock cuts this stream-line at A and the axis of symmetry at C. The sonic velocity point on the downstream side of the shock is B, the stagnation point is D, the obstacle corner is E, and the perpendicular from A meets the obstacle side at F. The methods of the previous section are now used to evaluate the field inside $ABCDEF$, where the rotational flow is mixed subsonic and supersonic. The problem is illustrated (Fig. 3).

The boundary conditions for this region consist of a knowledge of the stream-function ψ, the Mach number M, and the slope of the downstream stream-lines along AC, and also of ψ along $CDEF$. It is also necessary at this stage to obtain v_r^2 and $(\partial S/\partial\psi)/\mathscr{R}$ at the shock on the downstream side. At every point of the shock wave the tangent makes the shock angle with the direction of the axis of symmetry. It is well known that for a given Mach number and deflexion angle there are two possible shock-wave angles. The larger angle corresponds to the strong shock and the smaller angle to the weak shock. For example, at points C and A on the bow shock wave where the angle of deflexion is zero, the shock conditions are strong and weak respectively. If G is the point on the bow shock wave where the stream-line experiences its maximum deflexion, then all points

from C to G correspond to strong shock conditions and all points from G to A to weak shock conditions. There is, of course, only one shock-wave angle possible for the maximum angle of deflexion, since the weak and strong

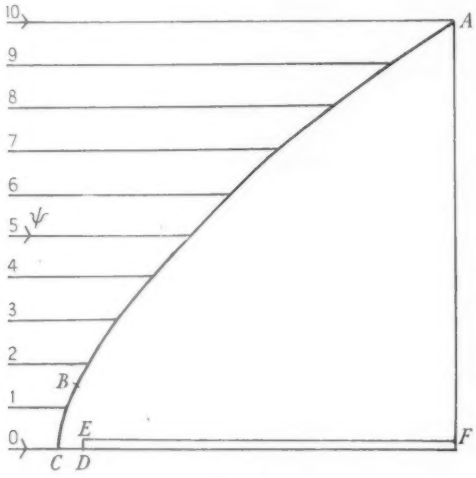

FIG. 3

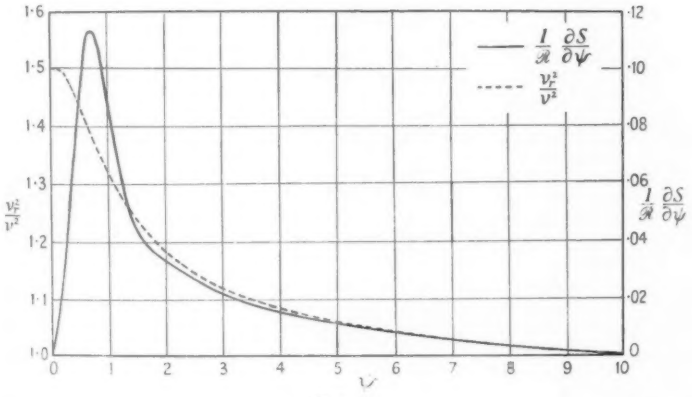

FIG. 4

shocks coincide at G. From the oblique shock chart of (**10**), the pressure-ratio p_2/p_1 can be read off for an initial Mach number of 1·8. Substitution of this pressure ratio in (8) will then give the flow parameter ratio at every point of the shock wave. The entropy has a constant value S_0 everywhere in the field upstream of the shock, but takes a different value S_r on every

stream-line downstream. The entropy increase $(S_r - S_0)$ is obtained at all points of the shock from (**11**). Since the stream-function ψ is also known at every point of the shock, we may plot $(S_r - S_0)/\mathscr{R}$ against ψ and read off the required quantity $(\partial S/\partial\psi)/\mathscr{R}$ at all points on the shock. v_r^2/v^2 and $(\partial S/\partial\psi)/\mathscr{R}$ are each plotted against ψ (Fig. 4).

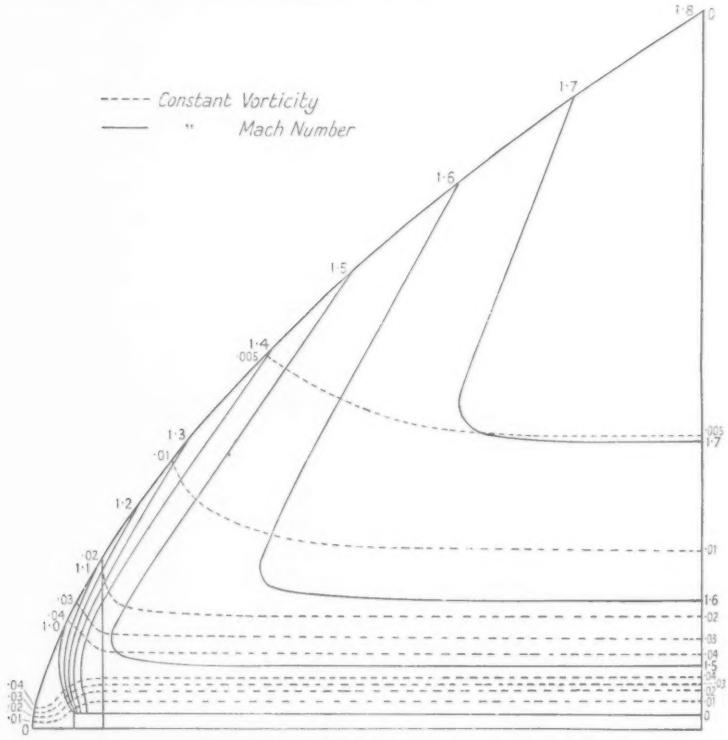

FIG. 5

The curves $v_r^2/v^2 = \text{constant}$ and $(\partial S/\partial\psi)/\mathscr{R} = \text{constant}$ are the stream-lines, and so it follows that Fig. 4 may be used not only for points on the shock wave, but also for all points downstream of the shock in the field to be examined.

As already mentioned, the field inside $ABCDEF$ was covered with a square net of non-dimensional mesh size $a = \frac{1}{10}$. Now it was shown in (**4**) that the only difficulties encountered in employing the relaxation method to mixed subsonic-supersonic problems occur in the neighbourhood of the sonic line. The method outlined there for overcoming such difficulties was employed in the present problem in the following way.

A value of ψ was assigned to every node of the square net covering the region $ABCDEF$. This assumed ψ-distribution must not violate the boundary conditions for ψ. Now the sonic line in the region starts at B and ends either at or near the obstacle corner E. Consequently, when the

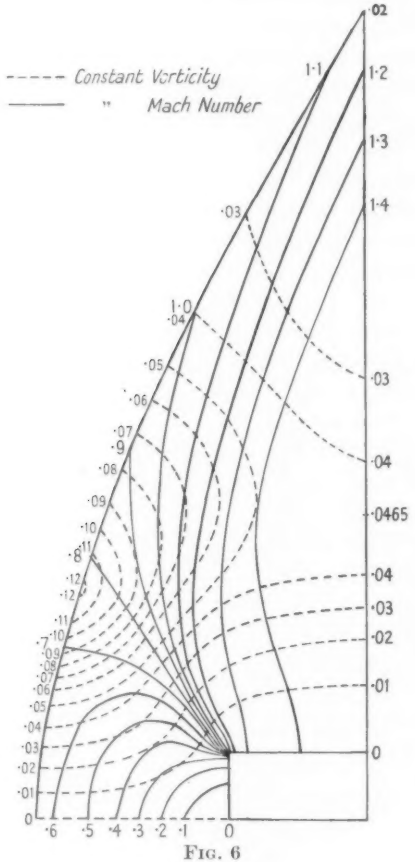

FIG. 6

shape of the sonic line is known, $BCDE$ will constitute a subsonic region and $ABEF$ a supersonic region. Using (9), R_0 can be calculated from the ψ-distribution at every node of the field. From Fig. 1 of (**4**) it is seen that for each value of R_0 there are two possible values of χ_0, a value less than 1·25 if the node is in the subsonic region, and one greater than 1·25 if the node is in the supersonic region. Although the sonic line is not known initially, the appropriate χ_0 can always be selected at each node. Thus F_0

is calculated at every node using (10). For the nodes near CD with comparatively low subsonic velocity and for the nodes near AF with comparatively high supersonic velocity, the modification in ψ is made solely with a view to the annihilation of the residuals F_0. At such nodes the relaxation pattern formulae (11) and (12) may be used in the elimination of the residuals. However, on approaching the sonic line from either side it is found that a modification of ψ often results in a value of R which is greater than the maximum possible one of 0·068. In such a case there is no possible value of χ. Consequently in modifying the value of ψ at nodes in the vicinity of the line BE with a view to eliminating the residuals, the value of R must be kept below 0·068. At such nodes the pattern formulae do not yield a definite result, and a method of trial and error is adopted. The sonic line is eventually obtained in the manner of (**4**). The complete field of flow showing the lines of constant Mach number is illustrated (Figs. 5 and 6).

In the flow of a subsonic compressible stream past a wedge (**4**) it was found that the sonic line met the wedge just in front of the apex. Consequently the field close to the obstacle corner in the present problem was examined in order to determine as accurately as possible where the sonic line met the obstacle. The net required to produce such information had a non-dimensional mesh size, $a = \frac{1}{160}$. It was found that the sonic line again met the obstacle just in front of the corner. As a detailed examination of the corner is not the primary object of this paper, the mesh size was not reduced further.

5. The rotational field

At any point in the rotational field of flow behind the bow shock wave, the vorticity is given by (**8**),

$$\omega = \frac{p}{\mathscr{R}} \frac{\partial S}{\partial \psi}.$$

This equation can be written in the non-dimensional form

$$\omega = \frac{p}{\gamma v_r} \frac{1}{\mathscr{R}} \frac{\partial S}{\partial \psi}, \tag{13}$$

where with a slight change of notation, ω, p, and ψ now stand for the non-dimensional quantities $(h/c_s)\omega$, $p/(p_s)_r$, and ψ/G respectively.

Now, as mentioned earlier, v_r^2/v^2 and $(\partial S/\partial \psi)/\mathscr{R}$ depend only on ψ and so the quantity $(\partial S/\partial \psi)/\gamma v_r \mathscr{R}$ has a constant value along every streamline behind the shock. The non-dimensional quantity p, like the Mach number M, is a function of χ at the point in question, and so (13) enables the non-dimensional vorticity to be calculated everywhere in the field

downstream of the shock. Lines of constant vorticity are shown in Figs. 5 and 6, along with the lines of constant Mach number.

On the shock wave itself, the value of the vorticity does not depend on the field downstream of the shock. Fig. 4, constructed from oblique shock-wave data, enables ω to be calculated from (13) without reference to the field downstream of the shock. Because p/ν_r decreases gradually with increasing ψ along the shock, the vorticity is found to be a maximum just before the point of inflexion on the graph of $(S_r - S_0)$ against ψ, which was obtained from (**11**). This point on the shock wave where the vorticity is a maximum is of some importance, since the stream-line starting there will always pass through regions of comparatively high vorticity.

A formula will now be derived for the angle between the stream-line and the constant Mach number line through any point in a rotational compressible field. Consider the field covered by two orthogonal families of curves $l =$ constant and $n =$ constant, the latter family being the stream-lines. The velocity q at a point is given by $q = q(l, n)$. Thus along a line of constant velocity,

$$\left(\frac{\partial q}{\partial l}\right)_n + \left(\frac{\partial q}{\partial n}\right)_l \left(\frac{dn}{dl}\right)_q = 0.$$

If ϕ is the angle between the constant velocity line and the stream-line through a point in the field, it follows that

$$\tan\phi = \left(\frac{h_n}{h_l}\frac{dn}{dl}\right)_q = -\frac{h_n}{h_l}\frac{(\partial q/\partial l)_n}{(\partial q/\partial n)_l},$$

where $h_l\,dl$ and $h_n\,dn$ are the elementary arc lengths along the stream-line and its orthogonal trajectory at the point. Now the vorticity at a point is given by

$$\omega = -\frac{1}{h_n}\left(\frac{\partial q}{\partial n}\right)_l - \frac{q}{L},$$

where L is the radius of curvature of the stream-line at the point. Elimination of $(\partial q/\partial n)_l/h_n$ leads to the result

$$\tan\phi = \frac{L\dfrac{1}{q}\left(\dfrac{\partial q}{\partial s}\right)_n}{1 + \dfrac{L\omega}{q}},$$

where ds is the elementary arc length taken along a stream-line.

Since c_s has the same value on every stream-line behind a bow shock, it can be deduced from Bernoulli's equation that a line of constant velocity is also a line of constant Mach number. In addition, it is easily shown that

$$\frac{1}{q}\left(\frac{\partial q}{\partial s}\right)_n = \frac{1}{M}\left(\frac{\partial M}{\partial s}\right)_n \frac{1}{1+(\gamma-1)M^2/2}.$$

The angle between the line of constant Mach number and the stream-line through a point is therefore given by

$$\tan\phi = \frac{\left(\frac{\partial M}{\partial s}\right)_n}{\frac{M}{L}\left(1+\frac{\gamma-1}{2}M^2\right)+\omega\left(1+\frac{\gamma-1}{2}M^2\right)^{\frac{3}{2}}}, \tag{14}$$

where all the quantities in (14) are non-dimensional. On the obstacle sides in the present problem, the radius of curvature is infinite and the vorticity zero. Thus the constant Mach number lines meet the obstacle everywhere at right angles.

It is worth while pointing out that in the rotational field of flow behind a bow shock, since c_s is constant everywhere, a line of constant dimensional velocity is a line of constant Mach number, constant non-dimensional pressure, and constant non-dimensional density. However, since $(p_s)_r$ and $(\rho_s)_r$ vary with r, lines of constant dimensional velocity are not lines of constant dimensional pressure or constant dimensional density.

6. Conclusion

The most significant feature of this paper is the adaptation of the relaxation technique to the evaluation of mixed subsonic-supersonic fields, changes in entropy being taken into account. The only difficulties occur in the neighbourhood of the sonic line, and these are overcome by the method outlined in (**4**) and in section 4 of the present paper.

The importance of taking into account the rotational nature of the flow behind the shock wave in the problem of the present paper is illustrated in Fig. 5, where it is seen that far downstream of the shock, where the flow is approximately parallel, the Mach number varies from 1·42 on the obstacle side to 1·80 on the first stream-line which passes through the shock without appreciable deflexion. If the flow behind the shock had been assumed irrotational, the Mach number of the flow far downstream would have been approximately 1·80 on every stream-line. Thus in the present problem the assumption of isentropic conditions behind the shock would have given a very inadequate approximation to the true field of flow. Even in the problem discussed by Maccoll and Codd (**2**), where the free stream Mach number is 1·50, the flow cannot be considered even approximately irrotational behind the shock, as the gain in entropy at the shock is sufficient to produce a parallel flow of Mach number 1·36 on the obstacle side far downstream of the shock.

The point on the shock wave at which the vorticity is a maximum is of major importance in relation to the rotational field of flow down-

stream of the shock, since the stream-line starting there is a locus of high vorticity.

Finally, the formula derived in this paper shows that the angle between the stream-line and the constant Mach number line through a point in a field of rotational flow is a right angle only if the stream-line has no curvature and the vorticity is zero at the point. This is the case on the obstacle sides in the problem of this paper.

REFERENCES

1. H. W. Emmons, N.A.C.A. Tech. Note 932 (1944).
2. J. W. Maccoll and J. Codd, M.O.S. Theoretical Research Report 17 (1945).
3. J. R. Green and R. V. Southwell, *Phil. Trans. Roy. Soc.* A, **183** (1943), 367–86.
4. A. R. Mitchell and D. E. Rutherford, *Proc. Roy. Soc. Edinburgh*, A, **63** (1951), 139–54.
5. G. Guderley, Wright Field Technical Report 39 (1947).
6. A. Busemann, N.A.C.A. Tech. Note 1858 (1949).
7. S. Goldstein and M. J. Lighthill, *Quart. J. Mech. and Applied Math.* **3** (1950), 297–302.
8. A. Vazsonyi, *Quarterly of Applied Mathematics*, **3** (1945), 29–37.
9. D. W. Holder, R. C. Tomlinson, and E. W. E. Rogers, A.R.C. Report 12,418 (1949).
10. H. W. Liepmann and A. E. Puckett, *Aerodynamics of a Compressible Fluid* (New York, 1947).
11. H. W. Emmons, A.R.C. Report 8150 (1944).

A NOTE ON KLITCHIEFF'S PAPER ON 'BUCKLING OF CONTINUOUS BEAMS ON ELASTIC SUPPORTS'

By A. CHARNES (*Carnegie Institute of Technology, Pittsburgh 13, Penn., U.S.A.*)

[Received 13 November 1950]

In a recent paper (**1**) J. M. Klitchieff arrives at an equation (5′) for a function Ω which may be written

$$m\Omega \sum_{k=-\infty}^{+\infty} \{[(2k+1)m-r]^2-m^2\}^{-1}\{(2k+1)m-r\}^{-2} = -1. \tag{1}$$

He is interested in the function $\Phi = m^3\pi^{-2}\Omega^{-1}$ for $r = 1$ and $m = 2, 3,...,$ and by approximating the sum of the series obtains the formula

$$\Phi = 2\pi^{-2}m^4(5m^2+1)(m^2-1)^{-2}(4m^2-1)^{-1}. \tag{2}$$

Professor E. Saibel has drawn my attention to the fact that he obtained by a different method the following expression for Φ, viz.

$$\Phi = 2^{-1}[1+\cos(\pi/m)]^{-1}. \tag{2′}$$

The two results contained in (1) and (2′) can be shown to agree. For the series (1) can be summed by residues (**2**) to give

$$\Phi = 4^{-1}\operatorname{cosec}^2\pi\left(\frac{r-m}{2m}\right)+\frac{m}{2\pi}\left[\cot\left(\frac{\pi(r-1+m)}{2m}\right)-\cot\left(\frac{\pi(r-1-m)}{2m}\right)\right], \tag{3}$$

which for $r = 1$ becomes

$$\Phi = 4^{-1}\operatorname{cosec}^2\left(\frac{\pi(m-1)}{2m}\right), \tag{4}$$

and it is easily shown that (2′) and (4) agree.

REFERENCES

1. J. M. Klitchieff, *Quart. J. Mech. and Applied Math.* **3** (1949), 257.
2. E. C. Titchmarsh, *Theory of Functions* (Oxford, 1949), pp. 114–15.

ING
TS'

for a

(1)

2, 3,...,

(2)

ained

(2')

or the

, (3)

(4)

B

T
th
T
se
ly
pe
a
an
m
T
pl
to
ph
pl
in
na
di

a
co
th
Ph
an
ve

O

BOOKS on MECHANICS and APPLIED MATHEMATICS of all publishers, supplied from stock or obtained to order. Catalogues on request. State interests.

FOREIGN DEPT.—Select Stock available. Careful attention to orders and inquiries. Books not in stock obtained under Licence.

SECOND-HAND DEPT., 140 GOWER STREET.—Select Stock of Second-hand recent editions. Large and small collections bought.

LENDING LIBRARY, Technical and Scientific

Annual Subscription, from 25s.

Prospectus post free on application

The Library Catalogue revised to December 1949. Pp. xii+1152. Demy 8vo. To subscribers 17s. 6d.; Non-Subscribers 35s. net (postage 1s.).

STATIONERY DEPT.—A comprehensive range of Sectional Designers Papers; Graph Books and Pads; Sheets and Pads of Logarithmic, 'Z' Charts, Circular Percentage, Reciprocal, Triple Co-ordinate, Polar Graph, Time Table (Gantt); Daily, Weekly and Monthly Charts; Planning Sheets, &c.; held in stock.

LONDON: H. K. LEWIS & Co. Ltd.
136 GOWER STREET, W.C.1

Business hours: 9 a.m. to 5 p.m. Saturday to 1 p.m.

Telephone: EUSton 4282 *Established 1844*

TENSOR ANALYSIS FOR PHYSICISTS

By J. A. SCHOUTEN 30s. net

This book is based on lectures given by the author in the University of Amsterdam. The first five chapters are concerned with setting out the mathematical theory underlying the use of tensors. A feature of this part is the author's facility for building up a vivid mental picture of concepts which are usually left in the more austere mathematical form of laws of transformation. The remaining five chapters deal with applications of the theory to some physical topics and include the consideration of physical objects and their dimensions, application to the theory of elasticity (including the quartz resonator), to classical dynamics, and to relativity. The last chapter discusses Dirac's matrix calculus.

Between Chapters V and VI there is a summary of the mathematical theory contained in the first five chapters so that those readers whose primary interest is Physics rather than Mathematics can find an epitome of the theory available in a convenient form.

OXFORD UNIVERSITY PRESS

HEFFER'S

of Cambridge

BOOKSELLERS

Antiquarian & New
English & European

Small or large collections of books gladly offered for

W. HEFFER & SONS, LTD.
Cambridge England

THE QUARTERLY JOURNAL OF MECHANICS AND APPLIED MATHEMATICS

VOLUME IV PART 3 SEPTEMBER 1951

CONTENTS

J. M. KLITCHIEFF: Buckling of a Triangular Plate by Shearing Forces 257

H. ŌKUBO: On the Two-dimensional Problem of a Semi-infinite Elastic Body Compressed by an Elastic Plane 260

J. G. OLDROYD: The Motion of an Elastico-viscous Liquid contained between Coaxial Cylinders. I 271

HAROLD JEFFREYS: The Surface Elevation in Cellular Convection . 283

S. TOMOTIKA, Z. HASIMOTO, and K. URANO: The Forces acting on an Aerofoil of Approximate Joukowski Type in a Stream bounded by a Plane Wall 289

A. A. TOWNSEND: The Passage of Turbulence through Wire Gauzes 308

H. B. SQUIRE: The Round Laminar Jet 321

A. M. BINNIE: The Effect of Friction on Surges in Long Pipe-lines 330

F. G. FRIEDLANDER: On the Half-plane Diffraction Problem . 344

L. C. WOODS: A New Relaxation Treatment of Flow with Axial Symmetry 358

A. R. MITCHELL: Application of Relaxation to the Rotational Field of Flow behind a Bow Shock Wave 371

A. CHARNES: A Note on Klitchieff's Paper on 'Buckling of Continuous Beams on Elastic Supports' 384

ICS

1951

257

260

271

283

289

308

321

330

344

358

371

384